# COAXIAL AND TRIAXIAL STRUCTURED FIBERS BY ELECTROSPINNING FOR TISSUE ENGINEERING AND SUSTAINED DRUG RELEASE

By

ABDURIZZAGH ALFITORI KHALF

Bachelor of Science in Chemical Engineering
Sirte University
Sirte, Libya
2002

Master of Science in Chemical Engineering
University of Stellenbosch
Stellenbosch, South Africa
2009

Submitted to the Faculty of the
Graduate College of the
Oklahoma State University
in partial fulfillment of
the requirements for
the Degree of
DOCTOR OF PHILOSOPHY
May, 2016

COAXIAL AND TRIAXIAL STRUCTURED FIBERS BY ELECTROSPINNING FOR TISSUE ENGINEERING AND SUSTAINED DRUG RELEASE

Dissertation Approved:

Dr. Sundar V. Madihally

Dissertation Adviser

Dr. R. Russell Rhinehart

Dr. AJ Johannes

Dr. Ranji K. Vaidyanathan

ACKNOWLEDGEMENTS

It is my pleasure to thank everyone who helped me get to where I am and have supported me through my research. I would like to thank my advisor, Dr. Sundar Madihally, for his guidance, support, and encouragement. I learned not only knowledge but also the working attitude. It was a great learning experience. I would also like to acknowledge my committee, Dr. R. Russell Rhinehart, Dr. AJ Johannes and Dr. Ranji K. Vaidyanathan for their guidance, assistance, and feedback. Many thanks to my lab mates, Jagdeep Podichetty, Kumar Singarapu, Christian Tormos, Carol Abraham, Kevin Roehm, Jimmy Walker and Carrie German, for their direct and indirect help with this research. I would also like to express thanks to the following departments for funding and help with analytical instrumentation.

Ministry of Higher Education Libya

Oklahoma Center for Advancement of Science and Technology

Department of Chemistry at Oklahoma State University

Dr. Krishna Bastola from the Department of Materials' Science and Engineering Oklahoma State University-Tulsa

Finally, I would like to thank my wife, Amal. She was always there cheering me up and stood by me through everything. Deep love to my dear son Aus his pleasant smile gives me strength to finish my work. Thank you to my parents, for their love and support throughout my life.

Name: ABDURIZZAGH ALFITORI KHALF

Date of Degree: May, 2016

Title of Study: COAXIAL AND TRIAXIAL STRUCTURED FIBERS FOR TISSUE ENGINEERING AND SUSTAINED DRUG RELEASE

Major Field: Chemical Engineering

Abstract: Coaxial and triaxial electrospinning are novel methods for fabrication of multilayered nano and micro-size fibers with desirable features such as co-solution blending, reinforced core, porous and hollow structure. However, the effect of type of fluids, solvent volatilities, polymer molecular weight, and co-solution blending properties (hydrophobicity/hydrophilicity) in multi-layered fibers have not been studied. In this work, coaxial electrospinning process was explored to determine the effect of type of core and solution rheology on jet stability and fibers formation using cellulose acetate (CA) as the shell material. Results from coaxial electrospinning of CA suggested that the fibers could be formed when the viscosity of the core is less than that of the sheath. Gelatin, chitosan, and mineral oil could be used as core fluids in the formation of core-shell and hollow CA fiber. Next, the coaxial process was scaled up to triaxial electrospinning to evaluate the effect of solvent volatility, type of polymer, polymer molecular weight, polymer solubility and polymer-solvent interactions at the interface and the mechanism of encapsulating the core fluid in multiaxial electrospinning. In triaxial electrospinning successful fiber formation was dependent on ensuring that the outer shell formed first, i.e., the relative solvent volatility of encapsulating core polymer to be lower than that of the shell polymer solvent. Based on the fundamental understanding of the formation of multiaxial fibers, I explored the use of these systems in a drug delivery application using biocompatible polymers of PCL blended gelatin (GT). In particular, I investigated the influence of hydrophobicity, hydrophilicity, drug-loading location, fiber size and co-solution blending properties in regulating the drug release in multi-layered fibers using Doxycycline (Dox) as a hydrophilic drug model. Drug release at 37°C over 5 days was controlled in coaxial GT-core and PCL/GT-core fibers while PCL-core had the least performance. The presence of additional layers decreased the burst release and tenability of drug release based on the selection of appropriate core-polymer. Thus, the unique fabrication process can be used to tailor the mechanical properties, biological properties and release of various factors, which can be potentially useful in a number of applications.

TABLE OF CONTENTS

LIST OF TABLES

LIST OF FIGURES

# CHAPTER 1

## INTRODUCTION

During the last decade, there has been an increasing interest in the electrospinning technology because of its capability to fabricate micro and nano fibers and flexibility to spin a variety of shapes and sizes of micro and nanofibers [1]. These micro and nano fibers offer unique properties such as high surface area per volume ratio, porous structure, strength characteristic, absorption characteristics. Important applications of micro and nanofibers include separation industries such as filtration, and biomedical applications, such as medicine, wound dressing, tissue engineering scaffolds and artificial blood vessels, textiles, energy and environmental applications such as fuel cells, solar cells, energy storage and carbon dioxide capture [2]. Electrospinning is the only technique that can produce fibers of the order of 100 nm [3] with capabilities for controlling the internal structure and surface properties. In electrospinning process sub-micron polymer particles, fibers or interconnected porous fiber meshes can be produced using an electrostatically driven jet of polymer solution [4].

In electrospinning, fibers are formed by an electrically charged jet of polymer solution [5]. While the electrospinning setup and process itself may be relatively uncomplicated, the variables concerned in producing a nano/microfiber mesh with relative uniformity are numerous. These include process parameters such as applied voltage; solution feed rate, the distance between spinneret and collector plate, and system parameters such as the type of polymer, polymer

concentration, type of solvent, solvent ratio, solution conductivity, surface tension, and solution viscosity [6].

Recently some modifications to electrospinning process have been made including collector plates and nozzle configurations. New spinnerets consisting of coaxial capillaries have been developed, which allow core-sheath fiber generation with improved control over fiber properties [7]. The latest development on electrospinning is introduced new types of nanofibers with unique structure and functions such as altered surface (hydrophobic and hydrophilic), mechanical and biological properties and the ability to manipulate the polymer solution composition. Because of these unique properties, electrospun fibers have been widely used and studied regarding many biomedical applications [8, 9]. However, forming solid fibers cannot impart all the required properties such as morphological, biological, and mechanical features. For example, embedded drug in solid fiber is subjected to fast release kinetics from the fiber surface exposed to the surrounding environment. To better control the release kinetics of embedded drugs, new modifications in fiber formation such as coaxial and triaxial electrospinning are developed. Recent studies showed that modified fibers have substantially increased surface area per unit volume. Bactericidal chemicals can be delivered to abate bacterial fouling in filtration applications [10]. However, there is limited understanding of governing conditions necessary to an electrospun wide variety of biomaterials. The specific aims of the research are given below:

**Aim 1: To investigate the effect of type core and sheath fluids on hollow and core-sheath cellulose acetate (CA) fibers' fabrication**.

- Explore the effect of type of core fluids on surface properties, size of hollow, and core–sheath cellulose acetate (CA) fiber.
- Evaluate the impact of the type of core material on the fiber tensile strength in dry and hydrated condition.

- Characterize fiber surface morphology and fiber cross-section to understand how the type of core material could affect the properties and final structure of coaxial fibers.
- Measure and compare the kinematic viscosity of spinning solutions of selected polymers to understand the observed differences and the optimum range of core and sheath fluids' viscosity needed during the electrospinning process.
- Investigate the effect of solvents' toxicity on cell function and long-term cell viability and the ability to regenerate tissues.

**Aim 2: To investigate the influence of solvent characteristics in triaxial electrospun fiber formation**.

- Evaluate the role of solvent volatilities, and molecular weights using cellulose acetate (CA, 30kDa), polycaprolactone (PCL, 45kDa, and 80kDa), mineral oil, and polyvinyl alcohol (PVA, 30kDa, and 100kDa) on triaxial electrospun fiber formation.
- Characterize fiber surface morphology and fiber cross-section to understand how changing the type of solvent and the type of sheath or core material could affect the properties and final structure of triaxial fibers.
- Analyze the chemical compositions in the fiber to confirm the presence of all components.
- Evaluate the strength of fabricated triaxial fibers in a dry and hydrated condition similar to aim 1. The tensile test is beneficial to identify the core distribution along the fiber length and the variation in the load carrying capacity between dry and hydrated conditions. Also, a comparison the strength of triaxial structured fibers in dry condition and hydrated condition could potential help in the usage of the produced fibers in applications that require some flexibility in addition to strength.
- Investigate the effect of solvents' toxicity and surface properties of triaxial fibers on cell function and cell viability for possible application in tissue regeneration.

**Aim 3: Controlling the release of therapeutic agents using multiaxial electrospun biocompatible hybrid fibers**.

- Fabricate hybrid polycaprolactone (PCL)/Gelatin (GT) electrospun fibers and tailoring the shape and thickness of the fibers for better control drug release of Doxycycline (Dox).
- Explore the effect of hydrophobicity and hydrophilicity interaction in drug loading and controlled release.
- Compare fabricated fibers from the single, coaxial and triaxial spinneret and characterize it for structural and morphology.
- Evaluate the cellular activity on the hybrid electrospun fibers of PCL/GT to understand the advantageous of blending PCL and GT for cells' attachment and proliferation.
- Study GT distribution and stability in the fabricated hybrid fibers using CFDA SE fluorescent staining.
- Model the permeability of multi-layered fibers by loading drug molecules at selected locations in a multi-layered component

**Summary**: Electrospinning is the most versatile and unconventional polymer processing technique for production of polymer nanofibers. Forming hollow nanofibers of CA has not been reported despite its potential for many applications. Hollow nanofibers have substantially increased surface area per unit volume of the fiber. Alternatively, bactericidal chemicals can be delivered from the inner core to abate bacterial fouling in filtration applications. Also, the selectivity of the filters can be altered in addition to adding growth factors for biomedical applications. Hydrophilic surface properties (CA) enhanced with hydrophobic core polymer (PCL) offer better balance and strength in hydrate condition.

Triaxial electrospinning showed to provide versatility to fabricate fibers with unique features. The stability of solution jet is the key factor that characterizes the optimum conditions of the

electrospinning process. Selection of solvents with appropriate boiling points relative to the outer sheath is critical: outer sheath should have a boiling point less than that in the inner cores. Tailoring the fibers with desirable structural features such as reinforced core, hollow, porous, multicoated and triaxial fibers will provide a unique feature for fabricated fibers. Fibers with such characteristics can be used to better-controlled release drug delivery system or to promote cell adhesion in tissue engineering.

Fabrication of fibrous mat containing doxycycline using co-axial/triaxial electrospinning of hybrid biodegradable, biocompatible PCL/Gelatin using different fibers' configurations, drug content, and drug loading location provides fibers with a suitable environment for cell proliferation and tissue regeneration.

# CHAPTER 2

# REVIEW OF LITERATURE

## 2.1 Electrospinning

Electrospinning is a fiber production method in which sub-micron polymer particles, fibers or interconnected porous fiber meshes are produced using an electrostatically driven jet of polymer solution [11]. Formals first patented electrospinning in the USA in 1934 [12]. The patent described the production of polymer filaments of cellulose acetate (CA) in ethylene glycol. The method involves dispersing the polymer solution using high voltage source. The drawback in this method is the difficulty in removing the fabricated fibers from the collector belt. From 1934 to 1971, many patents describing the experimental setup for production of polymer filaments were approved [13-16]. In recent years, the electrospinning process has regained attention due to a surge of interests in nanotechnology [17]. The major advancement in electrospinning was in 2003 when coaxial electrospinning was introduced [18]. The new modification gained considerable attention in the field of bioscience due to the mechanical, biological and structured properties of core-sheath fibers being easily manipulated by varying the material composition. The process is also called co-electrospinning, where two liquids are pumped independently through a coaxial spinneret and core-sheath jet, is drawn by the effect of an electric field to generate core-sheath structured fibers [19]. Section 2.4.1 further discusses the process of coaxial electrospinning.

## 2.2 Types of electrospinning

Traditional spinning methods such as melt, dry and wet spinning cannot produce woven or non-woven fibers with diameters as small as 100 nm. The only technique that can produce fibers as small as 100 nm is electrospinning. However, electrospinning is slow compared to the other fiber spinning processes. For instance, dry spinning has a yarn take-up rate of 200-1500 m/min, while electrospinning has a take-up rate of 30 m/min [20]. Thus, various electrospinning methods to improve fiber production rates such as multiple needle electrospinning, multi-jet electrospinning, and bubble electrospinning and nano-spider process have been investigated.

### 2.2.1 Multi-needle electrospinning

In multi-needle, electrospinning (**Figure 2.1a**) the polymer solution is forced through multiple needles connected to a high voltage supply. Syringe pump uses to pump the spinning solution to the spinneret setup. Different spinning solutions can be pumped independently to two different set in the same multiple spinneret setups. Due to the large mass of spinning, solution delivered a high voltage is needed for continuous electrospinning. The drawbacks of this method include blocking at the tip of the needles, unstable electric field strength and the variation in fiber size distribution. Although, a high flow rate, (1-18 mL/h) could be used in multi-needle systems for a higher production rate, the repulsion from adjacent jets in multi-needles is still an issue, also the system cannot produce smart advanced structure fibers such as core-shell fibers [21].

### 2.2.2 Multi-jet electrospinning

The multi-jet electrospinning setup (**Figure 2.1b**) consists of the high voltage supply, collector plate, hollow needle as spinneret and grounded needle as the auxiliary electrode. The multi jets produced when the auxiliary electrode is placed near the spinneret. The auxiliary electrode significantly enhances the electric field strength, which helps in the formation of multiple jets. The critical parameters that affect the number of multiple jets and fiber production rate are positions,

diameter, and length of the auxiliary electrode. Although, the fibers yield is 7-10 time larger than conventional electrospinning using same flow rate (3mL/h) bending instability, and splitting of the jets are still issue that needs to be addressed [22, 23].

### 2.2.3 Bubble electrospinning

Bubble electrospinning (**Figure 2.1c**) is a needless technique where the jets initiate from the surface of a polymer bubble instead of a cylindrical needle. The impact of the gas ($CO_2$, atmospheric air or $N_2$) passed underneath the polymer solution bath causes the generation of bubble structure. The jet travels from the bubble surface at the polymer bath located at the bottom to the collector placed on the insulating floor where fibers collected. Aligned fibers can be obtained by moving substrate connected to high voltage [24, 25].

### 2.2.4 Nano-spider electrospinning technique

Nano-spider technique (Figure 2.1d) uses electrode covered by the polymer solution to generate electrospinning jets. From 30 to 120 kV voltage is applied between the electrode that is partly submerged in the polymer solution and a collector device. The charged fibers are directed towards the oppositely charged collector where solvent evaporate rapidly during its travel to the target. Dry nanofiber layer accumulated randomly on the collector device. Elmarco Company uses the technique for large-scale production of electrospun fibers [26].

### 2.2.5 Needle electrospinning technique

Typical needle electrospinning setup consists of spinneret contacted to a high voltage supply (**Figure 2.2**); where the positively charged solution is pulled toward a collector plate by the effect of electric field. The electric force is generated between two electrodes one connected to the nozzle ejecting the polymer solution, and the other connected to a conductive collector. When the charge build-up at the nozzle (near 15 kV), droplet deforms into a conical structure referred to as Taylor

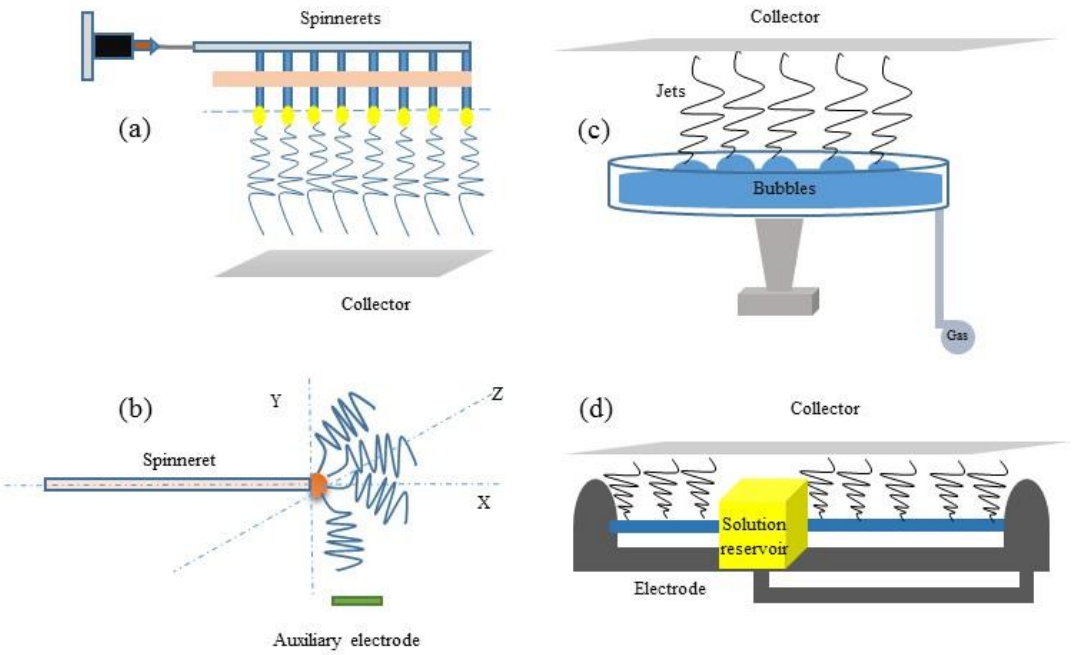


**Figure 2.1** Schematic diagram of electrospinning methods. a) Multiple needles electrospinning, b) Multi-jet electrospinning, c) Bubble electrospinning, d) Nano-spider electrospinning technique.

cone. Taylor cone can be described as the shape of the drop of the polymer solution attached to an orifice by the effect of surface tension and viscoelastic stresses before the jet is issued [5]. Increasing the electrical force above the surface tension of the polymer solution breaks the Taylor cone and polymer jet ejects from the apex of the Taylor cone. This jet deviates in a course of violent whipping from bending instabilities brought about by repulsive charges existing along the jet length. The jet stretching stops when the solvent evaporates from the surface of the jet resulting in the thinning of the fiber [14]. For successful electrospinning, it is necessary to form a stable Talyor cone, which will lead to the deformation of the jet into continuous uniform fibers with narrow distributions [27]. It is recommended not to start collecting fibers until Taylor cone reaches a steady state at the tip of the spinneret. Steady state is typically achieved within 1-2 minutes and after that time, fibers are collected.

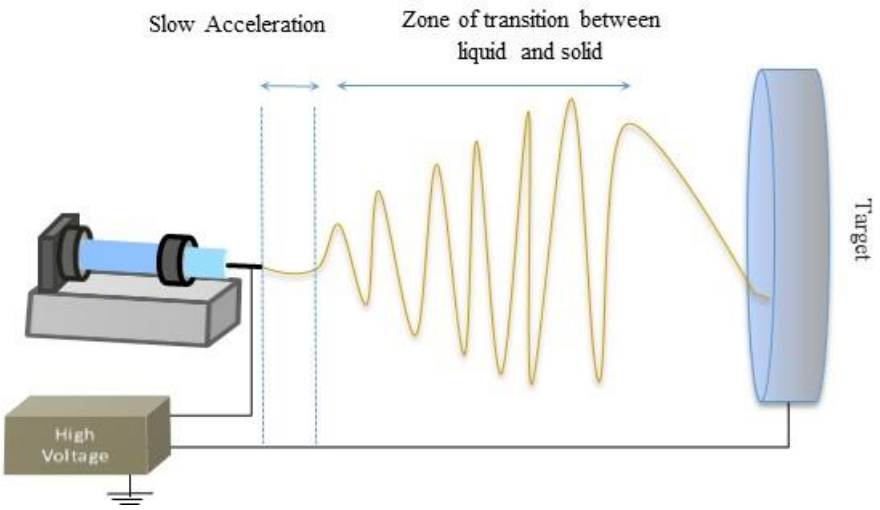


**Figure 2.2** Schematic diagram of electrospinning needle system.

### 2.3 The mechanism governing electrospinning process and solvent-polymer interactions

Polymers are consisting of long chains of molecules with repeating units known as monomers. These monomers are joined in linear or branched chains allowing the polymer chains to fit close together or cross-linked to provide harder material [28]. A polymer is said to be amorphous when the arrangement of the linear molecules is completely random. Polymers that are of higher crystallinity have higher yield strength, modulus and harden. When crystalline polymers are stretched, the polymer chains are oriented in the direction of the stress and destroy the spherules structure [29]. The intermolecular and solvent interactions in polymers are substantially affected by the state of polymer molecules as amorphous (random orientation) or crystalline (highly ordered structure). Polymer molecules will open or separate from the crystal structure to allow solvent molecules to break the crystal apart to dissolve them [30]. The solubility of polymers not only depends on the type solvent but the solvent-polymer interaction. The solvents that made of polar molecules are good at dissolving polymers that are composite of polar groups. If the intermolecular interactions between the polymer and the solvent are weak, the polymer will not dissolve. The size of solvent molecules could also influence the polymer-solvent interaction. If the size of the solvent

molecules is small, they will diffuse readily into the polymer structure and there will be a significant number of solvent molecules surrounding the chain [31]. In general, the polymer-solvent interaction must be equal to that of the intermolecular interaction between same molecules in the polymer and solvent to merge completely and produce a homogeneous solution known as an ideal spinning solution, which is needed for successful electrospinning [32].

In electrospinning process, the charged jet is held as a droplet shape by the effect of electric force and surface tension force. When the electric field overcomes the liquid surface tension force the Taylor cone is broken and a core-shell jet of spinning solution ejects from the apex of the cone. Because of the influence of electric field, the jet goes in a course of whipping and spinning instability. In the last stage of the instability reign the elongation of the jet stops by solidification of the jet, the solvent is evaporated and expelled, resulting in dry thinning fibers. Low boiling point solvent causes the polymer molecules to evaporate faster from the charged jet surface and diffuse easily from the inside of the charged jets to the outer surface. A critical factor for smooth electrospinning is the relative solvent volatility [33]. This mechanism of solvent evaporation and whipping instability can be explained by the evaporation of solvent molecules from the charged jet surface and then solvents from the inner core diffuse to the outer surface. During electrospinning, the homogeneity of the jet is not constant. The rapid solvent evaporation from the jet surface is mostly the cause of the jet inhomogeneity in the radial direction. This inhomogeneity along with stretching and jet instabilities are the two primary factors responsible for the final structure and morphology (porous nanofibers, fibers skins) of the electrospun fibers [34]. The jet drying time decreases rapidly with the decrease of the initial jet radius. For well-spun fibers, it must take account of the evaporation of solvent molecules from the fluid jet surface. The instability region (stretching and elongation) of the liquid jets is a cause of the interactions between the acting forces (viscoelastic, surface tension, and drag) and applied electrostatic forces [35, 36]. The electrical forces (**Table 2.1**) lose their influence on the charged jets due to the solidification of the surface of

charged jets. If the volatility of the polymer solution is very low, it will delay the mass transfer of solvent molecules resulting in wet fiber formation and poor electro-spinnability. Thus, the intrinsic properties of the solvents used in the spinning solution like boiling point and vapor pressure govern the evaporation rate. Some modeling efforts to understand the phase behavior of polymers is explored [37].

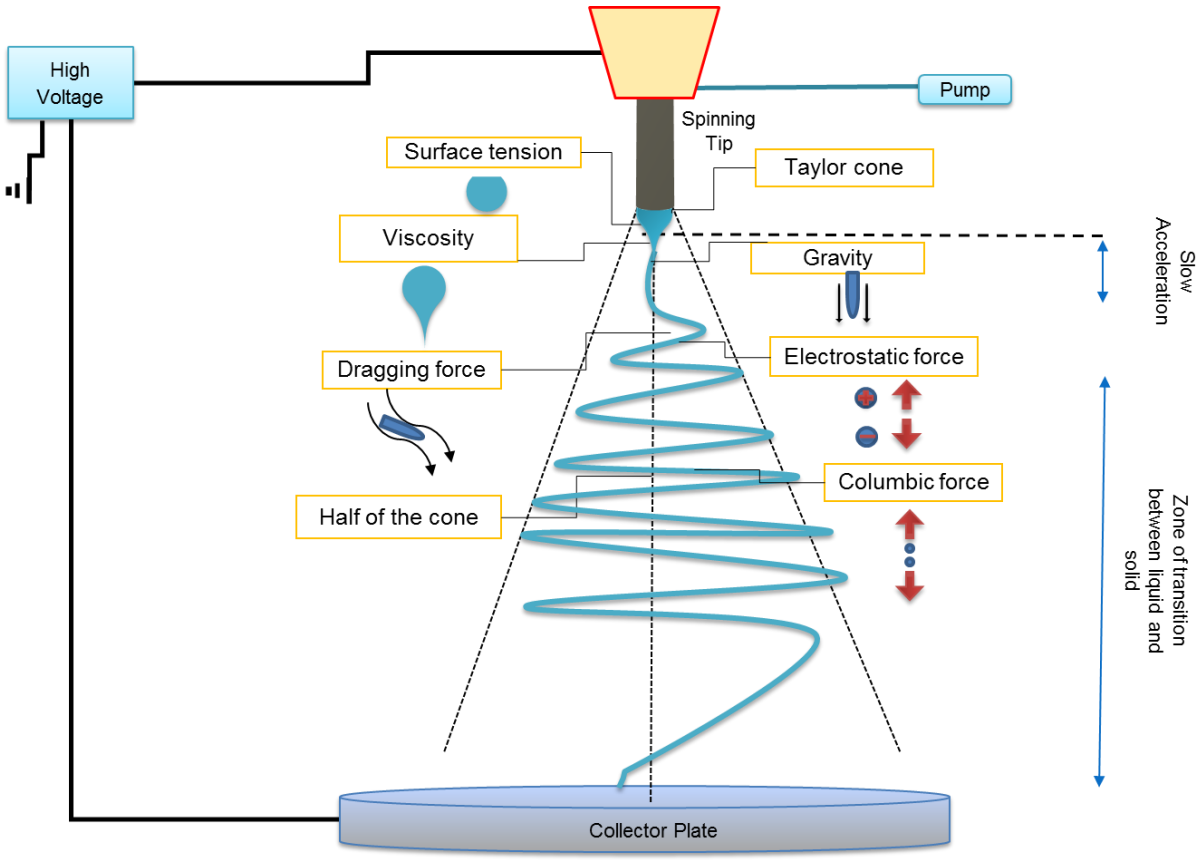


**Figure 2.3** Formation of Taylor cone at the tip of the spinneret.

**Table 2.1** The acting forces on the charged jet during electrospinning.

| Force | Description |
|---|---|
| Gravitational | The force exerted by gravity on the jet. |
| Electrostatic | The force that carries the jet to the collector. |
| Columbic | The force that responsible for the stretching of the jet during its flight time. |
| Viscoelastic | The force that prevents the jet from whipping and stretching. |
| Surface tension | The force that acts against stretching the surface of the jet. |
| Drawing | The force that results from the friction between the surface of the jet and surrounding air. |

## 2.4 Recent development in needle electrospinning technique

### 2.4.1 Coaxial electrospinning

Recent advances in electrospinning technology are focused on tailoring the fibers with desirable structural features such as core–sheath, core–sheath, hollow, porous and triaxial-channel fibers for use in various applications (**Figure 2.4)**. Core-sheath fibers are formed by coaxial electrospinning, where a coaxial spinneret composed of an outer and inner needle is most commonly used. Coaxial electrospinning can generate fibers from various solution pairs, core–sheath, hollow and functional fibers that may contain particles [38].

The core-sheath structure allows electrospun fibers to function as vehicles for delivery of a loaded drug [39]. The high surface area per volume ratio and core-sheath structure of electrospun nanofibers scaffold have potential use in tissue engineering and controlled drug delivery system [40]. With the incorporation of the hollow structure, the mechanical properties could decrease and ability to alter biological properties could be restricted. Surface topography of the fibers' influences spreading characteristics and activity of cells in cellular regeneration. Polymer solutions have to be compatible with growth factors and drugs to be used for the controlled and sustained release to

minimize deposition on the fibers; hydrophilic polymers are suitable for hydrophilic growth factors and drugs and lipophilic polymers for lipophilic growth factors and drugs. A third component could be introduced to the blended system to modify properties of the binary polymer. For example, polymethylmethacrylate (PMMA) could be added to the polycarbonate/poly (vinylidene fluoride) blend to improve the interface adhesion. In single spinneret electrospinning, the loaded drugs subjected to an initial burst release of the functional molecules at the fiber surface and expose to the surrounding environment [41]. More recently, some have developed emulsion electrospinning technique to prepare core-shell nanofibers with drug encapsulated [42]. In this process, a discontinuous phase solution containing particles/droplets (drug +water) is dispersed into a continues phase polymer solution (organic phase). The core-shell structured fibers are formed [43, 44] where the hydrophilic drug is loaded in the core and hydrophobic drug in the shell polymer [45]. The primary drawback associated with emulsified solution compared to coaxial electrospinning is the need for stabilizing the emulsion to avoid phase separation. However, the presence of the emulsifying agent in the fabricated fibers may not be desirable and could also affect the release rate and drug loading characteristics [44].

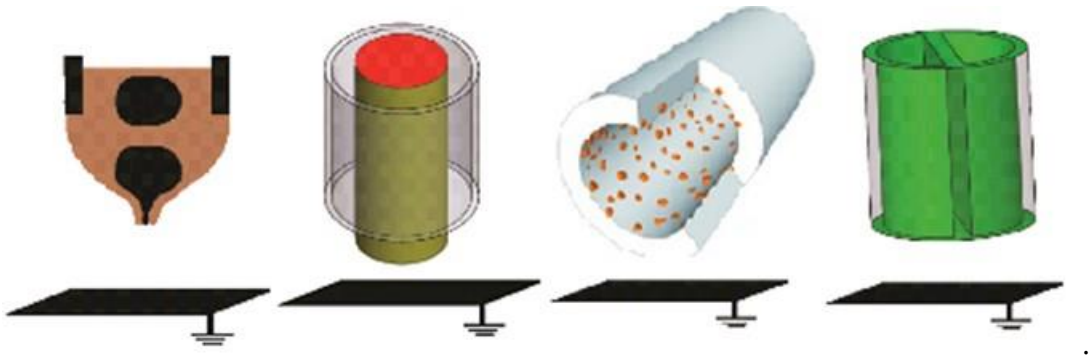

**Figure 2.4** Schematic structure of a combination of coaxial electrospun fibers [46]

.

### 2.4.2 Triaxial electrospinning

In triaxial electrospinning, three polymer solutions are supplied into a compound Taylor cone through a spinneret. Charged liquid at the nozzle orifice is drawn out by an electric field to form a

jet. Reasons for these modifications include: i) producing triaxially structured fibers with high control on fiber properties, ii) controlling the delivery approaches of multiple drugs, iii) improving the mechanical properties with the hollow fiber morphology, and iv) altering the biological properties. In triaxial electrospinning technique, selected polymers could be loaded with nanoparticles. These nanoparticles have a beneficial use for controlling drug release and or enhancing cell proliferation and migration. Triaxial fiber could also be used to deliver two different drugs with the dual delivery system by using the intermediate layer that acts as an isolation layer between and the shell and core materials [47]. Furthermore, triaxial fibers can be formed with different features such as hydrophobicity, hydrophobicity, and mechanical strength. Upon formation of the fiber, the outer sheath can be extracted, exposing the desired inner sheath allowing fibers of polymers that cannot be electrospun on their own. However, there are many possible applications for triaxial electrospinning technique; still, there is limited research on triaxial electrospun fiber due to the complexity of the process.

**2.5 Blending natural and synthetic polymers**

Different research groups [48-50] have explored several types of synthetic and natural polymers in electrospinning. Natural polymers are suitable for cell attachment and cell proliferation due to the surface topography of the fibers that influence spreading characteristics and activity of cells [51] while synthetic polymers have poor surface functionality toward cells due to the low hydrophilicity [52]. Thus, coaxial and triaxial electrospinning provide an efficient method for fabrication of desirable biocomposite for particular applications. For example, blending natural and synthetic polymers provided a new biomaterial with appropriate mechanical, physical and chemical properties, which is favorable for cell adhesion and polymer degradation rate. Other potential applications for hybrid-structured fibers include wound dressings, drug delivery, medical implants, filtration and catalysis [53]. For example, Wei Fu et al.[54] reported on the effect of mechanical properties and fibers wettability of the hybrid electrospun scaffold of PCL/gelatin and collagen

/PLCL on cell adhesion and proliferation behaviors and showed that collagen/PLCL scaffold is good candidates for vascular tissue engineering. Chong et al.[55], investigated the used of hybrid electrospun fibers in dual-side cellular growth by cultivating fibroblast cells on both sides of a thin PCL/gelatin scaffold for possible utilization in a dermal analog to assist in skin cover and regeneration. However, most of these works and other research have been focusing on describing the influence of various electrospinning parameters on morphology and structure of electrospun fibers or describing the chemical structure and biological activities. A few reports are describing the use of electrospun hybrid fibers in drug delivery with complex fiber structure such as coaxial and triaxial.

**2.6 Polymeric biomaterials evaluated in electrospinning**

Unique properties of polymeric electrospun fibers such as micro-scale pattern (mimic biological environment), high surface area to volume ratio, order structure, and porosity enable the polymeric fibers to be an excellent candidate for various applications in the biomedical field. Electrospun fibers that are biodegradable and biocompatible are attractive for use as implantable scaffolds or in drug delivery. The degradation rate of the fiber is important in controlling the drug release rate. The degradation rate of the polymer may vary by the type of polymer and intended application. A material characteristic such as polymer molecular weight and molecular weight distribution, surface properties (hydrophilicity and hydrophobicity), melting temperature, crystallinity, roughness and rigidity have a significant effect on the degradation kinetic of the polymer. Crystalline and amorphous materials are more likely to degrade faster since enzymes mainly attack the amorphous zones in the polymer. The degree of crystallinity could be one of the causes of rapid degradation of some polymers [56]. It is important to select a biodegradable material with a suitable degradation rate in a way that does not influence the release rate of the drugs.

Popular biodegradable electro-spinnable polymers are polycaprolactone (PCL), cellulose acetate (CA), gelatin (GT) and polyvinyl alcohol (PVA). **Figure 2.5** shows the chemical structure of PCL, CA, GT, and PVA. PCL is a biocompatible, biodegradable, semi-crystalline and non-toxic polymer. PCL is a synthetic polyester has gained much attention due to its well-known advantages such as low cost, low melting point (60℃), nontoxicity and elastomeric properties. PCL has average molecular weight ranges from 3000 to 85000 g/mol and has been diluted in several types of solvents, including chloroform, acetic acid, dichloromethane toluene, methanol, benzene, and tetrachloride [57]. Cytotoxicity, biocompatibility and degradation rate of PCL have been widely studied in short and long term's implantations [58-60]. PCL has good biocompatibility with living cells and biodegradable only in the present of bacteria and fungi but not easily degradable in animal and human bodies due to the absent of desirable enzymes, which cause the degradation process takes much longer time. PCL has been studied to form many medical devices [61], or scaffolds for tissue regeneration of in vivo and in-vitro cell culture using serum added media. PCL membranes fabricated using chloroform show elongation up to 1000% before the break [62]. To alter the hydrophobic characteristics of the surface, PCL has been blended with many natural polymers and utilized in drug delivery [63]. For instance, PCL blended gelatin loaded metronidazole has been used as an anti-infective membrane using a long-term subcutaneous implantation model and showed excellent comprehensive properties in vitro and in vivo [64]. Han et al. [65] also had electrospun PCL blended poly trimethylene carbonate (PTMC) and used it to encapsulate the herbal medicine shikonin. The fabricated fibers PCL/PTMC loaded shikonin were evaluated for antibacterial activates against two types of bacteria. They found that the release rate of the drug was depending on the polymer concentration and drug loading content in the fibers.

PCL has also been explored in coaxial electrospinning to form core-shell structure's fiber for positional applications in drug delivery and tissue regeneration [66]. Hui et al. [67] prepared core-shell electrospun fibers consisted of PCL as core and thermosensitive polyethyleneglycol-poly(N-

isopropyl acrylamide) (PEG–PNIPAAm) as a shell. They utilized salicylic acid as a drug model loaded in the core PCL. They evaluated the effect of polymer feed rate and thermosensitivity of shell material on the release behavior of the drug. They found that increase the temperate near the melting temperature caused the shell material to melt allowing most drugs to release in a short time. Others have also reported on blending PCL with chitosan to improve the biocompatibility and hydrophilicity.to support adhesion and proliferation of stem cells [68-71].

PVA is another synthetic hydrophilic polymer that has been explored for wide range biomedical applications, including tissue regeneration and drug delivery. PVA is a biodegradable and water-soluble biocompatible polymer and has been attractive in various biomedical applications, because of its solubility in an aqueous environment. However, electrospinning of single PVA fiber is limited due to the high hydrophilicity of PVA and rapid desolation of PVA in water [72]. Researchers have studied the effect of the degree of hydrolysis on electro-spinnability and fibers' stability of PVA in water [72, 73]. Others also reported on tailoring the chemical and physical properties to improve the mechanical and water resistance properties of PVA. For instance, PVA has been blended with chitosan to improve the biocompatibility and cell attachment [74, 75]. Also, electrospinning PVA combined gelatin showed improving in electrospun fibers' properties [76].

Another popular polymer of broad interest is CA, an acetylated derivative of the most abundant natural polysaccharide cellulose. Fabrication of CA fibers by electrospinning has evinced more interest in recent years due to the good thermal stability, biodegradability and chemical resistance of CA [77]. Several researchers have investigated the effect of type of solvent and solvent ratio on the average diameter of the electrospun CA nanofibers [78, 79]. Single and co-solvent systems studied include dioxin, dichloromethane (DCM), N, N-dimethylacetamide (DMA), ethanol, water, acetone, Dimethylformamide (DMF) and chloroform. CA has been attractive in a wide range of applications such as membrane in the separation process, cigarette filter, and biomedical films. Lately, CA has been proposed for tissue engineering and explored in drug delivery [80-83].

Cellulose nanofibers blended with carbon nanotubes have been developed as a way to promote conductivity [84]. Xiao-mei et al.[81] studied the drug release behavior of three ester prodrugs of naproxen (methyl ester, ethyl ester and isopropyl ester loaded in electrospun CA fibers. They found that the prodrug loaded fiber showed a rapid drug release at the early time and sustained release over an extended duration of time (150 h). Characterization of CA electrospun fibers showed that the three ester prodrugs of naproxen were compatibility with CA and distributed uniformly within the fibers. Recently, Chantarodsakun et al. [85] reported on controlling release of 6-gingerol from CA electrospun fibers. They showed that CA fibers loaded 6-gigerol with the antioxidant characteristic could be effectively used to controlled delivery of 6-gigerol via a transdermal route.

To tailor CA fiber with desirable structural CA has been electrospun into core-sheath fiber by coaxial electrospinning of CA with polyethylene glycol (PEG) as a smart material for thermal energy storage and temperature regulation [86]. CA was also coaxially electrospun to form CA/PVA core-sheath fibers and was used to evaluate the effect of declination on wicking behavior of fabricated CA/PVA fibers [87]. Coaxial fibers of CA/PVA have promising applications in biosensor strip and other biomedical applications that require high wicking rate.

In order to obtain cell adhesive fibers, gelatin is used in this project. Gelatin has been widely studied and exposed in various biomedical applications due to its excellent biocompatibility and biodegradability. Important biomedical applications of gelatin include tissue engineering of bone, skin and cartilage; surgical treatments and wound or burn dressings [88-90]. Several studies have been done to examine the relationship between the properties of electrospun gelatin solution such as solvent composition and morphology and mechanical properties of formed fibers [91, 92]. Because of the strong polarity of gelatin, there is a limited number of organic solvents available for dissolving gelatin. Solvents utilized to dissolve gelatin include acetic acid, 2,2,2-trifluoroethanol (TFE), Hexafluoroisopropanol (HFIP) and hexafluoro-2-propanol (HFP) [93]. Several studies have been conducted to improve and enhance the mechanical strength of gelatin by incorporated it with

other synthetic biodegradable polymer such as PCL and PLLA [94-102]. Gelatin prepared by a hybrid network of biodegradable polymers was also explored in coaxial electrospinning [103-107] and utilized in drug delivery [108-112]. This literature review helps in concluding that PCL, PVA, CA, and gelatin are more attractive than other biopolymers because of the unique characteristics they offer such as strengths, degradation, bioactivities and bendability as detailed in **Table 2.2**. **Figure 2.6** compares the key properties related to PCL, PVA, CA and gelatin polymers [113, 114].

**Table 2.2** Characteristics functions of PCL, gelatin, CA and PVA polymers.

| **Property** | **Advantage** |
|---|---|
| Biodegradability | Tailorable degradation kinetics.' |
| Environmental Compatibility | Microstructures mimic extracellular matrix (ECM) |
| Fabrication | Ability to control size, shape, thickness and drug release rate |
| Functional groups | Favorable cell responses |
| Blending Compatibility | Improve stress, crack resistance and drug loading efficiency |

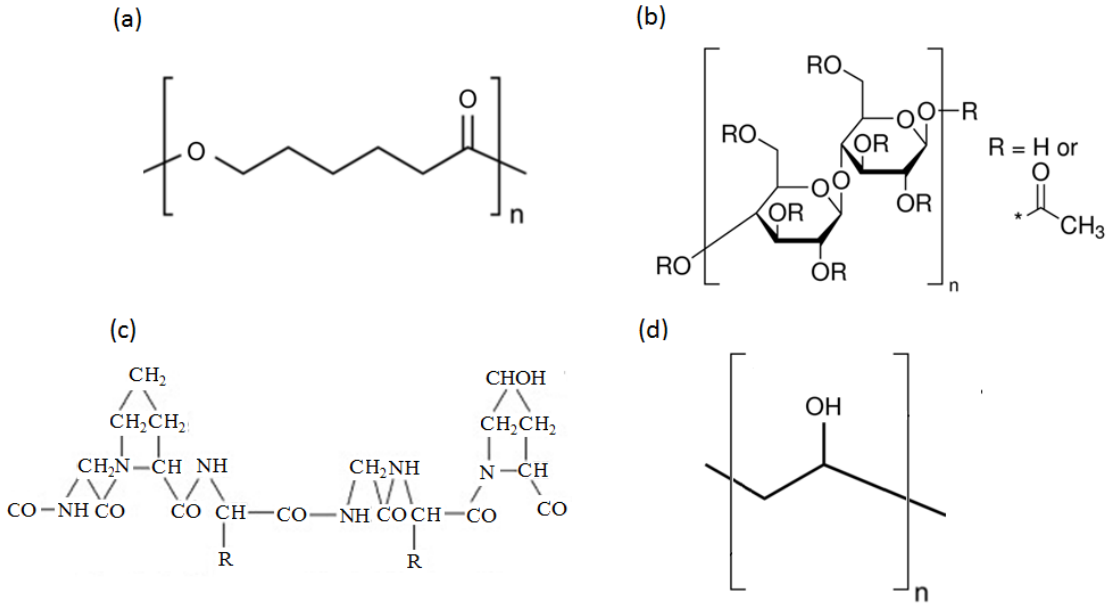


**Figure 2.5** Chemical structure of synthetic and natural polymers. a) PCL, b) CA, c) gelatin and d) PVA [77, 115, 116].

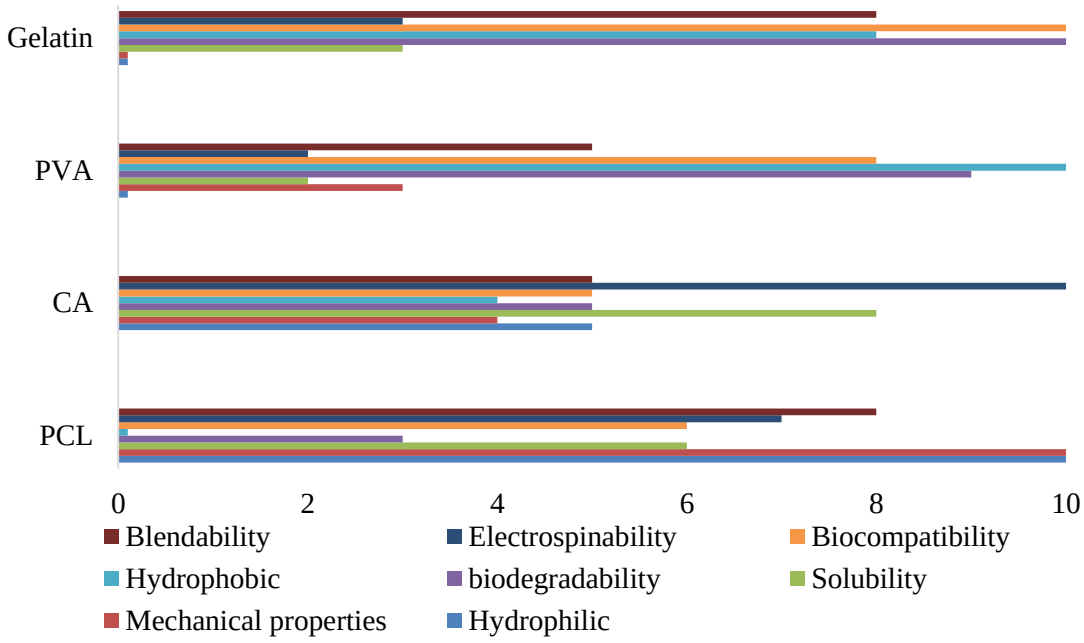


**Figure 2.6** Comparison of performance characteristics of PCL, CA, PVA, and gelatin.

### 2.7 Electrospinning in biomedical applications

There are several methods used to fabricate scaffold for tissue engineering and wound dressing, and various procedures were adopted for drug delivery and enzyme immobilization. Methods used to fabricate scaffold in tissue engineering such as solvent casting, freeze-drying [117], phase separation [118, 119] and electrospinning [120]. Tissue engineering is the use of biology and engineering principles for the development of functional substitutes that restore, improve or repair damaged tissues and or organs [121]. The loss or failure of an organ or tissue is one of the most costly health problems [122]. Repair or replace the damaged organs and or lost tissue is based on three essential components, cells, growth factors and scaffold [123, 124]. The scaffold is the main elements, which can be formed into the shape of tissue that needs to be substituted, and it interacts with cells and growth factors to regenerate the tissue. Thus, one of the most challenges in tissue engineering scaffold is the ability to fabricate biodegradable and biocompatible polymeric materials that mimic the extracellular matrix with mechanical properties similar to the native tissue with proper degradation rate, so it dissolves as the cells grow on the scaffold [99]. Most of the

engineered tissues are fabricated using polymers as scaffold material important properties associated with polymeric scaffolds are material chemistry, type of polymer, polymer molecular weight, solubility, and surface properties [121]. Electrospun fibers have shown an ability in the fabrication of biomaterial-based scaffolds with the capability of modification of their chemical, biological and mechanical properties for the regeneration of specific target tissues by coaxial or multiaxial electrospinning of multiple materials and or blends of natural and synthetic polymers with controlled dimension and arrangement [125-127]. Blending natural and synthetic polymers provide biomaterials nanofibers with controlled degradation rate and improved biological and mechanical properties and unique structure such as hydrophobic and hydrophilic surface structure. The heterogeneous structure can be prepared with desirable properties of synthetic polymer function providing better mechanical properties while natural polymer improves surface functionality for better cell adhesion and growth in tissue engineering [128]. The core-shell structural scaffold has been developed to improve and regulate engineering skin biomechanics functionality to match the native tissue biomechanics [129].

**2.8 Electrospun fibers as drug-delivery systems**

The idea of controlled drug delivery is to deliver the well-controlled amount of drug for an adequate period to a target site in the body [130]. Controlled drug delivery allows the release of therapeutic agent loaded electrospinning, nanoparticles or microspheres at a controlled rate and timely manner to avoid undesired side effects and high doses of the drug. Another important feature of controlling drug delivery is that the blood level of the drug remains constant between the maximum value and minimum value for an extended period. This process helps in avoiding the toxicity that could occur at high blood drug level and preventing the drug from depleting in the blood in a short time [131].

Encapsulation, the drug in the fiber core, provides protection, and prolonged drug release [47]. In electrospinning, successful drug, encapsulation is depending on the ensuring the distribution of the

drug molecule into the electrospun fiber, drug characteristics such as stability and solubility as well as the morphology of the fibers could significantly affect drug encapsulation efficiency [132]. Therefore, different electrospun fibers with differing types of structures have been investigated in controlled drug-delivery systems [133, 134] and have been developed for generating novel structural electrospun fibers capable of encapsulating functional molecules or therapeutic compounds and offer protection to the therapeutic agent from surrounding environment [109, 135]. Electrospinning technique resolves the limitations in the traditional methods of drug delivery. Size and internal structure of electrospun fibers can be controlled (**Figure 2.7**) by varying process and or system parameters [136].

Electrospun medicated fibers with the multilayered structure using a coaxial /triaxial fluid process provide altered release time profiles based on loading location and distribution of the drug in the fibers [137]. Drugs can be physically adsorbed by fibers (surface immobilization) or directly loaded into polymer solution before electrospinning [138]. The adsorption capacity of fibrous mats for a drug are described using adsorption isotherms such as

single parameter Langmuir model $\frac{m}{m_{max}} = \left(\frac{k_L C_e}{1+k_L C_e}\right)$ and

the two-parameter Freundlich model $logm = \frac{1}{n}\log C_e + \log K_F$

where m is the amount of drug absorbed per unit weight of the fibrous matrix, $m_{max}$ is the maximum adsorption capacity for single layer, Ce is the equilibrium concentration of the drug remaining in the solution when the absorbed amount is m, $K_L$ is the Langmuir constant and $K_F$ is the Freundlich constant. Using uniaxial electrospinning of PAA, adsorption of doxycycline was described [139] to both the equations. Using these equations one could determine whether the drug is physically adsorbed and what the maximum ration of the drug to the polymer is.

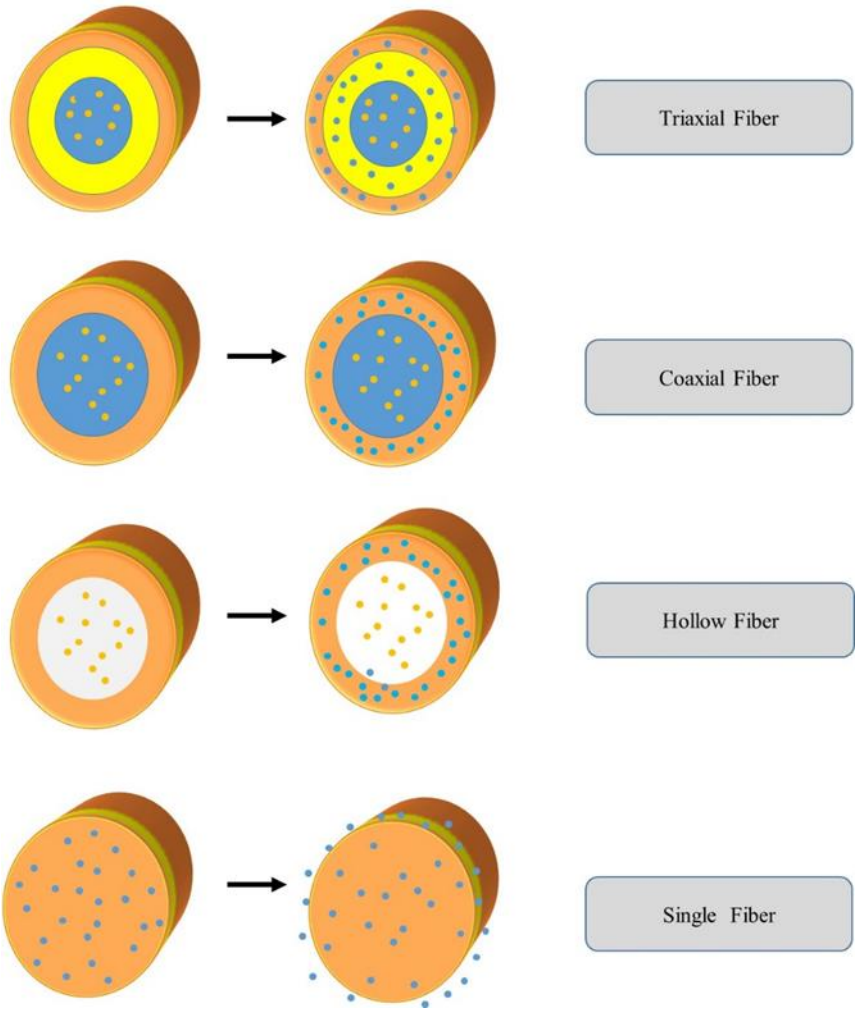


**Figure 2.7** Types of electrospun fiber structures loaded drug.

Many types of drugs have been incorporated into the electrospun fibers such as growth factors, genes, DNA, proteins, inhibitors and antibodies [130, 140, 141]. Using these results, it is well understood that the solvent-drug compatibility affects drug release rates and/or result in poor encapsulation in single electrospun fibers [147]. For example, in order to avoid undesirable solubility issues of hydrophilic cisplatin in nonpolar solvents such as chloroform/methanol, some have selected to use solvents such as dichloromethane and dimethylformamide to ensure solubility of both the polymer and cisplatin [148]. A detailed strategy for single fibers has been recently reviewed [149]. A similar concept also extends to co-axial and tri-axial electrospinning while

selecting solvents and polymers. Many results comparing various therapeutic agents show (**Table 2.3**) similar characteristics of phase separation when the polymer is not compatible with the drug. Extended list of using coaxial fibers in delivering water soluble bioactive components has been summarized elsewhere [150].

**Table 2.3** Various coaxial and triaxial fiber configurations for drug delivery applications.

| Polymer core/shell | Drug type | Application | Comments | Ref |
|---|---|---|---|---|
| PCL/PCL | Ampicillin | hydrophilic drug from hydrophobic polymer | Some sustained release of the drug up to 72 hr was noticed but there was non-uniform mixing of the drug with the polymer | [142] |
| PCL /PCL | Dipyridamole | hydrophobic drug in hydrophobic polymer | Higher concentration of drug led to thinner, and faster diffusion of the drug with reduced burst release | [143] |
| PCL /Gelatin | Metronidazole in PCL | hydrophilic drug in hydrophobic polymer | Increased drug concentration increased burst release despite loaded in the core region and there was non-uniform mixing | [144] |
| PCL/ PEG | Salicylic acid in PCL | Relating the shell thickness to the drug release rate | Thicker hydrophilic shell leads to reduced penetration of water and difficulty in diffusion of hydrophobic salicylic acid loaded in hydrophobic PCL core | [145] |
| PEG/PCL | BSA in PEG | Protein delivery | Smaller-sized fibers had a faster release rate than larger size fibers | [61] |
| PEG/PLA | Salicylic acid in PEG | Evaluating the effect of pores in the sheath on drug release | Increase core feed rates reduced pore on shell and increased drug release from the core relative to non-porous fibers | [146] |
| PEG /PBSc | Triclosan in PEG and curcumin in PBSc | Release of hydrophobic and hydrophilic drugs | Release of triclosan and curcumin was dependent on the media and their hydrophobicity and fiber structure. | [147] |
| Protein /PCL-PEG | BSA or PDGF as proteins | Control release of a growth factor using PEG as a porogen | Release rate protein from the core was affected by MW and concentration of small MW PEG in PCL | [148] |
| PDLLA /PHB | dimethyl oxalylglycine | Control release of hygroscopic drug | With PHB core drug showed linear release after initial burst release, unlike PDLLA core where only burst release was noted. | [149] |
| PLGA-HA /Collagen | Amoxicillin in Collagen | Evaluating hydrophilic drug releases from hydrophilic shell | Increased polymer content in the shell decreased the rate of release of the drug, despite following initial burst release. | [150] |
| Zein /acetic acid | Ferulic acid in Zein | Evaluating the effect of using acetic acid to stabilize core fibers | Using acetic acid as the sheath fluid helped improving the release rate of hydrophilic drug from the protein core. | [151] |

| | | | | |
|---|---|---|---|---|
| Zein/Zein | Ketoprofen | Hydrophobic drug from protein fibers | Using a blank or low concentration of Zein solution in the shell is essential to prevent burst release of the drug. | [152] |
| CA/ Acetone-DMAc-ethanol | Ketoprofen in CA | hydrophobic drug releases from hydrophilic CA | Using the same solvent mixture in the sheath helped obtain uniform small diameter fibers with negligible difference in release rate of the drug | [153] |
| PVP/CA | Amoxicillin in PVP | hydrophilic drug releases from PVP | The drug release behavior from the fibers was dependent on the pH of the medium; high pH resulted in higher release | [154] |
| PVP/EC | Maraviroc and Metronidazole | Release of hydrophobic drug when loaded in hydrophobic EC shell | PVP used as a sacrificial core, and the hydrophobic drug release depended on the shell thickness. Also, hydrophilic drug was not compatible as crystals were observed on shell surface. | [155] |
| PolyCD /PMAA | PROP in PolyCD | Control release of hydrophilic drugs | The core polymer with high molecular weight was able to spontaneously encapsulate the drug | [156] |
| PVA /PMMA | Ciprofloxacin in PVA | Periodontal disease and skin, bone, and joint infections. | Lower amount of PVA in the core prevented the burst release and achieved long sustained drug release | [157] |
| PMMA-Nylon | Ampicillin | Release of hydrophilic drug in a hydrophobic solvent. | There was a burst release proportional to the drug dosage and fiber examination after released showed unstable shell structure. | [158] |
| PVP/ PCL /PCL | KAB in PVP KAU in PCL | Dual release of model molecules by loading in core or outer shell | Selecting a less water-miscible solvent for the intermediate material is important to minimize the diffusion of dye loaded in the core layer | [47] |
| EC/EC/EC | Ketoprofen | Provide zero-order drug release | For successful triaxial electrospinning, it is important to ensure that the core, middle, and outer laminar fluids form a stable Taylor cone in a concentric manner | [159] |

Polycaprolactone (PCL), Poly (ethylene glycol (PEG), Poly-(3-hydroxy butyrate) (PHB), (poly (DL-lactic acid) (PDLLA), Platelet-derived growth factor (PDGF), Poly(butylene succinate)(PES), Poly (lactic-co-glycolic acid (PLGA), Hydroxyapatite (HA), Poly(lactic acid) (PLA), N,N-dimethylacetamide (DMAc), Poly-cyclodextrin (polyCD), Poly(methacrylic acid) (PMAA), Propranolol hydrochloride (PROP), Polyvinyl alcohol (PVA), Polyvinylpyrrolidone (PVP), Ethyl cellulose (EC), fluorescein isothiocyanate-conjugated bovine serum albumin (fitcBSA)

### 2.9. Modeling the drug release behavior

Loading the drug molecules in the shell component will result in burst release in the initial stage where the drug molecules are on or near the fiber surface because of rapid solvent evaporation during the electrospinning process [160] which treat's short-term treatment only. Whereas coaxial/triaxial fibers are designed to provide dual release profiles consisting of an immediate and

sustained release from the fiber core [161, 162] also, the drug can be programmed for multi release pattern [163-165]. To determine the time constants and the thickness necessary to regulate the release rate from different fibers the drug release mechanism needs to be well understood. The release mechanisms of a drug or therapeutic agent from the drug-delivery device can be classified into three major mechanisms' diffusion, swelling followed by diffusion and degradation [166]. Diffusion occurs within the bulk polymer or through layers as in multilayered fibers. Several factors could affect the drug release rate. These factors include: a) fiber composition such as hydrophilicity, hydrophobicity, and biodegradability, b) Fiber geometer such as thickness and structures, c) Drug loading locations and d) Solubility and stability of drug compound, in addition to the drug- polymer compatibility and the interactions between polymer-solvent-drug.

Drug present in the electrospun scaffold relies on first liquid from the surrounding penetrating the polymeric layer. This dissolves the drug so that it could diffuse or leach out of the polymeric matrix into the surrounding. The porosity of the matrix must be accounted in the model equation. Many methods have been proposed to model these activities with the intent of understanding the diffusivity of the polymeric matrix. One of the earliest models was developed by Higuchi relating the drug release rate from planar surfaces and spherical particles using Fickian diffusion. However, there could be non-Fickian diffusion due to structural changes such as fiber swelling and fiber stress relaxation. In order to determine whether the drug release depends on those events, Korsmeyer-Peppas model proposed a generalized power-law model [167], which may be modified to include the burst release. To determine the mechanism of drug release, first 60% drug release data is fitted into the model, and the exponent “n” value is calculated. If n is less than 0.45, then the process is Fickian diffusion limited, if n is between 0.45 and 0.89 it is non-fickian anomalous diffusion limited, and if n is 0.89 and greater then other factors are contributing for the drug transport (referred as case-II and super case-II transport). Using n values one could understand whether the drug is Fickian diffusion limited or Case II-transport limited future alterations in the fibrous

architecture can be made. This model has been extensively used in various electrospun drug release studies (**Table 2.4**). When the drug release is found to depend on the swelling and relaxation (based on n value), then some have explored additional models to understand the diffusional characteristics in that region [171]. Others have used a desorption model to further understand the compatibility of the drug with the polymer [170]. In this case, a scaling factor is considered to understand how

**Table 2.4** Examples of modeling on drug release from electrospun fibers.

| **Type** | **Polymer** | **Drug model** | **Release model** | **Drug release** | **Ref** |
|---|---|---|---|---|---|
| Coaxial | CA<br>PMMA/Nylon | Ketoprofen<br>Ampicilin | $\frac{M_t}{M_\infty} = \frac{M_b}{M_\infty} + k_{kp}t^n$ | 98% 144 h<br>30 days | [168]<br>[158] |
| Hollow | PEO | Gentamicin | | 70% 40 min | [169] |
| Uniaxial | PCL and<br>Lutrol F127 | Acetazolamide<br>timolol maleate | $\frac{M_t}{M_\infty} = \alpha\left[1 - e^{-\frac{\pi^2 t}{8\tau}}\right]$ | 50% <240 h<br>Acetazolamide<br>50% <240 h<br>timolol maleate | [170] |
| Uniaxial | PDLLA | Chlortetracyclin<br>e, tetracycline | $\frac{M_t}{M_\infty} = 1 - \left(1 - \frac{k_0}{C_0 L}t\right)^N$ | 53% 50h<br>tetracycline<br>56% 50h<br>Chlortetracycline | [171] |
| Coaxial | PCL, PLGA,<br>PVA, PLLA | Metoclopramide | $M_t = \left[\frac{2\pi h D \varphi C_s}{\ln(r_0/r_i)}\right]t$ | 55% uniaxial<br>70% coaxial | [166] |
| Coaxial | PVP,<br>HPMCAS | Paracetamol | $\frac{M_t}{M_\infty} = \left[e^{-tk_a} + e^{-tk_b}\right]$ | 50% 10 min 85%<br>1 h | [172] |

$M_t$ is the amount of drug released at time t, $M\infty$ is total drug release at infinite time, $M_b$ is the burst release, $k_{kp}$ is the release rate constant, $\alpha$ is the ratio of the drug at the fresh surface of the fiber to

the sum of the surface and in the fiber, $\tau$ is the characteristic time, L is the diffusional length of the sample, N is the exponent (1 for films and 2 for cylinders), $k_0$ and $C_0$ are constant related to the drug diffusion coefficient, h is the height of the cylinder, $r_0$ is the radius of the total fiber and $r_i$ is the radius of the core fiber, D is the diffusion coefficient, $\varphi$ is the partition coefficient for the drug from the core to shell, Cs is the steady state concentration, ka and kb are constants corresponding to each blended polymers.

Polyvinylpyrrolidone (PVP), Hydroxy-Propyl-methyl Cellulose Acetate Succinate (HPMCAS), Paracetamol (PCM), Poly(D,L-lactide) (PDLLA), Chlortetracycline Hydrochloride (CTC), tetracyclinehydrochloride (TC), Poly ε-caprolactone (PCL), Poly(lactic-co-glycolic acid) (PLGA), Poly(vinyl alcohol) (PVA), Poly (L- lactic acid) (PLLA), Poly(acrylic acid) (PAA), Polyethylene oxide (PEO), Cellulose (CA)

much of the drug is expelled to the surface relative to that present in the bulk. However, whencoaxial or triaxial fibers are used, there are multiple layers. The behavior of each layer may be different. In this regard, considering the radius of each layer, one could evaluate whether the shell controls the drug release [166] relative to the partition coefficient. Alternatively, compartmental modeling is approach where each compartment is treated as a first order model [172]. However, in order to manipulate each layer in the multiaxial system, one has to understand the resistance each layer offers to the intended drug and manipulate the composition accordingly. However, the drug release behavior of a hybrid core fibers with biocompatible outer surface using the same solvent system in micro-size fibers have not been studied. This would help in tailoring the fiber permeability and achieve a drug release profile from hydrophilic and hydrophobic core reservoirs. Hence, my study focused on, first, forming coaxial fibers from PCL and GT in five different configurations and analyzed the matrix porosity, volume fraction, surface morphologies, internal structures and altering the inner core to regulate the drug release profile by utilizing the chemical nature of the drug and the polymers. The second phase of the study involves modeling the permeability of multi-layered fibers by loading drug molecules in multi-layered component and tailoring the shape and thickness of the fibers for better control drug release.

# CHAPTER 3

## CELLULOSE ACETATE CORE–SHELL STRUCTURED ELECTROSPUN FIBER: FABRICATION AND CHARACTERIZATION

### 3.1 Introduction

Recent advances in electrospinning technology are focused on tailoring the fibers with desirable structural features such as core–sheath, hollow, porous and multi-channel fibers. Core–sheath fibers are formed by coaxial electrospinning, where a coaxial spinneret composed of an outer and inner needle is used [173]. Coaxial electrospinning can generate core–sheath, hollow and functional fibers from various solution pairs that may contain particles [174]. The high surface area per unit volume and core–sheath structure of electrospun fibers scaffold has a potential use in water filtration, tissue engineering and controlled drug delivery system [175]. Surface topography of the fibers influences spreading characteristics and activity of cells needed in tissue regeneration. The core–sheath structure allows electrospun fibers to function as vehicles for drug delivery [176]. Polymer solutions have to be compatible with growth factors and drugs to be used in the controlled and sustained release to minimize deposition outside the fibers; hydrophilic polymers are suitable for hydrophilic growth factors and drugs and lipophilic polymers for lipophilic growth factors and therapeutic agents [48].

Many synthetic and natural polymers have been explored in coaxial electrospinning. Natural polymers are suitable for cell attachment and cell proliferation due to the surface topography of the fibers that influence spreading characteristics and activity of cells [149] while synthetic polymers have excellent tailorable mechanical properties but lack cellular influence [177]. Thus, coaxial electrospinning offers an effective method for fabrication of desirable biocomposite for particular applications. Popular biodegradable electrospinable polymers are polycaprolactone [58], Chitosan, [178], gelatin and cellulose acetate (CA). PCL is non-toxic, biocompatible and biodegradable and has gained significant attention due to its low melting point (60 °C) and elastomeric properties [179]. It has been studied to form many medical devices or scaffolds for tissue regeneration of in vivo [180] and in vitro [181] cell culture. PCL has been blended with many natural polymers to alter the hydrophobic characteristics of the surface and has been extensively evaluated in core–sheath structures [182]. Gelatin and chitosan have been widely studied and explored in various biomedical applications due to their excellent biological activity [183]. Gelatin and chitosan nanofibers have been evaluated in tissue engineering of bone, skin and cartilage; surgical treatments and wound [88, 90].

CA has gained significant attention in electrospinning as a long linear chain polymer with good electrospinniability [79]. Electrospun CA nanofibers blended with carbon nanotubes have been developed as a way to promote conductivity. CA semipermeable membranes are commonly used in applications such as dialysis, ultrafiltration, and reverse osmosis [184]. Regenerated cellulose via deacetylation of CA membranes has additional chemical resistance to many organic solvents and aqueous solutions, and low nonspecific absorption. Many solvents have been explored in forming electrospun CA fibers [185] including organic solvents such as acetone and acetic acid. Increased CA concentration showed improved fiber size [186]. Mixing other solvents such as dimethylacetamide [187], and Dioxane [188] to acetone improved CA spinnability. CA nanofibers showed good thermal stability, biodegradability and chemical resistance [79] and had been

proposed for tissue engineering, and drug delivery [153]. However, CA biocomposite nanofibers with improved mechanical properties have not been reported despite their potential in many applications [189]. For example, hollow fibers will have increased surface area per unit volume, and formed composites with bactericidal polymers can abate bacterial fouling in filtration applications. Filter selectivity can be altered by adding various factors.

This work evaluated how the mechanical and biological properties of electrospun CA fibers altered by reinforcing the fiber with different core materials. Comprehensive fibers analysis of identifying and examining fibers morphology and surface structure were carried out to understand the interaction between system and process parameters during coaxial electrospinning process. These results show significant improvement in CA–PCL core–sheath structures.

## 3.2 Materials and methods

### 3.2.1 Materials

CA Mn = 30,000 GPC, octane 99 %, acetone 99.9 %, 1-2 dioxin, Type A Gelatin (porcine 300 Bloom), chitosan medium molecular weight, PCL (80 kDa, Mn = 80,000, and PCL 10 kDa, Mw = 14,000) were purchased from Sigma-Aldrich (St. Louis, MO). Mineral oil 99.9 % was from Rexall (Goodlettsville, TN). PCL (43 kDa, Mw = 43,000–50,000) was obtained from Polysciences (Warrington, PA). All other chemicals were used as received.

### 3.2.2 Generation of electrospun fibers

CA was dissolved in 2:1 (v/v) acetone:dioxene mixture. PCL was dissolved in 1: 9 (v/v) methanol and chloroform mixture. Chitosan was dissolved in 1:19 (v/v) mixture of acetic acid and water while gelatin was dissolved in 1:9 (v/v) mixture of acetic acid and water. All solutions were prepared fresh at room temperature.

The custom-built coaxial electrospinning setup (**Figure 3.1**) used in this study consisted of two syringe pumps (74900 series, Cole-Parmer Instrument Company, Vernon Hills, IL) to pump shell and core solutions separately, syringes, needles, high voltage power supply (ES30P-5W/DAM, Gamma High Voltage Research, Ormond Beach, FL), earth grounding, and a collection mandrel. CA spinning solution (14 wt%) was loaded into a 10 mL syringe. Syringes were connected to the spinneret via 30-cm long PTFE tubing (from Sigma Aldrich, St. Louis, MO). Shell and core solutions were pumped at controlled flow rates as indicated in **Table 3.1**. Fibers collected for 10 min were used to examine the surface morphology and the cross section of the formed fibers. The core was removed by immersing formed fibers in octane for 24 h and then air dried at room temperature. Randomly distributed fibers were collected on a flat plate for tensile analysis.

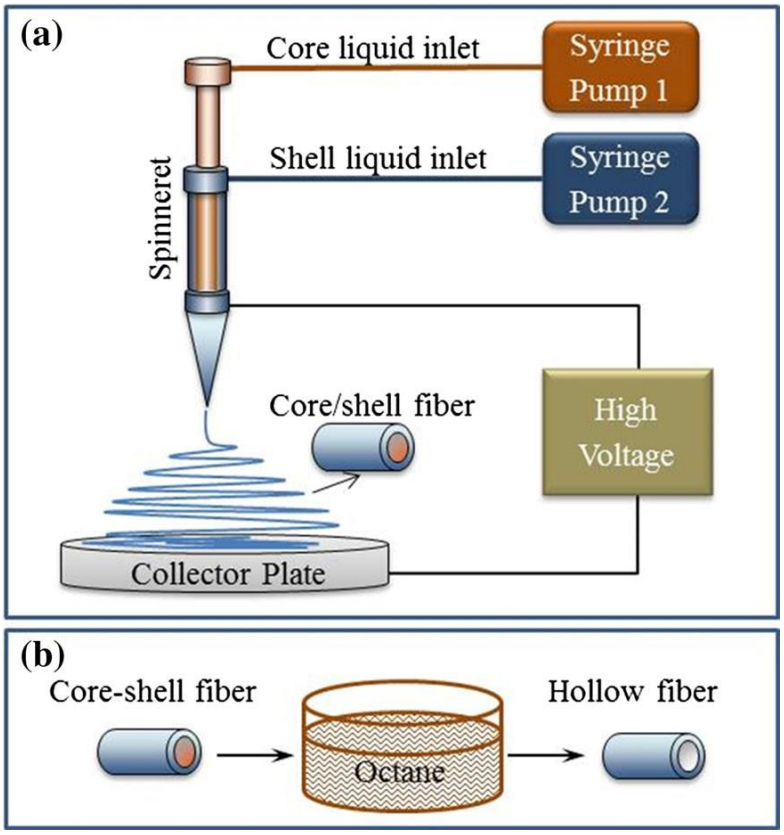


**Figure 3.1** Core–shell fiber formation. a) Schematic of coaxial electrospinning setup. b) Schematic of fiber core extrication.

### 3.2.3 Viscosity measurement

Solution viscosities were measured at shear rates ranging from 0.0001 to 1,000 $s^{-1}$ using a C-VOR Viscometer (Bohlin Instruments Ltd., Cirencester, UK). Solutions were loaded into a viscometer fitted with a standard-size recessed end concentric cylinders' geometry, 15 mm stator outer diameter, 14 mm rotor inner diameter and 0.7 mm gap.

**Table 3.1** Ranges of operating parameters.

| Parameter | Operation value |
|---|---|
| CA Shell solution concentration | 12–17 wt% |
| Core solution concentration | 1–20 wt% |
| Shell flow rate | 0.5–3 mL/h |
| Core flow rate | 0.001–2 mL/h |
| Spinning distance | 5–12 cm |
| Solvent ratio | 1/1, 1/2, 3/1,2/1 (v/v) |
| Voltage applied | 5–20 kV |
| Core needle ID | 0.03–0.7 mm |
| Shell needle ID | 0.15–1.5 mm |

v/v is volume percent or volume/volume percent; ID is needle internal diameter

### 3.2.4 Microstructure characterization

Samples were analyzed by scanning electron microscope (Jeol JOEL 6360USA Inc., Peabody, MA), similar to a previous publication [175], with some minor modifications. In brief, fibers were first frozen in liquid nitrogen, cut into 2-mm long strips, attached to an aluminum stub using a double sided conductive tape and sputter-coated with gold for 1 min. Digital micrographs were collected from random locations at 15 kV accelerating voltage. Micrographs were analyzed for fiber sizes using Sigma Scan Pro (SPSS Science, Chicago, IL) image analysis software. More than

30 fibers were randomly quantified using three different images per condition. Obtained values were then used to determine the fiber size distribution, average fiber size, and standard deviation.

### 3.2.5 Differential scanning calorimetry

Thermal properties were characterized using a Q2000 differential scanning calorimeter (TA instruments New Castle, DE) equipped with refrigerated cooling system (RCS) 90. Five to ten mg of fibers were sealed in aluminum pans. The experiments were run between 25 and 250 °C range in nitrogen atmosphere at 10 °C/min ramp rate.

### 3.2.6 Fourier transform infrared spectroscopy

Samples were analyzed by a Thermo-Nichole-50 FTIR spectrometer equipped with a DTGS detector. Dry samples were loaded, and spectral scans were obtained at ambient conditions at a resolution of 4 $cm^{-1}$ with an accumulation of 64 scans, using the associated software. Peaks were analyzed by plotting the data in Sigma Plot 12 software (SPSS Science, Chicago, IL).

### 3.2.7 Tensile analysis

Tensile testing was performed at room temperature in dry and hydrated conditions using samples collected on a flat collector plate, similar to the previous publication [190]. For hydrated conditions, samples were immersed in water for 1–2 min prior to testing. Fibers collected on the flat plate for the same duration of time were peeled and cut into 8 cm long × 1 cm wide rectangular strips and loaded into the tensile test machine (INSTRON 5542, Canton, MA) outfitted with a 100 N load cell. Scaffolds were strained to break at a cross head of 10 mm/min. Data collected using Merlin (INSTRON, Canton, MA) software was exported to MS Excel and analyzed for stiffness from the slope of tensile strength (N) vs extension (%) in the linear region. The break point was measured on the load-extension curve. Experiments were repeated three times for each fiber type, and the average, and standard deviations were calculated.

### 3.2.8 Cell culture

Human Umbilical Vein Endothelial Cells (HUVEC-2) derived from single donors were obtained from BD Biosciences [59] and cultured in Medium 200 phenol red free (PRF) supplemented with Low Serum Growth Supplement (containing 2 % v/v fetal bovine serum, 1 µg/mL hydrocortisone, 10 µg/mL human epidermal growth factor, 3 ng/mL basic fibroblast growth factor, and 10 µg/mL heparin) following vendor protocols. The cells were maintained in a 37 °C, 5 % $CO_2$/95 % air, humidified cell culture incubator. When confluent or for seeding on different structures, cells were detached with trypsin/EDTA (Invitrogen Corp.), and then trypsin neutralization solution (Invitrogen Corp.) was added. Cells were centrifuged at 125 g for 5 min and dispersed in growth medium. Twenty five thousand viable cells stained with CFDA-SE were seeded onto tissue culture plastic surface, and fibers.

Cell viability was assessed using carboxyfluorescein diacetate-succinimidyl ester (CFDA-SE, Invitrogen Corp. Carlsbad, CA) stain after 1 day, as described previously [191]. In brief, CFDA-SE content from the cytoplasm of live cells was extracted by three cycles of repeated freezing and thawing. The CFDA-SE content in the spent medium and the cytoplasm were assessed for fluorescence intensity using a spectrofluorometer at 485 nm excitation and 52 nm emission. The cell-containing samples were also fixed in 3.7 % formaldehyde for 30 min at room temperature. The samples were dried using ethanol followed by a brief vacuum drying and then sputter coated with gold at 40 mA prior to observing under an SEM. Experiments were conducted in triplicates ($n = 3$). Reported valued were represented as mean ± SD. A significant difference between two groups was analyzed using ANOVA with 95 % confidence interval. Differences in the results were considered statistically significant when $p < 0.05$.

### 3.3 Results and discussion

#### 3.3.1 Fabrication of CA solid (single) fiber

Solid single CA fiber was processed using single spinneret [192]. 17 kV applied voltage, 15 cm spinning distance, 1 mm sheath spinneret inner diameter and 0.25 mm core spinneret inner diameter were found to be optimum for single fiber electrospinning. Fabricated solid CA fibers formed using 14 % CA in 2:1 acetone/dioxane solvent mixture appeared to be slightly different in size (**Figure 3.2a**). Formed fiber quality could be improved by varying process and or system parameters. Since the study focus on fabrication of core–sheath structural fiber we did not try to improve the uniformity of CA solid fibers. Fibers had an average diameter of 0.60 (±0.20) µm with a wide range of fiber diameters. Produced CA single fibers were used as control material in the comparison of fibers characteristics in the three configurations (CA single, CA hollow, CA–PCL).

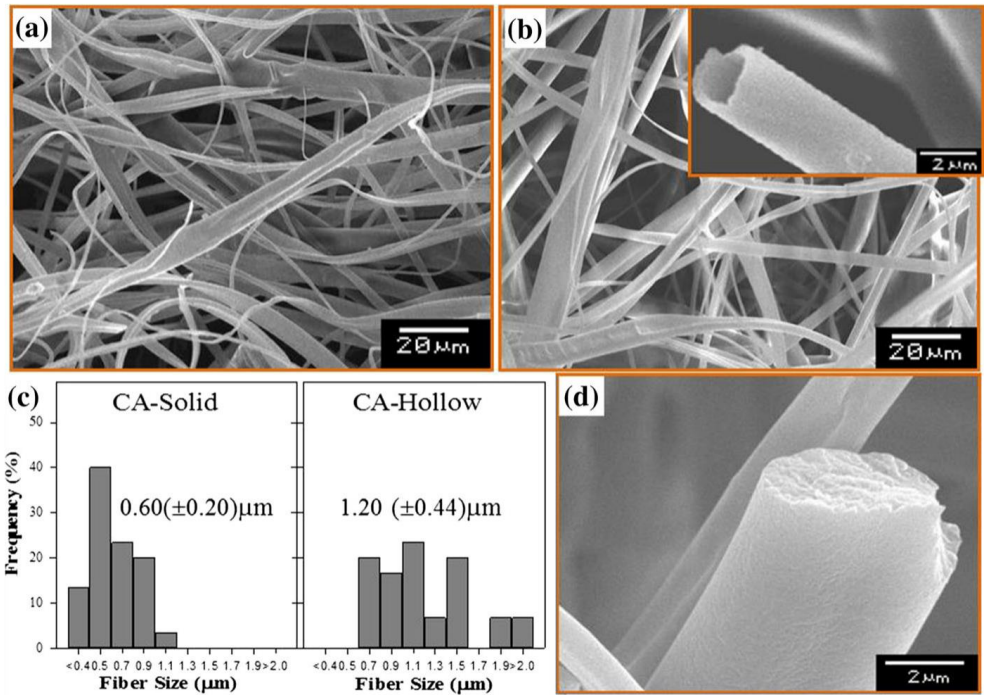


**Figure 3.2** Micrographs of electrospun CA fibers. a) Solid fiber. b) Hollow fiber fabricated form 14 wt% CA and oil. Inset is high magnification micrographs showing the cross section. c) Fiber size distributions of CA-solid electrospun and CA-hollow fibers. d) CA chitosan electrospun fibers from 14 wt/v% CA and 2 wt/v% chitosan.

### 3.3.2 Fabrication of CA hollow fiber

Visual classification of the spinning solutions was carried out during the coaxial electrospinning process. The behavior of the coaxial jet was classified as either dripping or whipping. Electrospinning produces fibers only during the whipping phase. A stable whipping jet was observed when optimum electrospinning conditions was achieved (**Table 3.2**). After the fabrication of core–sheath fiber, the core mineral oil was selectively extracted by immersion in octane, which has a good phase-separating ability and good extractability. Octane showed an ability to remove the mineral oil without effecting the CA present in the outer sheath and the overall morphology of electrospun fibers (**Figure 3.2a**). Analysis of the SEM micrographs (**Figure 3.2b**) of hollow CA fibers showed uniform fibers distribution without the presence of beads in the fibers structure formed using 14 % CA in 2:1 aceton/dioxan mixture. Comparison of fibers with and without octane treatment showed no change in the morphology and uniformity of electrospun CA fibers after core extraction. The average fiber diameter and standard deviation of electrospun fibers were evaluated. Obtained results showed that hollow fibers were nearly double in size, i.e., 1.2 (±0.44) μm and the distribution of fibers was broad.

**Table 3.2** Summary of core and shell fluid compositions utilized.

| Fluid | Polymer | MW (kDa) | Conc (wt%) | Solvent/co-solvent | Observation |
|---|---|---|---|---|---|
| Shell | CA | 30 | 14 | Aceton/dioxan (2/1) | Uniform, beads free – |
| Core | Oil | – | – | – | – |
| Core | PCL | 80 | 20 | Chloroform/methanol (90/10) | Separation of two components |
| Core | PCL | 43 | 20 | Chloroform/methanol (90/10) | Uniform, beads free |
| Core | PCL | 10 | 20 | Chloroform/methanol (90/10) | Non-uniform |
| Core | PCL | 10 | 9 | Chloroform/methanol (90/10) | Non-uniform beaded fibers |
| Core | Chitosan | 125–800 | 2 | Water/acetic acid (95/05) | No fiber formation |
| Core | Gelatin | 75 | 10 | Water/acetic acid (90/10) | No fiber formation |

### 3.3.3 Fabrication of CA–PCL fiber

PCL molecular weight of 10, 43, and 80 kDa were evaluated for their ability to electrospun core–sheath structure fiber. At high molecular weight (80 kDa), the strength of core solution increased eventually led to prevent sheath solution from dragging and encapsulating the core solution. Obtained micrographs (**Figure 3.3a**) showed uniform fibers with no beads. However, fibers appeared to be broken along the length of the fibers indicating an inability of sheath polymer to wrap the core polymer. SEM image of a fracture cross-section of CA–43 kDa PCL (core) showed (**Figure 3.3b**) the presence of both the core and outer sheath, suggesting the presence of both PCL and CA. Formed structures were uniform, and no beads were present. Interestingly, measured fibers sizes indicated that 43 kDa core and 80 kDa core fibers had similar fiber sizes and were comparable to that of CA-hollow fibers. The distribution of fiber thickness in CA–PCL 80 kDa and CA–PCL43 kDa fibers was similar to that of hollow fibers. However, that of 10 kDa PCL was nearly half the size of 43 kDa and was comparable to that of solid CA fibers. These results show that the MW (with respect to solution concentration) of the core solution has a significant impact on the morphology, quality and final CA core– sheath structures. 10 kDa PCL with 9 and 20 % concentration were electrospun to better understand the effect of concentration on coaxial jet stability and fiber uniformity. Fibers produced from coaxial electrospinning of 20 % CA–PCL 10 kDa were uniformly distributed (data not shown), similar to CA solid fibers. Fibers produced from CA–PCL10 kDa 9 % had an average diameter of 0.7 (±0.21) μm, similar to that of CA–PCL10 kDa 20 % (0.6 (±0.16) μm) and solid CA fibers. Varying the concentration from 9 to 20 % showed no significant effect on the overall fiber uniformity (**Table 3.2**). However, the effect of PCL concentration of high MW and flow rate to better understand the effect on overall fiber size still need further investigation.

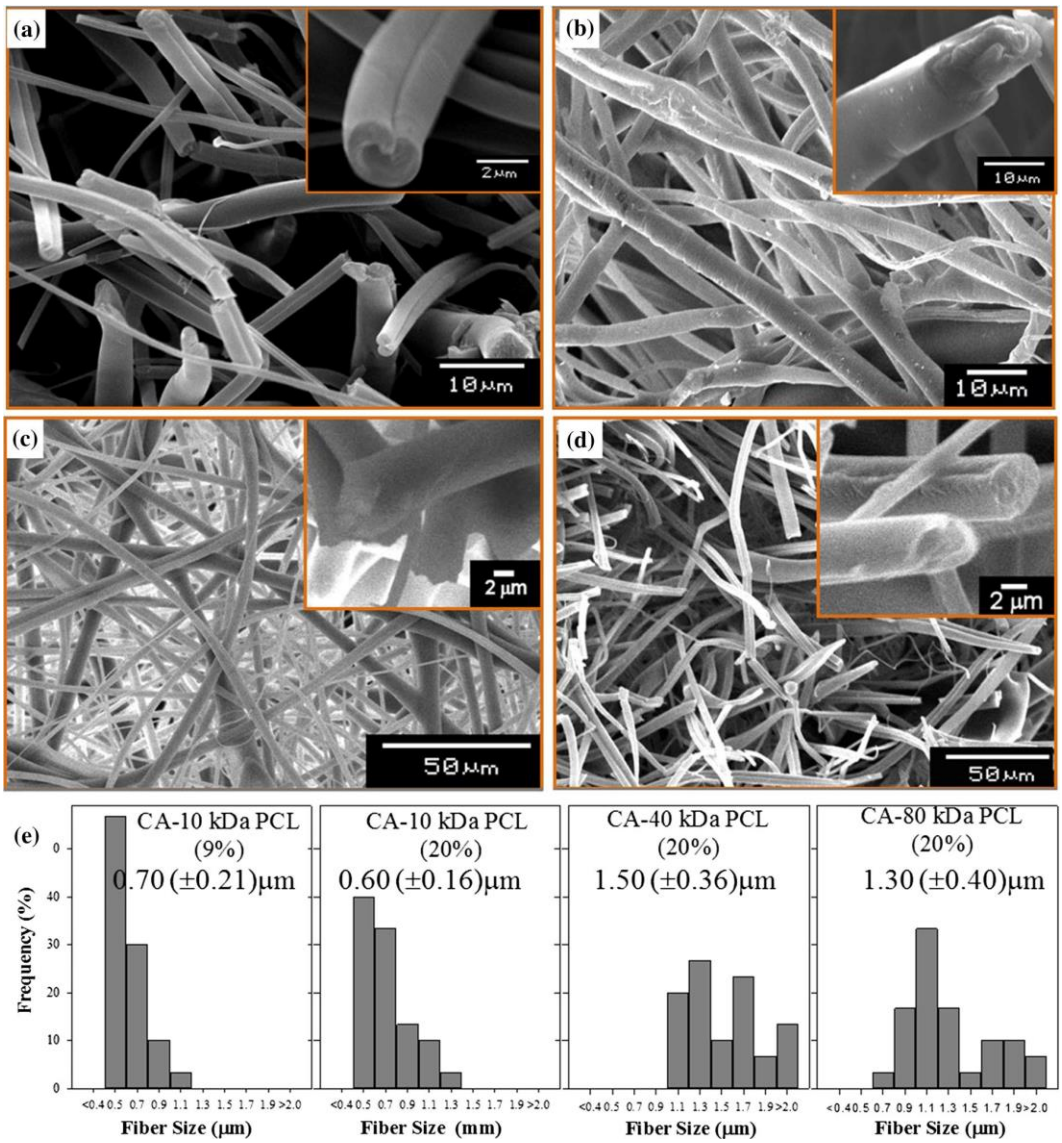


**Figure 3.3** Scanning electron micrographs of CA–PCL core shell fibers. a) 80 kDa PCL shell core, b) 43 kDa PCL shell core, c) 9 % 10 kDa PCL shell core, d) 20 % 10 kDa PCL shell core, e) Fiber size distributions of CA–PCL core–shell fibers showing the effect of MW. Insets in these micrographs are cross sectional view of solid fibers.

### 3.3.4 Fabrication of CA–chitosan and CA–gelatin fiber

Coaxial electrospinning of both CA–gelatin and CA– chitosan showed difficulties in maintaining a stable coaxial structured jet. The jet was formed, but there was a tendency to electrospray rather

than electrospinning and the spinning solution often blocked the tip of the spinneret. **Figure 3.2d** is SEM image of CA– chitosan fibers. No fibers formed for CA–gelatin at any given condition. The lack of spinnability and/or poor spinning performance of both gelatin and chitosan was due to the incompatible solvent system of gelatin and chitosan solutions mixture, leading to solvent interaction between core and shell solutions that owed to the separation of two components. The volatility of the sheath polymer solvent was also high, which delayed the mass transfer and diffusion of the core solvent molecules resulting in wet fiber formation. Other parameters such as surface tension interactions between polymer molecules and solvent, voltage applied, solution conductivity and solution concentration could also affect the spinning trajectory [173, 193].

### 3.3.5 Presence of PCL inside CA fibers by DSC analysis

Melting temperature of CA is near 225 ℃ [194], PCL is 60 ℃, and chitosan undergoes thermal degradation at 270 ℃ prior to melting. To understand the presence of PCL in CA–PCL fibers, DSC analysis was performed on fibers. For the four conFigureurations CA solid, CA–PCL (43 kDa PCL), CA hollow and CA oil, a similar melting temperature was observed (**Figure 3.4**). In CA hollow fibers, a broad bump was observed between 70 and 110 ℃, probably due to the presence of octane. Thermograms of CA–PCL coaxial fibers demonstrated two melting temperatures attributed to the existence of PCL and CA. Both melting temperatures appeared to be shifted. For PCL, it was around 57 ℃ while that for CA was 217 ℃. This could be attributed to the interaction between PCL and CA components. Further investigations varying the flow rates of both the components would provide a better understanding of the interactions between PCL and CA [181].

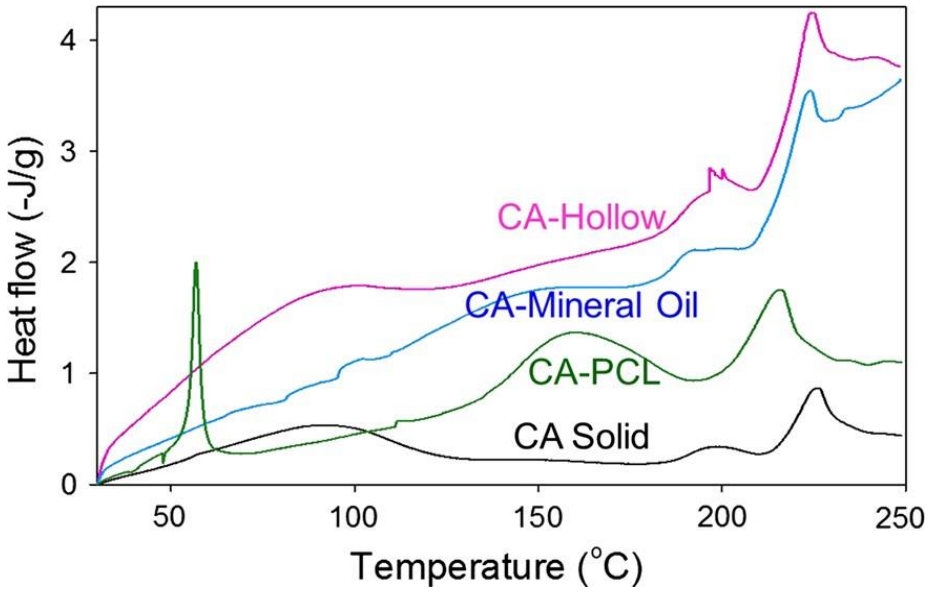


**Figure 3.4**. Thermograms of various CA fibers.

### 3.3.6 Presence of mineral oil in the fibers by FTIR.

Spectroscopy of solid CA fiber and pure mineral oil showed (**Figure 3.5**) signature absorption peaks. In solid CA fibers, a wide stretching band of the hydroxyl groups at 3,470 $cm^{-1}$, C–H stretching at 2,920 and 2,850 $cm^{-1}$, and symmetric (or CH3) and asymmetric (or CH2) bending of C–H at 1,370 and 1,460 $cm^{-1}$ respectively were observed. Three strong C=O peaks also appeared at 1,030, 1,210 and 1,740 $cm^{-1}$. Relative to CA, unique absorption peak of mineral oil was at 720 $cm^{-1}$ due to the out of plane CH bond. The same absorption band appeared in CA-mineral oil and CA hollow suggesting the presence of the mineral oil residual after oil core removal. The content of the carbonyl group was the same in CA solid, CA mineral oil and CA hollow. The increased peaks in carbonyl group peaks in CA-mineral oil could be attributed to the presence of similar bonds in CA, octane, and residual mineral oil. The peak at 1,370 $cm^{-1}$ was higher than at 1,460 $cm^{-1}$ in CA solid, CA mineral oil and CA hollow, unlike the mineral oil alone. The FTIR of the four CA configurations CA solid, CA–PCL, CA mineral oil, and CA hollow present characteristic

functional groups of CA, PCL and mineral oil, with an indication of the presence of residual of mineral oil and octane in CA hollow configuration. However, evaluating the CA mineral oil fibers cross section at different sample locations after octane treatment showed no presence of mineral oil. In applications that require full removal of mineral oil further warming the octane, solution could help complete remove of mineral oil.

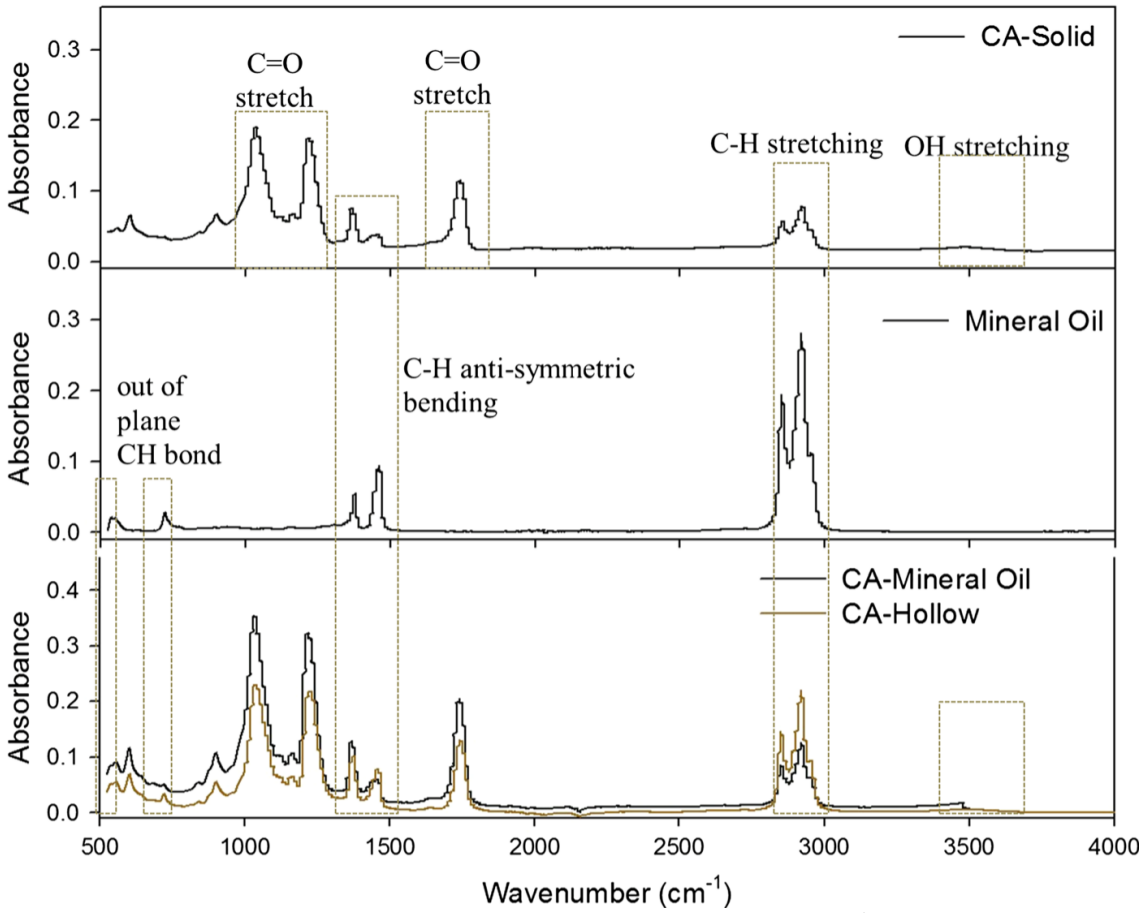


**Figure 3.5** FTIR spectra at various frequencies with a resolution of 4 $cm^{-1}$.

### 3.3.7 Comparison of solution viscosity

The viscosity of the utilized solutions was evaluated to understand the observed differences in core and sheath viscosities. In general, CA and gelatin solutions (**Figure 3.6**) had similar trends although the shear rate had different effect on viscosity at low and high rates. Mineral oil, chitosan

solution, and 10 kDa 9 % PCL solutions had a lower viscosity than CA solution. Also, the effect of shear rate was different at high and low shear rates; viscosity of 20 % solution of 10 kDa PCL was slightly higher than CA but then drastically decreased with shear rate. The viscosity of 43 kDa PCL solution was much higher than all the other solutions, but also showed a drastic decrease in viscosity with increasing shear rate. The viscosity of 80 kDa PCL solution could not be measured due to instrument error, attributed to very high viscosity. We then calculated the viscosities of core–sheath fluids (**Table 3.3**) at flow rate utilized during electrospinning with the assumption of completely developed laminar flow [195]. The viscosity of CA at 0.45 $s^{-1}$ was 46 Pa s, which was much higher than solutions that showed core–sheath formation. This suggests that when the ratio of core viscosity to sheath viscosity is less than one, coaxial stable jet can be formed under the application of a suitable voltage. In addition, both the solutions need to be compatible without precipitation which requires miscibility of polymeric components. The lower limit for solution viscosity is set by polymer characteristics such as MW, and functional groups rather than viscosity characteristics.

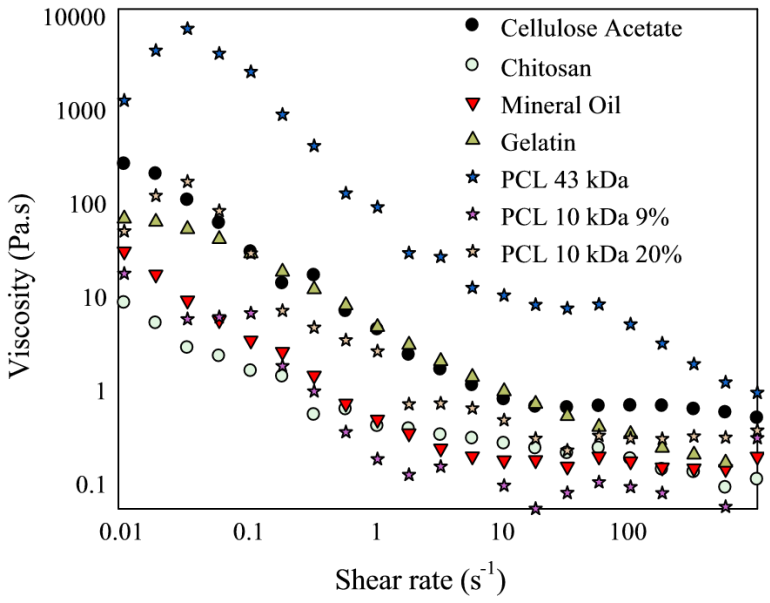


**Figure 3.6** Viscosity profile of CA, mineral oil, chitosan, gelatin and PCL (43 and 10 kDa).

### 3.3.8 Tensile behavior

The tensile strength of the fibers was evaluated in dry and hydrated conditions. Load–extension curves (**Figure 3.7a**) showed that the introduction of hollow core reduced the load-carrying capacity significantly relative to solid CA fibers. Break point and the slope of the line (i.e., stiffness coefficient) in the linear region were determined (**Figure 3.7b**). Large standard deviations were observed which could be attributed to changes in size, density, and orientation of fibers between samples. Both break load and the stiffness were reduced in hollow CA fibers relative to solid CA fibers in a dry condition, probably due to the increased fiber size with decreased polymer content per unit area. This was further confirmed by the load–extension curves (**Figure 3.7a**) of 10 kDa 9 % PCL core fibers which had fiber sizes similar to that of solid CA fibers; initial load-extension of CA–10 kDa PCL (9 %) was similar to that of solid CA fibers. Interestingly, 9 % 10 kDa PCL had more load carrying capacity and stiffness relative to 20 % 10 kDa PCL. This could be due to the fact that CA is much stronger than PCL in dry state while PCL has better elongation characteristics [190] than CA; the 9 % 10 kDa PCL was more like solid CA fibers due to reduced amount of PCL. However, CA–20 % 10 kDa PCL showed better stretching compared to CA solid, and CA–9 % 10 kDa, attributed to PCL. Also, 43 kDa PCL core fibers had similar initial load-extension curve to that of CA solid. When CA–80 kDa PCL fibers were analyzed, some sections within the same sample showed load–extension behavior of CA solid fibers, while others are showing trends similar to CA–43 kDa PCL fibers, indicating the separation of two components. Obtained results showed that CA fibers with loaded PCL (10 kDa) core have better elastic elongation compared with the CA solid and hollow. Since CA is used in hydrated conditions in most applications including water filtration, tissue regeneration, and textiles. We evaluated the formed core– sheath fibers in hydrated condition (**Figure 3.7c**). CA-solid fibers showed a significant reduction in the load carrying capacity, break point, and stiffness (**Figure 3.7d**) relative to dry condition. This is expected based on the weak mechanical properties of CA in hydrated conditions relative to dry conditions. Further, CA-hollow fibers were very fragile and could not be successfully mounted on to the equipment in

hydrated conditions (data not shown). CA–10 kDa (9 %) PCL fibers also showed similar behavior to solid CA fibers suggesting a little contribution from the core 10 kDa PCL. However, significant improvements in the break load were observed in the CA–PCL 43 kDa fibers, relative to the CA solid suggesting that the presence of PCL is helping improve the overall CA fiber strength. Nevertheless, CA–PCL fibers with 43 kDa as the core showed marginal elongation relative to dry conditions. No reduction also suggests the uniform distribution of the core in the entire sample. This also suggests the appropriate molecular weight of PCL allowing sheath solution CA to drag and encapsulate the core liquid PCL allowing more control of hydrophobic core polymer (PCL) in CA–PCL fibers. Thus, much of the strength is attributed to the hydrophobic PCL core. This could potentially help in the usage of CA in applications under hydrated conditions.

**Table 3.3** Viscosity and shear rate values of core and shell electrospinning solutions.

| Solution | Shear rate at needle tip (1/s) | Viscosity (Pa s) |
|---|---|---|
| CA | 0.45 | 46 |
| CA | 4.23 | 1.42 |
| Mineral oil | 4.23 | 0.5 |
| Chitosan | 4.23 | 0.66 |
| Gelatin | 4.23 | 4.5 |
| PCL 10 kDa-9 % | 4.23 | 0.45 |
| PCL 10 kDa-20 % | 4.23 | 8 |
| PCL 43 kDa-20 % | 4.23 | 10.2 |

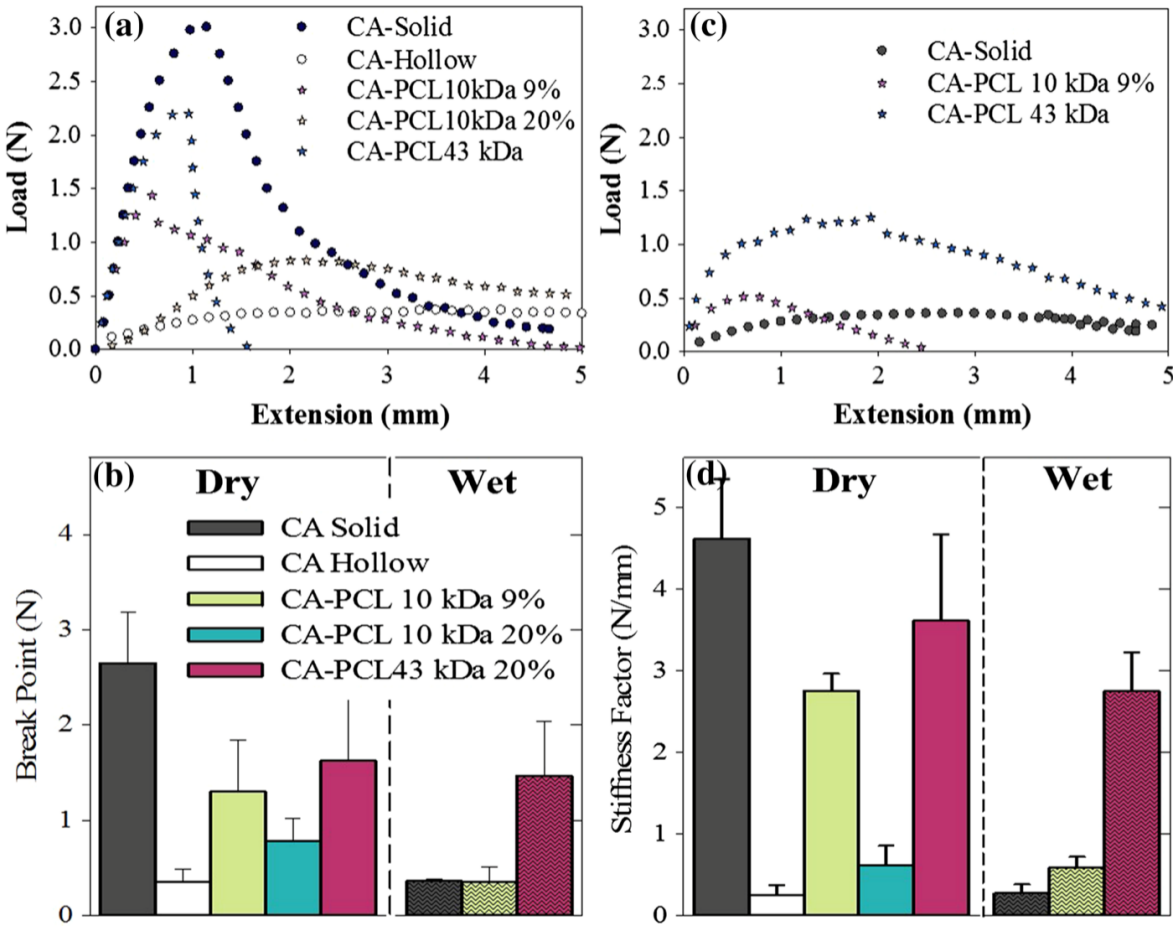


**Figure 3.7** Effect of tensile load on various core–shell CA fibers. a) Representative tensile strength-extension curves in a dry condition, b) Break strength, c) Representative tensile strength-extension curves in hydrated condition, d) Stiffness calculated from the linear region. Each bar in (b) and (d) is an average of at least three pooled samples from different experiments and error bars correspond to standard deviations. Patterned bars correspond to the hydrated conditions.

### 3.3.9 Cell viability and Spreading

The activity of HUVEC-2 cells was evaluated to understand the utility of CA–PCL 43 kDa core shell fibers. Since fiber size influences cellular activity [175], we tested the effect of cellular activity using CA-hollow fibers and CA–PCL 43 kDa fibers which showed similar fiber sizes.

First, we tested the viability after one day of culture using an approach described previously [191]. We have shown that cell viability can be accurately assessed by pre-staining the cells with CFDA-SE, without the concerns of non-specific adhesion of fluorochromes to matrix elements. When the cytoplasmic content obtained from freeze thaw cycle (**Figure 3.8a**) was analyzed, no differences were observed between the tissue culture plastic surfaces (TCPS) to those on electrospun surfaces. In addition, the supernatants collected after 1 day showed no significant difference between all the surfaces. This suggested that cell behavior was identical in all substrates and was comparable to TCPS. Also, the new formulations are not toxic, as the loss of cells due to death was similar in all conditions. Then we evaluated the morphology of cells using scanning electron microscope. These results (**Figure 3.8b, c**) revealed that the cells on both hollow CA fibers and CA–PCL fibers attached to the fibers. They were entangled throughout the matrix. The cell features in different surfaces demonstrate no significant difference regarding the cell morphology and spreading. This desirable feature is indicative of a good cell attachment, implying the cytocompatibility of the electrospun membranes. Although, PCL has good mechanical strength, however, shows poor cell adhesion. Since both types of CA fibers showed good cell adhesion and proliferation properties, no differences are observed between the CA-hollow and CA– PCL with low amount of serum, this suggests that the PCL is completely encapsulated in the CA. However, we need to understand the effect of these on cell function**,** long-term cell viability (Hong and Madihally 2010), and ability to regenerate tissues.

### 3.4 Summary

In this study, we showed that electrospun CA hollow and core–sheath fibers can be prepared by coaxial electrospinning. PCL molecular weight of 10, 43, and 80 kDa were evaluated for their ability to electrospun core–sheath structure. The configuration of 43 kDa PCL solution showed

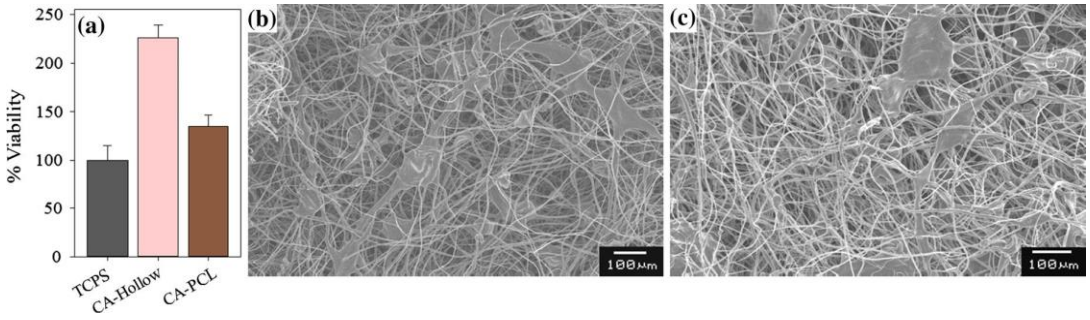


**Figure 3.8** Endothelial cell interaction on core–shell fibers. a) Cell viability as measured by CFDA-SE staining. Each bar corresponds to average (n = 4 from different experiments), and error bars correspond to standard deviations. b) Micrograph showing the distribution of cells on CA hollow fibers. c) Micrograph showing the distribution of cells on CA–43 kDa PCL fibers.

better jet stability. Gelatin and chitosan could be used as a core fluid, but the operation range is limited, and their electrospinning solutions perspiration requires an expensive solvent. In hydrated conditions, CA–PCL fibers showed significant improvement in break stress and strain relative to solid or hollow CA fibers. DSC and FTIR analysis confirmed the presence of CA and PCL. Incubation with human umbilical vein endothelial cells showed attachment and spreading, suggesting no toxicity. Anticipated impact that inherent to the formed CA hollow and CA core–sheath fibers include: (1) high surface area per volume ratio to enhance cell attachment, larger fiber diameter relatively means of increasing the porosity and pore size to attain desired mass transport; (2) distinctive mechanical properties (high strength to weight characteristics) for tissue that requires greater stiffness and strength; (3) hydrophilic surface properties (CA) enhanced with hydrophobic core polymer (PCL) for better balance and strength in hydrate condition.

# CHAPTER 4

# INFLUENCE OF SOLVENT CHARACTERISTICS IN TRIAXIAL ELECTROSPUN FIBER FORMATION

## 4.1 Introduction

Electrospinning is a versatile polymer processing technique in which sub-micron polymer particles, fibers or interconnected porous fiber meshes can be produced using an electrostatically driven jet of polymer solution [196]. A high voltage is applied to polymer solution using two electrodes: one connected to the nozzle ejecting the polymer solution and the other connected to a conductive collector. When the charge build-up at the nozzle (near 15 kV), droplet deforms into a conical structure referred to as Taylor cone. Increasing the electrical force above the surface tension of the polymer solution breaks the Taylor cone and polymer jet ejects from the apex of the Taylor cone. This jet deviates in a course of violent whipping from bending instabilities brought about by repulsive charges existing along the jet length. The jet is stretched where the solvent evaporates, resulting in the thinning of the fiber [197]. Important properties inherent to electrospun fibers include high surface area per volume ratio, porous structure, highly ordered structure, high rate of adsorption and high strength to weight characteristics [198, 199]. However, there is a growing interest in modifying the solid fibers to impart necessary morphological, biological, and mechanical properties [149]. For example, the fabrication of co-continuous fibers of cellulose acetate (CA) blended polyurethane has improved the mechanical properties of CA [200]. While the electrospinning setup itself is relatively uncomplicated, the variables concerned in producing a nano

and micro sized fiber with relative uniformity are numerous [175]. Process parameters such as applied voltage could significantly affect the shape and size of the droplet at the tip of spinneret from which the jet is generated. The optimum range of applied voltage varies with the type of polymer solution from 5 to 25 kV. Solution flow rate influences the size, porosity and geometry of fibers. Increasing the flow rate to a high value causes wet and incomplete drying because of decreased time for solvent evaporation. A minimum flow rate is required to replace the lost of the polymer solution from the jet being ejected from the Taylor cone at the tip of the spinneret. Changes in polymer concentration affect both viscosity and surface tension of the solution, which determines solution electro-spinnability. Solution viscosity controls the polymer chain entanglement when polymer jet travels from the spinneret to collector. Exceeding the solution viscosity limit could cause blocking and disruption of solution flow. In the past two decades, many changes have been made in the basic principles of electrospinning process [201]. New spinnerets consisting of coaxial capillaries allow fiber generation with improved control over fiber properties to control the release kinetics of embedded drugs [202-205]. Fibers with unique structure and functions can be formed such as (i) altered surface (hydrophobic and hydrophilic), and (ii) multilayered structure. These structures are useful for delivering bactericidal chemicals to abate bacterial fouling in filtration applications. Also, natural and synthetic heterogeneous structure can be prepared with desirable properties of synthetic polymer function providing mechanical properties while the natural polymer is promoting cellular attachment and growth in tissue engineering [206]. Due to these unique properties, electrospun coaxial and or multilayered structures have been widely studied [207-209]. However, there is limited understanding of governing conditions necessary for electrospun triaxial fibers.

Many have evaluated the effects of type of solvent and solvent content (phase separation and fast solvent evaporation) on the solid fiber diameter, shape, surface morphology, mechanical properties and crystallinity [210]. These studies are extended to some composite fibers and or blended polymers in single-phase process. However, the effect of solvent volatility and relative polymer

molecular weights on uniform encapsulation of the core polymer in coaxial and or triaxial electrospinning process is not well understood. Selection of solvents with an appropriate boiling point for each layer in coaxial and or triaxial electrospinning is critical as rapid solvent evaporation from the jet surfaces could cause instabilities in fiber formation. In this study, we explored the effect of type of solvent, solvent volatilities, and polymer MW on uniform triaxial fiber formation. We utilized combinations of polycaprolactone (PCL), cellulose acetate (CA), polyvinyl alcohol (PVA), and mineral oil. PCL is non-toxic, biocompatible and biodegradable synthetic polyester and has gained much attention due to its low melting point (60 ℃) elastomeric properties. It has been studied to form many medical devices or scaffolds for tissue regeneration of in vivo and in-vitro cell culture using serum added media [211]. To alter the hydrophobic characteristics of the surface, PCL has been blended with many natural polymers and also has been extensively evaluated in core-sheath structures [212]. CA fibers have good thermal stability, biodegradability, and chemical resistance [213]. CA fibers are proposed for tissue engineering, and drug delivery [133, 214]. PVA is a biodegradable, and biocompatible polymer explored in various biomedical applications [215]. Mineral oil was used as an inner core layer due to ease of spinning with CA solution [216], and selective extraction with octane to obtain the hollow structure. Different solvent mixtures were analyzed based on their boiling points, estimated using a process simulator. Solution viscosities were evaluated at various shear rates. Obtained fibers were analyzed by scanning electron microscopy, and fiber sizes were characterized using digital micrographs. Differential scanning calorimetry (DSC) and FTIR were performed to determine components in the triaxial fibers. Tensile tests (both wet and dry) were assessed to determine the use of different layers. 24-h viability of human umbilical vein endothelial cells was evaluated. These results show that triaxial fibers can be formed with different features such as hydrophobicity, hydrophobicity, and mechanical strength. Upon formation of the fiber, the outer sheath can be extracted, exposing the desired inner sheath allowing fibers of polymers that cannot be electrospun on their own.

Understanding the mechanism of coaxial and triaxial jet formation will assist in the fabrication of uniform multi-functional fibers with controlled features.

## 4.2. Experimental

### 4.2.1. Materials

Cellulose acetate (CA) $M_n$ = 30,000 GPC, octane 99%, acetone 99.9%, 1–2 dioxin, Polycaprolactones (PCL 80 kDa, $M_n$ = 80,000), polyvinyl alcohol (PVA 100 kDa, $M_n$ = 80,000–120,000 and PVA 30 kDa, $M_n$ = 30,000) 99% hydrolyzed were purchased from Sigma–Aldrich (St. Louis, MO). Mineral oil 99.9% was from Rexall (Goodlettsville, TN). Polycaprolactone (PCL 45 kDa, $M_w$ = 43,000– 50,000) was obtained from Polysciences (Warrington, PA). All other chemicals were used as received without further purification.

All polymer solutions were freshly prepared by stirring for 24 h. CA was dissolved at 14 wt% at room temperature using a mixture of acetone and dioxin (2:1 v/v) (**Table 4.1**). PCL spinning solution at 20% mass concentration was prepared at room temperature in a mixture of chloroform and methanol (9:1 v/v) or other solvent mixtures. PVA was dissolved in distilled water under heating at 80℃, and after the solution was cooled, other solvents were added. The polymer solutions were then transferred to a 10 mL plastic syringe fitted with 10 cm long plastic tubing and connected to the electrospinning setup.

### 4.2.2. Electrospinning setup

The electrospinning setup (**Figure 4.1**) consisted of two syringe pumps (74,900 series, Cole-Parmer Instrument Company, Vernon Hills, IL), 10 mL syringe (Luer-Lok Tip; Becton Dickinson and Company, Franklin Lakes, NJ), custom-built spinneret, high voltage power supply (ES30P-5W/DAM, Gamma high Voltage Research, Ormond Beach, FL), earth grounding, and a collection mandrel. The triaxial spinneret consisted of three concentric needles; inner core needle had an

inner diameter of 0.58 mm, the intermediate needle had an inner diameter of 2.1 mm, and the outer sheath needle had an inner diameter of 3 mm.

The spinning solutions were loaded into a 10 mL syringe via 30 cm long PTFE tubing (Sigma-Aldrich, St. Louis, MO) connecting the syringe to the spinneret. Solutions were pumped to the spinneret at controlled feed rate. The core fluid (mineral oil) was pumped to the core spinneret at a varied flow rate ranging from 0.01 to 1 mL/h. The intermediate and outer sheath solutions were pumped to the spinneret at flow rates ranging from 0.1 to 2 mL/h. The spinning distance (distance from the spinneret to ground collector) was set at 8 cm. A 17 kV voltage was applied between the needle and the conductive collector.

**Table 4.1** Summary of conditions and polymers evaluated.

| **Outer sheath** | **Intermediate** | **Inner FR** | **Outer FR** | **Observation** |
|---|---|---|---|---|
| 14%CA (dio/ace) 1:2 | 20%PCL (chl/me) 9:1 | 0.01–1 | 0.1–2 | No fiber formation |
| 14%CA (dio/ace) 1:2 | 20% PCL (acc/chl/ me) 4:5.4:6 | 0.5 | 2 | Uniform fibers |
| 20%PCL (chl/me) 9:1 | 14%CA (dio/acc) 1:2 | 0.5 | 2 | Uniform fibers |
| 20%PCL (chl/me) 9:1 | 10%PVA (water) | 0.1 | 3 | Uniform fibers |
| 10% PVA (water) | 20%PCL (acc/chl/me) 4:5.4:6 | 0.01–2 | 0.1–3 | Dripping |
| 14%CA (dio/acc) 1:2 | 10%PVA (water) | 0.01–1 | 0.01–2 | Dripping |

All polymer compositions are based on wt%. Chloroform (chl), Methanol (me), Dioxane (dio), Acetic acid (acc), Acetone (ace), Dimethylformamide (Dime), Distill water (water), FR = Flow rate.

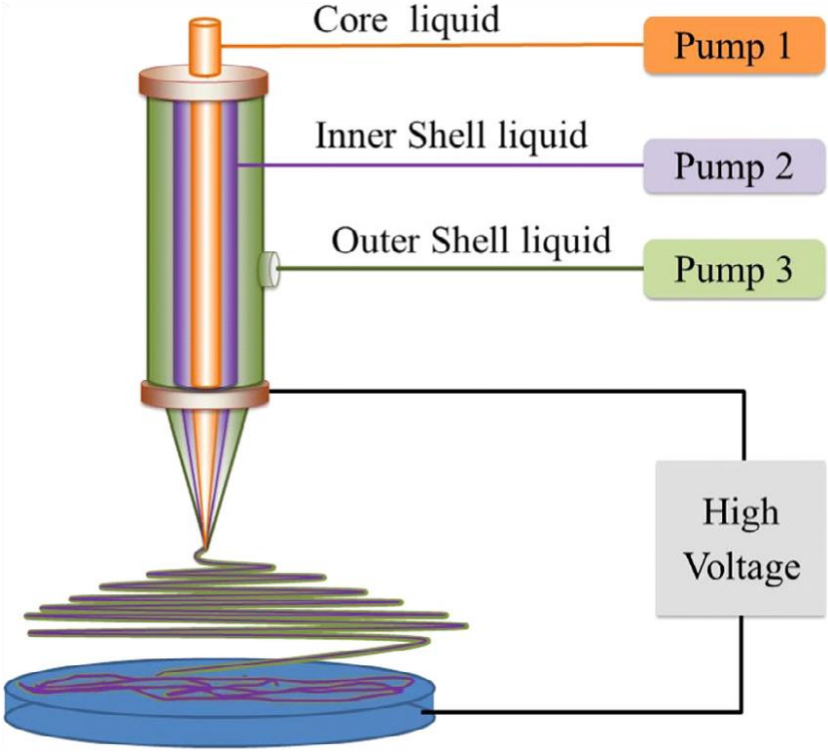


**Figure 4.1** Schematic of tri-axial electrospinning setup.

All experiments were conducted at 25 C and humidity was at 55% relative humidity, except while testing the effect of humidity. During that time, humidity was completely saturated. The ranges of operating parameters evaluated in this study are summarized in **Table 4.2.** Mineral oil (inner core) was selectivity removed by immersing fibers in octane for 24 h, as described in a previous publication [216]. Obtained fibers were then air dried at room temperature.

### 4.2.3. Characterization

Samples were analyzed by JOEL 6360 (Jeol USA Inc., Peabody, MA) scanning electron microscope similar to our previous publication [14], with minor modifications. In brief, fibers were first frozen in liquid nitrogen, 2 mm × 2 mm pieces were cut, and attached to an aluminum stub using a double-sided conductive tape and sputter-coated with gold for 1 min. Digital micrographs were collected at 15 kV accelerating voltage. Fiber sizes and shapes were quantified using digital

micrographs and image analysis software Sigma Scan Pro (SPSS Science, Chicago, IL). Three images of each sample were analyzed; nearly 30 fibers were randomly quantified per condition. Obtained values were then used to determine the fiber size distribution, average fiber size, and standard deviation.

### 4.2.4. Solvents properties and boiling point determinations

Solvent mixture boiling points were determined using CHEMCAD (Chemstations, Inc. Houston, TX), which has built-in access to DIPPER thermophysical database. Compounds of interest were selected from the component list. Maximum operating temperature (T) and pressure (P) were set to 25 C and 1 atm. While accessing liquid (X) and vapor (Y) composition of mixtures, Non-Random Two-liquid (NRTL) thermodynamic model was selected due to its applicability for polar liquid mixtures at low pressures. TPXY plot was selected at constant pressure and used to generate T-XY diagram needed for determining the boiling points. Since XY plots were mass fraction based but the used solvent mixtures were volume based, volume fractions were converted to mass fractions, using density and molecular weight of each component. From the plot, boiling point of the mixture was estimated at any given mass fraction (**Table 4.3**).

**Table 4.2**Viscosity and shear rate values of electrospinning solutions.

| **Fluid** | | **Shear rate in the needle (s1)** | **Viscosity (Pa s)** | **Solvent mixtures** |
|---|---|---|---|---|
| CA | Sheath | 0.45 | 46 | Diaxane:acetone |
| | Core | 4.23 | 3.5 | |
| 20% PCL 45 kDa | Core | 4.23 | 55 | Chloroform: methanol |
| | Sheath | 0.45 | 650 | |
| 10% PVA 80 kDa | Core | 4.23 | 0.3 | DI water |
| 14% PVA 30 kDa | Core | 4.23 | 0.5 | DI water |
| Mineral oil (0.1 mL/h) | Core | 4.23 | 0.5 | – |

**Table 4.3** Boiling point of solvent mixtures utilized in the study.

| Solvent mixtures | Volume ratio | Mass fraction | BP (℃) |
|---|---|---|---|
| Acetone/dioxin | 1:2 | 0.4/0.6 | 65.8 |
| Acetic acid/chloroform | 2:3 | 0.32/0.68 | 69 |
| Chloroform/methanol | 9:1 | 0.94/0.06 | 54.6 |
| Water/methanol | 9:1 | 0.92/0.08 | 93 |
| Water/dimethylformamide | 9:1 | 0.91/0.09 | 102 |

### 4.2.5. Viscosity measurement

Solution viscosities at various shear rates were measured in the range of 0.0001–1000 1/s at room temperature using a C-VOR Viscometer (Bohlin Instruments Ltd., Cirencester, UK). Solutions were loaded into viscometer fitted with a standard-size recessed end concentric cylinders, 15 mm stator outer diameter, 14 mm rotor inner diameter and 0.7 mm gap distance.

### 4.2.6. Differential scanning calorimetry

Thermal properties were characterized using a Q2000 Differential scanning calorimeter (TA Instruments New Castle, DE) equipped with a refrigerated cooling system (RCS) 90. Five to 10 mg of fibers were sealed in aluminum pans. The experiments were run between 25 and 250 ℃ range in a nitrogen atmosphere at 10 ℃/min ramp rate.

### 4.2.7. Fourier transform infrared spectroscopy

Samples were analyzed by a Thermo-Nicolet 6700 FTIR spectrometer equipped with a DTGS detector under the transmission mode. Dry samples were loaded, and spectral scans were obtained at ambient conditions from 400 to 4000 $cm^{-1}$ at a resolution of 4 $cm^{-1}$ with an accumulation of 64 scans, using the associated software. Peaks were analyzed using Sigma Plot 12 software (SPSS Science, Chicago, IL).

### 4.2.8. Tensile analysis

Tensile testing was performed at room temperature in dry and hydrated conditions, similar to previous publications [217]. In brief, fibers from different configurations were collected on a flat plate for the same duration of time and peeled from the collector plate. Samples were cut into 8 cm long 1 cm wide rectangular strips and loaded into the tensile test machine (INSTRON 5542, Canton, MA) outfitted with a 100 N load cell. The specimens were fully immersed in water for 1 min before testing in a hydrated condition. Fibers were strained to break at a cross head of 10 mm/mm. Data collected using Merlin (INSTRON, Canton, MA) software was exported to MS Excel and analyzed for stiffness from the slope of tensile strength (N) vs. extension (%) in the linear region. The breakpoint was marked and measured on the load-extension curve. Experiments were repeated three times per fiber type and the average and standard deviations were calculated.

### 4.2.9. HUVEC cell culture

Human Umbilical Vein Endothelial Cells (HUVEC-2) derived from single donors was obtained from BD Biosciences (San Jose, CA). Medium 200 phenol red free (PRF), Low Serum Growth Supplement (LSGS containing 2% v/v fetal bovine serum, 1 µg/mL hydrocortisone, 10 ng/mL human epidermal growth factor, 3 ng/mL basic fibroblast growth factor, and 10 µg/mL heparin), trypsin/EDTA, trypsin neutralizer solution, and carboxyfluorescein diacetate succinimidyl ester (CFDA-SE) were obtained from Invitrogen Corp. (Carlsbad, CA). HUVEC-2 was cultured in Medium 200PRF supplemented with LSGS following vendors' protocols. The cells were maintained in a 37 ℃, 5% $CO_2$/95% air, humidified cell culture incubator. The media was changed every two days. When confluent or for seeding on different structures, cells were detached with trypsin/EDTA, and then trypsin neutralization solution was added. Cells were centrifuged at 180 g for 7 min and dispersed in the growth medium. Viable cells were counted using Trypan blue dye exclusion assay.

Cells were then incubated in growth medium containing 2 μM CFDA-SE at 37 ℃ for 20 min followed by washing the excess stain with growth medium. Twenty-five thousand cells were seeded onto tissue culture plastic (TCP) surface, and 3D matrixes.

The specimens containing cells were washed in MSCGM, and cytoplasmic CFDA SE stain was extracted from live cells by three cycles of repeated freezing and thawing [191]. The CFDA-SE content in the spent medium and the cytoplasm was assessed by fluorescence intensity in Gemini XS spectrofluorometer (MDS Technologies, Santa Clara, CA) at the excitation and emission wavelengths of 485 nm and 525 nm, respectively.

After one day, the cell-containing samples were fixed in 3.7% formaldehyde for 30 min at room temperature. The samples were dried using ethanol followed by a brief vacuum drying and sputter coated with gold at 40 mA before observing under a scanning electron microscope to evaluate the distribution of fibers and cells, similar to the fibers described above.

### 4.3. Results and discussion

#### 4.3.1. Formation of PCL/CA/Hollow fibers

Previously we reported on the formation of coaxial CA and hollow fibers [216]. In this work we first validated the use of triaxial electrospinning spinneret in formation of structured triaxial fiber. In electrospinning, the first criterion is obtaining stable jet so we questioned whether PCL/CA/Hollow fiber can be formed by adding an outer stream of PCL. The outer stream was PCL dissolved in chloroform and methanol. The intermediate solution was CA in a mixture of acetone and dioxin, and mineral oil was loaded in the core. Water-soluble polyvinyl pyrrolidone could also be used instead of mineral oil as the core to obtain hollow fibers of CA [218]. Visual observation of the jet behavior and Taylor cone formation showed no solvent–solvent interaction or jet broke during triaxial electrospinning of PCL/CA/mineral oil. The Taylor cone appeared to be more stable along the length of the jet. Therefore, no adjustment was made for the volatility of

spinning solutions due to the appropriate boiling points of the compounds. Qualitative analysis of the formed fibers showed that 1.5 mL/h outer/intermediate flow rate and 0.2 mL/h core flow rate were the optimum. After extraction of core mineral oil, fibers were analyzed by scanning electron microscopy SEM (**Figure 4.2**). Micrographs showed the presence of all three concentric layers, suggesting success in forming PCL/CA/hollow triaxial fibers.

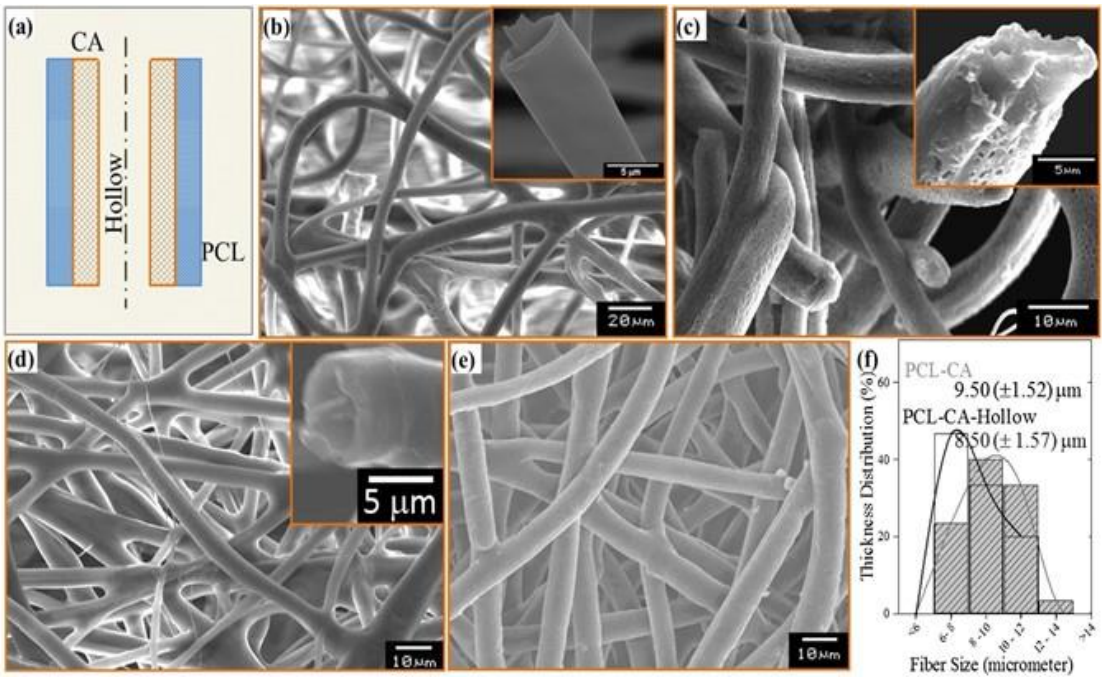


**Figure 4.2** Outer PCL configuration with inner CA. (a) Schematic showing the configuration. (b) 80 kDa PCL sheath with CA-hollow structure. (c) 80 kDa PCL sheath with the CA-hollow structure formed under high humidity. (d) 45 kDa PCL sheath with CA-hollow structure. (e) 45 kDa PCL sheath with CA core. Insets in these micrographs are a cross-sectional view of single fibers. (f) Fiber size distributions of core-sheath fibers.

Next, we examined the effect of 80 kDa and 45 kDa of PCL MW for triaxial fiber formation while keeping all other parameters constant including the CA molecular weight (30 kDa). Solution of 45 kDa PCL showed better electrospinning performance relative to 80 kDa PCL solution. Fibers

prepared from 45 kDa PCL were much more uniform than 80 kDa PCL. Increased MW could increase the strength of sheath solution, which influences the dragging and encapsulation mechanism of the intermediate and core components. The stable jet was obtained only when the intermediate polymer MW was smaller or equal to that of the outer sheath.

Since environmental parameters such as temperature and humidity affect the fiber characteristics [137], we questioned how humidity would affect formed triaxial fibers. Results showed that when relative humidity was above, 30% pores formed on the surface of the fiber, similar to other reports [219]. The presence of pores on the surface of fibers could contribute to increasing the surface area, which would be useful for drug delivery applications. We also quantified the fiber diameters of PCL/CA fibers with and without the addition of the core compound. Results showed that PCL/CA fiber had an average diameter of 9.50 (±1.52) μm (**Figure 4.2f**) while that of PCL/CA/Hollow fiber was smaller 8.50 (±1.57) μm.

However, the distributions of fiber sizes were similar suggesting that the addition of inner core may not change the overall fiber diameter at identical process and solution parameters. If different fiber sizes are required, then one has to change process parameters (including applied voltage, and nozzle-collector distance) and solution parameters (including polymer concentration, solution viscosity, and solution conductivity) have been extensively studied and shown to affect fiber size. For example, application of a lower voltage (15 kV) with a lower concentration of CA (8%wt/v) and increasing the collector plate distance (15 cm), hollow CA fibers with smaller diameters can be obtained [218].

### 4.3.2. Formation of CA/PCL/Hollow fibers

We questioned whether switching the polymer streams would also form triaxial structure. However, fibers did not form using a solvent mixture of chloroform and methanol for the intermediate PCL43 kDa solution due to the high volatility and low boiling point of the solvent

mixture, which limited the outer CA sheath solution wrapping ability. The jets behavior showed blocking and clogging at the tip of the spinneret, prohibiting the fibers formation (**Figure 4.3**). To confirm the reason better, we evaluated the boiling points of solvents mixture. These results showed (**Table 4.3**) that acetone–dioxin mixture has a boiling point of 65.8 ℃ while chloroform–methanol mixture has 54.6 ℃. Thus, the intermediate PCL component solvent mixture evaporated faster from the charged jet, which significantly weakened the outer sheath solution wrapping ability and the capability to maintain the triaxial jet. When the volatility of the intermediate solution is high, it will weaken the outer sheath encasing ability, which leads to poor electro-spinnability and wet fibers formation. The solvent molecules first evaporated from the charged jet surface and then mass diffusion takes place from the inside of the charged jets to the outer surface [220]. Because of the higher volatility of the intermediate PCL solvent, it was required to lower solvent boiling point by adding acetic acid. Which significantly strengthened the sheath jet stability allowing full control of CA polymer to encapsulate the intermediate PCL polymer. After removing the core mineral oil by immersing in octane, triaxial CA/PCL/Hollow layers were visible under SEM (**Figure 4.3d**). To confirm that PCL was uniformly distributed, we selectively stripped the outer CA by immersing in acetone (referred as 0/PCL/Hollow fibers). Micrographs showed (**Figure 4.3e**) 0/PCL/Hollow fibers slightly smaller than the CA/PCL/Hollow fibers. When fiber diameters were determined, results showed that CA/PCL/Hollow fibers had an average diameter of 11.6 (±3.92) µm (**Figure 4.3f**), relatively larger than 0/PCL/Hollow fibers. After removal of CA from the triaxial fibers, fibers had a thickness of 10.1(±2.29) µm, suggesting that the CA layer thickness is 0.75 µm.

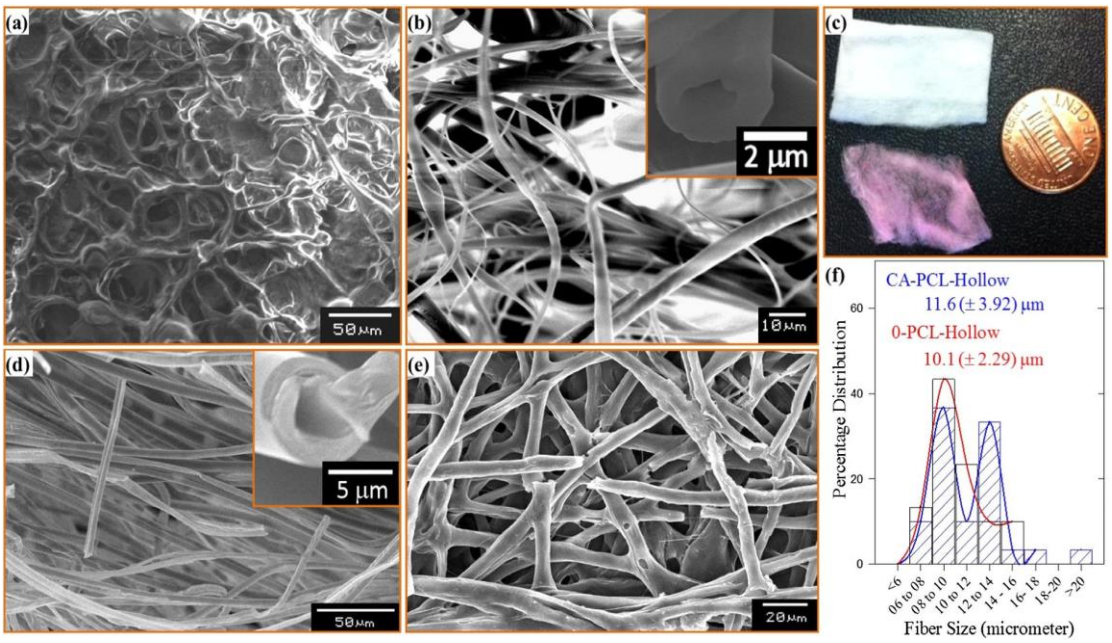


**Figure 4.3** Outer CA configuration with inner PCL. (a) Sample obtained by interchanging CA and 80 kDa PCL. (b) CA sheath with 80 kDa PCL hollow structure after modifying PCL solvent. Inset in this micrographs is a cross-sectional view of single fibers. (c) Photograph of formed fibers comparing the effect of solvent modification. (d) CA sheath with 45 kDa PCL hollow structure after modifying PCL solvent. Inset in this micrographs is a cross-sectional view of single fibers. (e) Fibrous structures remaining after selective removal of outer CA in acetone overnight. (f) Fiber size distributions of core-sheath fibers with 45 kDa PCL.

### 4.3.3. Formation of PCL/PVA/Hollow fibers

The intermediate solution (PVA) showed poor processability due to the low volatility and high boiling point of PVA solvent. However, other research groups have demonstrated the possibility of improving PVA spinnability by adding surfactants [221]. We did not try to improve electro-spinnability of PVA since it was the intermediate solution. However, the jet stability was governed by the sheath solution and the solution flow rate. All other configurations showed fiber formation at sheath solution flow rate of 1.5 mL/h except for PCL/PVA/mineral oil. When PCL solution flow

rate was at 1.5 mL/h bending instability increased, the jet broke to spray droplets, and splitting and electrospray were observed. We questioned whether this is due to high flow rate a large volume of solution is drawn from the spinneret, which caused the jet to electrospray without any sufficient stretching, and the residual solvent might bring the fibers to fuse together. To test this possibility, we lowered the PCL solutions flow rate to 0.5 mL/h so that the smaller amount of solvent will have more time for complete evaporation. At this flow rate spinning jet have had sufficient and slower time to dry and produce clean dry fibers. **Figure 4.4b** shows micrographs of formed structures of PCL/PVA/Hollow fibers. Quantification of micrographs for the fiber diameters showed that PCL/PVA/Hollow fibers had an average diameter of 7.16 (±1.59) µm (**Figure 4.4c**), relatively smaller compared to other configurations.

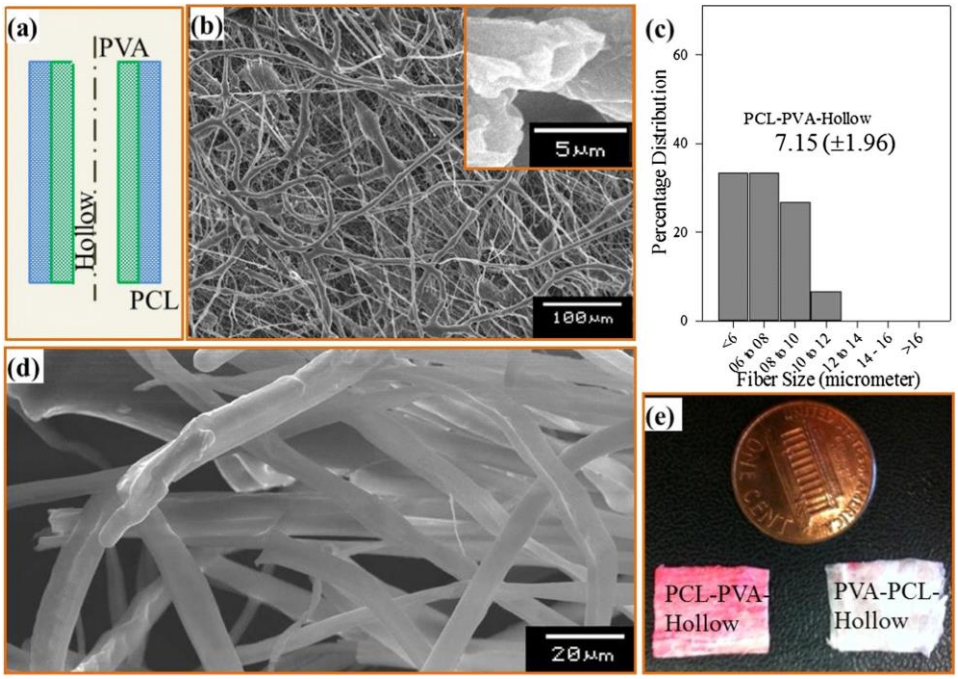


**Figure 4.4** Outer PCL configuration with inner PVA. (a) Schematic showing the PCL/PVA/Hollow configuration. (b) 80 kDa PCL Sheath 100 kDa PVA hollow structure. Inset is a micrograph showing single fibers. (c) Fiber size distributions of core-sheath fibers with 80 kDa PCL. (d) 45 kDa PCL sheath with PVA-hollow structure. (e) Photographs showing the fibers in different configurations.

### 4.3.4. PVA/PCL/Hollow and CA/PVA/Hollow fibers

When sheath solution of PCL was switched with an intermediate solution of PVA keeping all other electrospinning parameters constant, PVA solution showed poor electrospinning performance and difficulty in maintaining a stable triaxial jet. This could be due to the high evaporation rate and fast spinning rate of the intermediate PCL solution, which limited the outer PVA sheath solution wrapping ability to maintain the triaxial jet stability during the electrospinning process. We utilized acetic acid along with chloroform and methanol to dilute PCL solution for a possible reduction in solution volatility of PCL solvent. Although the jet visually appeared to be more stable over most of its length, poor electro-spinnability of PVA was an issue. Wet and fused PVA/PCL/Hollow fibers (**Figure 4.5f**) were obtained after the removal of core mineral oil.

No fibers formed from triaxial electrospinning of CA/PVA/mineral oil. The lack of spinnability and or poor spinning performance of CA sheath and intermediate PVA could be due to the incompatible solvent system of CA solution mixture to that of PVA owed to weaken in polymer jet or unsuitable molecular arrangement. Results showed that electrospinning of triaxial PVA is not possible due to the solvent miscibility. The addition of PVA solution to CA solutions (**Figure. 4.5d**) in a beaker resulted in spontaneous precipitation; same behavior was observed at the tip of the triaxial spinneret.

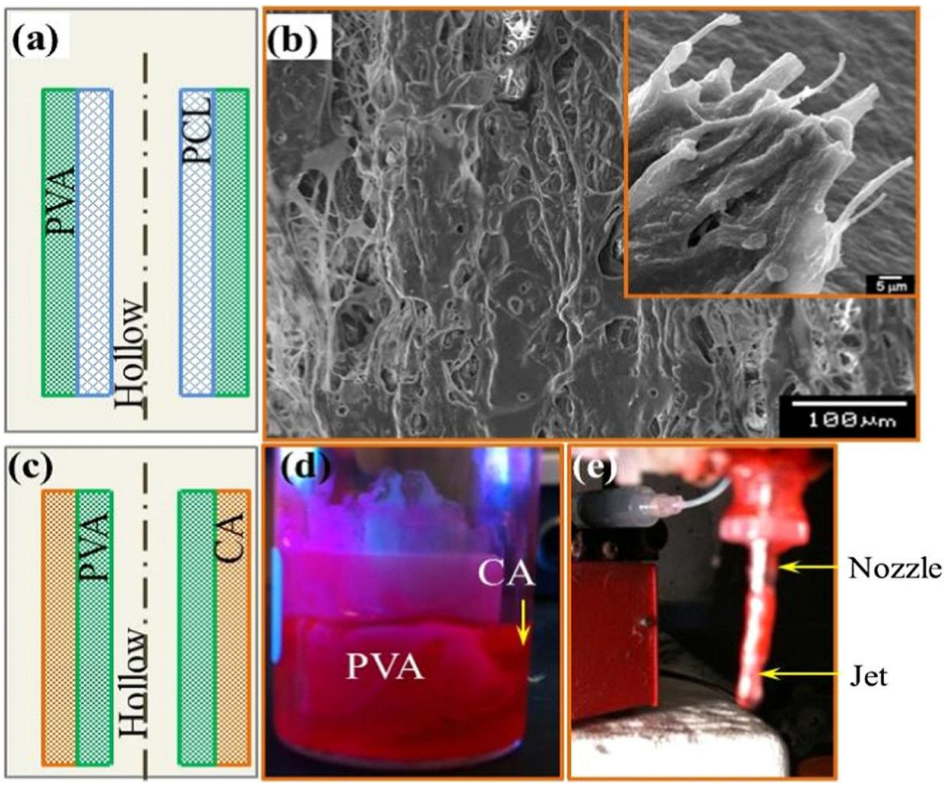


**Figure 4.5** PVA configurations with PCL and CA. (a) Schematic showing the PVA/PCL/Hollow configuration. (b) Micrograph of a structure formed using PVA-PCL Hollow fiber configuration. Inset is the high magnification showing merger of fibers. (c) Schematic showing CA/PVA/Hollow fiber configuration. (d) Precipitation with the interaction of two non-identical polymer molecules (CA/PVA) in CA solution. (e) Clogging issues at the tip of the spinneret.

### 4.3.5. DSC analysis

DSC analysis was performed to understand the presence of different components in the fabricated fibers. For CA/PCL/Hollow configuration, a strong at 60 ℃ was detected, which corresponds to the melting point of PCL. A weak peak was detected at 225 ℃, which corresponds to the melting process of CA located between 170℃ and 240 ℃ (**Figure 4.6**). The reduction in the percentages of CA (intermediate component) is due to the difference in mass flow friction between components. The total mass contribution from CA and PCL in the fibers were 40% and 60% respectively. The

increase in PCL mass percentage is due to the difference between MW and concentration compared to CA. Further investigations varying the flow rates of both the components would provide a better understanding of the interactions between PCL and CA. The Same behavior was observed for PCL/CA/Hollow configuration. Stripping of the outer CA in CA/PCL/Hollow configuration demonstrated similar strong melting peak of PCL at 65 ℃ and a tiny minimum peak of CA at 226 ℃ (**Figure 4.6**) confirming the distribution of intermediate PCL along the fiber.

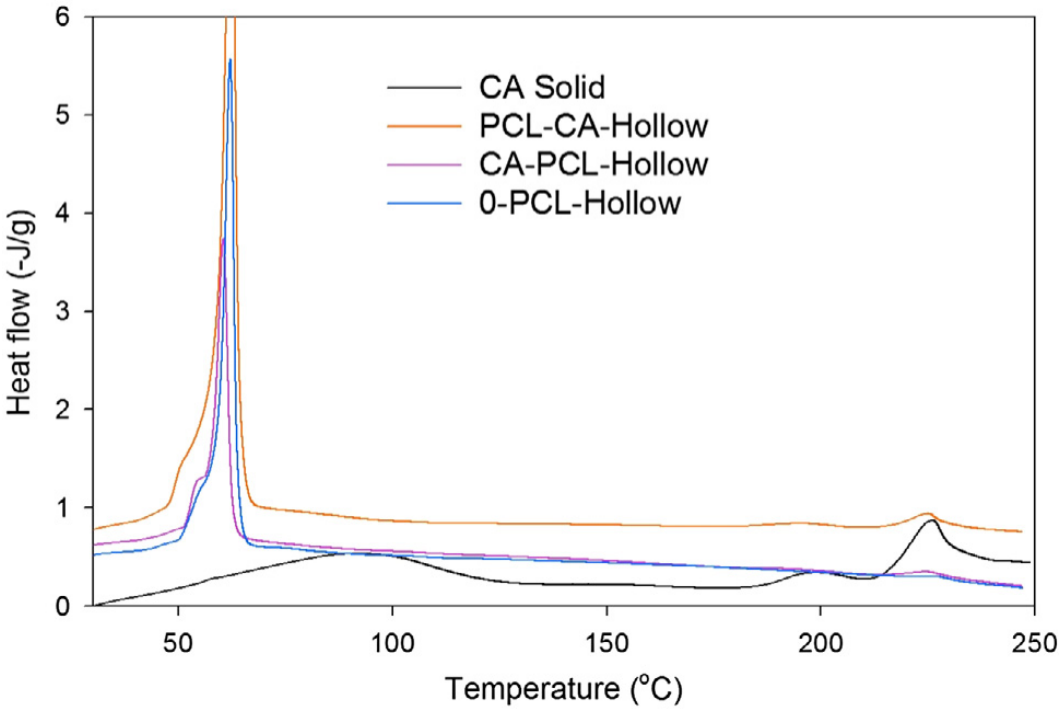


**Figure 4.6** DSC thermograms of various triaxial fibers.

### 4.3.6. FTIR analysis

FTIR spectrum results are shown in **Figure 4.7** where the absorption lines are identified. In CA/PCL/Hollow configuration, a characteristic stretching bands of PCL consist of asymmetric $CH_2$ stretching at 2890 $cm^{-1}$, symmetric $CH_2$ stretching at 2980 $cm^{-1}$ and carbonyl stretching at 1750 $cm^{-}$

$^{1}$ which all found identical to what reported by others [135]. Other stretching bands which attributed to CA are hydroxyl groups at 3500 $cm^{-1}$, C–H stretching at 2920 and 2850 $cm^{-1}$, and symmetric (or $CH_3$) and asymmetric (or $CH_2$) bending of CAH at 1370 $cm^{-1}$ and 1460 $cm^{-1}$ respectively were observed. Three strong C=O peaks also appeared at 1030, 1210 and 1740 $cm^{-1}$. Relative to CA, the unique absorption peak of mineral oil was at 720 $cm^{-1}$ due to the out of plane CH bond. The same absorption band appeared in CA-mineral oil and CA hollow suggesting the presence of the mineral oil remaining after core removal. The content of the carbonyl group, CH, and $CH_2$ groups was identical in all configurations except when the outer CA in CA/PCL/Hollow configuration was stripped out where it demonstrated minimum peaks of CA (**Figure 4.7**). The FTIR spectrometer of the three configurations, CA/PCL/Hollow, PCL/CA/Hollow and 0/PCL/Hollow present characteristic chemical functional groups of CA and PCL, with an indication of the presence of PCL and CA in all certified configurations. Further heat treatment could help in removing residual mineral oil from fabricated fibers.

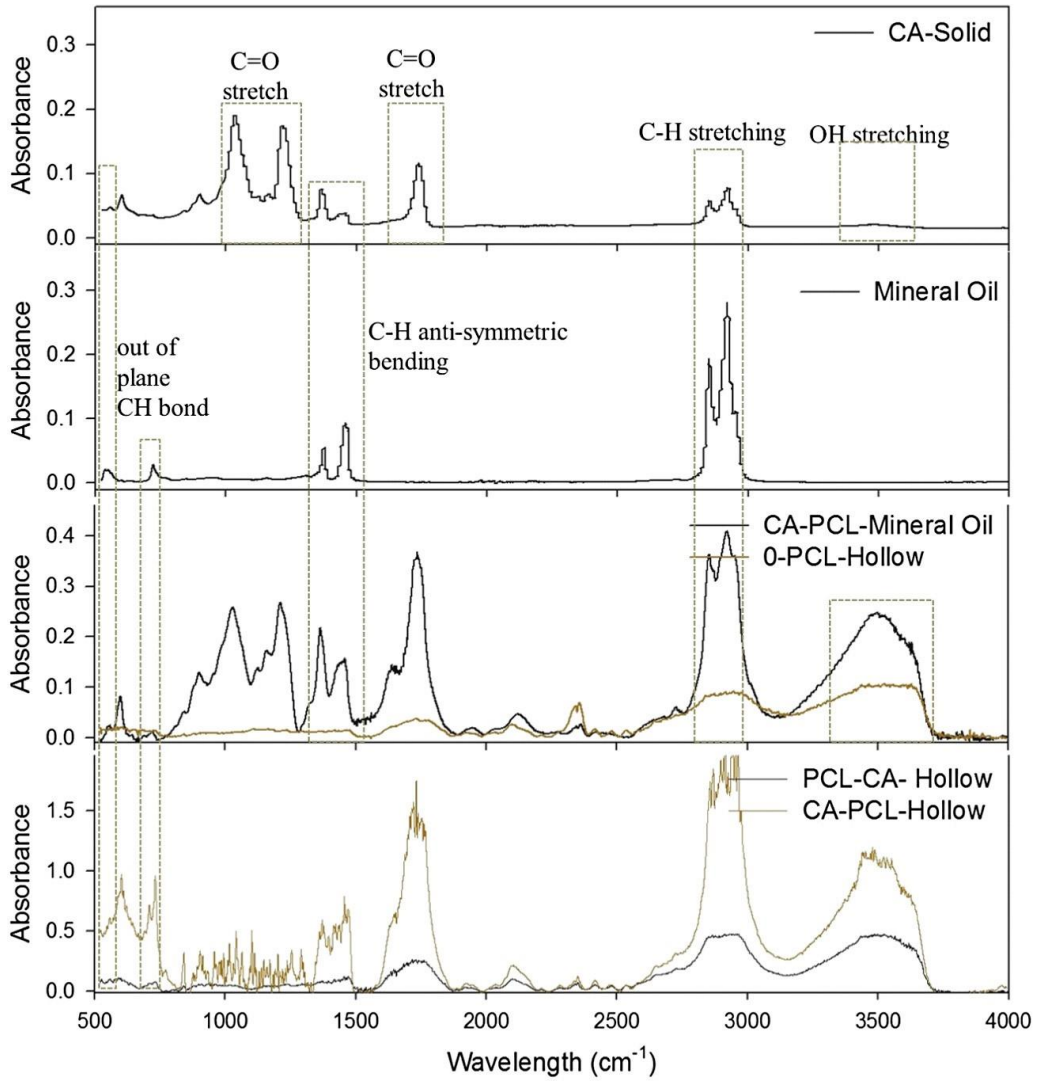


**Figure 4.7** FTIR spectra of CA fibers at various frequencies obtained at ambient conditions at a resolution of 4 $cm^{-1}$.

### 4.3.7. Tensile behavior

The tensile strength of the triaxial hollow structured fibers was evaluated in dry and hydrated condition, and load–extension curves (**Figure 4.8 a and b**) were plotted. The presence of PCL on top of the hollow CA fibers showed a significant increase in load-carrying capacity. Similarly, the presence of PCL layer underneath the CA layer increased the load carrying capacity but not to the

extent of PCL/CA/Hollow fibers. PCL/PVA/Hollow fibers had the least load carrying capacity. Extensions also followed a similar pattern.

Samples were tested in hydrated conditions to assess the contribution of hydrophilic CA. The difference in the strength of dry and wet fibers was in the range of 50–60%, probably due to the presence of PCL. Hence, formed triaxial fibers provide a way to improve the mechanical property of the hollow fibers while retaining the functionality of the outer sheath. Fibers with improved mechanical strength could help in using CA in applications under hydrated conditions. When 43 kDa PCL core and CA sheath fibers were evaluated in the dry condition, the sample showed load–extension curves behavior similar to that at the hydrated condition. The observed similarity could be attributed to the presence of the core hydrophobic PCL. In the third configuration of PCL/PVA/Hollow structure, no significant changes were observed in the load carrying capacity between dry and hydrated condition. This could be as a result of the full control of hydrophobic sheath material of PCL and low density of intermediate hydrophilic material PVA due to the weak interaction between PCL and PVA as a result of the poor electrospinning performance of PVA polymer during the process.

To better understand these characteristics, break point and the slope of the line (i.e., stiffness coefficient) in the linear region were determined for all three configurations. Both break load (**Figure 4.8c**) and the stiffness (**Figure 4.8d**) reduced significantly in dry PCL/CA/Hollow structure fibers relative to that at the hydrated condition. The wide deviations could be attributed random orientation of fibers in the measured samples. In hydrated condition, CA/PCL/Hollow structure fibers showed a reduction in a break point and stiffness relative to dry conditions. PCL/PVA/Hollow structure showed similar tensile behavior to dry condition and low break strength and stiffness compared with that of PCL/CA/Hollow. This could attribute to the reduction in fibers size and weak interaction between the sheath material PCL and intermediate material PVA.

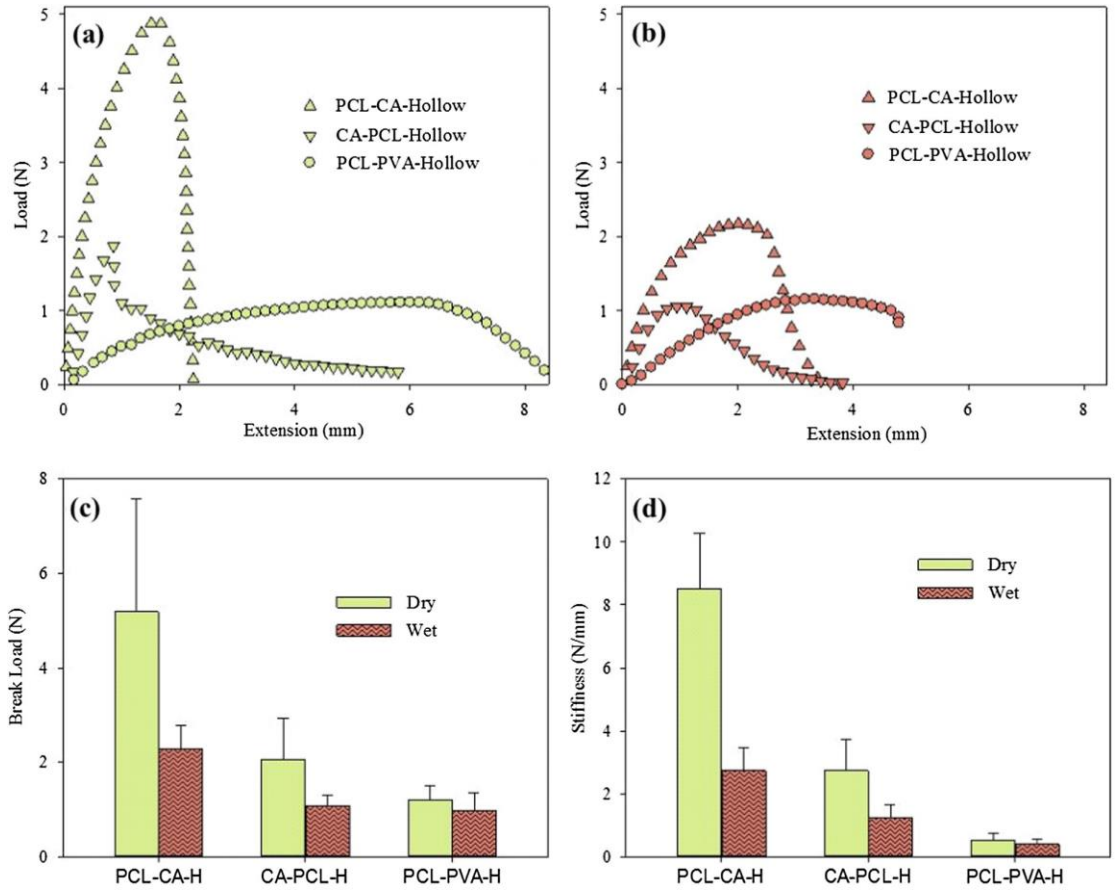


**Figure 4.8** Effect of tensile load on various triaxial fibers. (a) Representative tensile strength-extension curves in dry condition. (b) Representative tensile strength-extension curves in hydrated condition. (c) Break strength. (d) Stiffness calculated from the linear region. Each bar is an average of at least three pooled samples from different experiments and error bars correspond to standard deviations.

### 4.3.8. The role of viscosity of spinning solutions in predicting fiber formation

We measured the viscosity of the utilized solutions to understand the observed differences in core-sheath and triaxial fiber formation. In general, CA and PCL solutions (**Figure 4.9**) had similar trends although the shear rate effect on viscosity was slightly different at the low and high rates. Mineral oil and PVA solution were consistently lower than CA and PCL solutions at all shear rates. Also, the effect of shear rate was slightly different at high and low shear rates. Fourteen percent

solution of 30 kDa PVA exhibited a viscosity slightly higher than ten percent 80 kDa PVA and both drastically decreased with increase in shear rate. The viscosity of 45 kDa PCL solution was much higher than all the other solutions, which also showed a drastic decrease in viscosity with increasing shear rate. We then calculated the viscosities of utilized solutions using the solution flow rate from electrospinning process with the assumption of completely developed laminar flow [222], where the velocity profile ($V_r$ at any given location in the radial direction) is given by

$$V_r = V_{max}\left(1 - \left(\frac{r}{R}\right)^2\right) \tag{4.1}$$

Where $V_{max}$ is the maximum velocity of the moving plate (m/s), R is the tube radius (m), and r is the radius corresponding the location where local velocity is determined. Then shear rate ($\gamma$) is the derivative of $V_r$ with respective to the radius. Differentiating Eq. (4.1) with respect to the radius gives.

$$\gamma = \frac{dV_r}{dr} = V_{max}\frac{2r}{R^2} \tag{4.2}$$

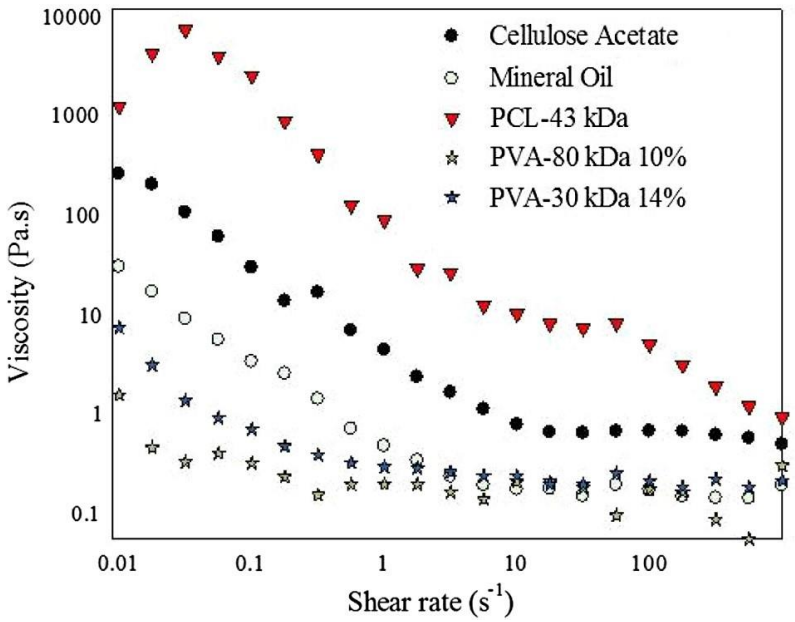


**Figure 4.9** Comparison of viscosity profiles for CA, mineral oil, PCL and PVA solutions used in the study.

To utilize Eq. (4.2), relating $V_{max}$ to the flow rate used in the spinning process is useful. For this purpose, average velocity $V_{average}$, the ratio of volumetric flow rate (Q) to the spinneret cross-sectional area ($\pi R^2$) was first related. Then, for laminar flow

$$V_{max} = 2 * V_{average} = 2 \times \frac{Q}{\pi R^2} \tag{4.3}$$

Substituting Eq. (4.3) for $V_{max}$, the maximum shear rate near the wall (r = R) is

$$\gamma = \frac{4Q}{\pi R^3} \tag{4.4}$$

Using Eq. (4.4), we calculated the shear rate and the corresponding viscosity for the electrospun conditions (**Table 4.3**). The viscosity of PCL at 0.45 $s^{-1}$ was 650 Pa s, which was nearly hundred times that of CA solution. Despite variations in the viscosity of 43 kDa PCL, CA and mineral oil, no significant difference was observed in the triaxial fibers. The obtained results suggest that fibers could be formed when the viscosity of the core is less than that of the sheath.

### 4.3.9. Cell viability and Spreading

The activity of endothelial cells was evaluated to understand the utility of the fabricated fibers in very low serum (2%) supplemented medium. Since fiber size significantly influences cellular activity [75]. First, we tested the effect of viability after one day of culture. Previously it has been shown that viability can be accurately assessed by pre-staining the cells with CFDA-SE [223]. Using this approach, cell viability was evaluated using CFDASE staining present in the cytoplasm of the cells after one-day culture.

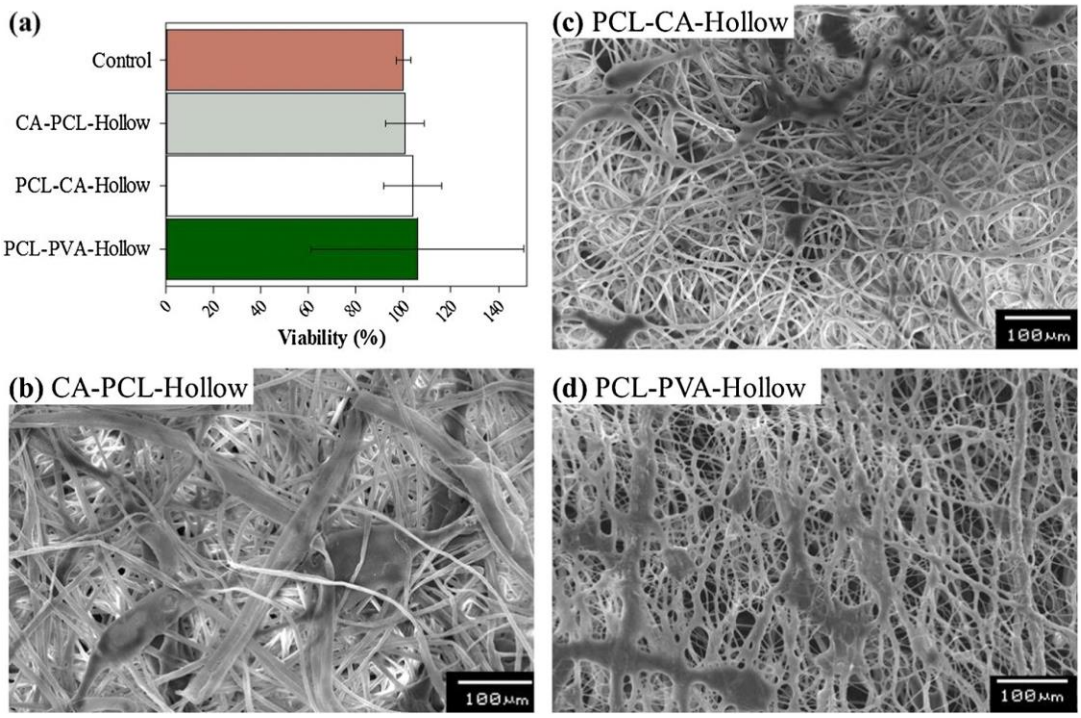


**Figure 4.10**. Endothelial cell interaction on core-sheath fibers. (a) Cell viability as measured by CFDA-SE staining. Each bar is an average of at least four pooled samples from different experiments and error bars correspond to standard deviations. (b) Micrograph showing the distribution of cells on CA hollow fibers. (c) Micrograph showing the distribution of cells on CA-45 kDa PCL fibers.

When the cytoplasmic content obtained from freeze thaw cycle (**Figure 4.10**) and analyzed, similar results were obtained suggesting that these substrates are not toxic. The supernatants collected after one day also showed no significant difference between all the surfaces. This suggested that cell attachment was identical in all substrates and was comparable to TCPS suggesting that the new formulations are not toxic to cells.

Then we evaluated the morphology of cells using scanning electron microscope. The showed (**Figure 4.10. b and c**) that the cells were attached to the fibers and entangled by them throughout the matrix. In some locations, cells showed numerous lamellipodia and filopodia with anchorage points to the fibers. The cell features on the different surfaces demonstrated no significant differences in morphology and spreading. This desirable feature is indicative of a good cell attachment, implying the cytocompatibility of the implants, as realized by the above quantitative analysis. Nevertheless, we need to understand the effect of these configurations on long-term viability cell growth and tissue regeneration [14].

### 4.4. Summary

Triaxial spinneret was successfully implemented. The fabricated triaxial structured fiber with increased thickness offer unique features, such as hydrophobicity, hydrophobicity, and mechanical strength. The stability of solutions volatility is the key factor that characterizes the optimum conditions of the triaxial electrospinning process. We investigated the solvent mixture properties on the triaxial jet stability include solvent boiling point and solvent incompatibility/miscibility. Solvents mixture (chloroform and methanol) of outer sheath PCL solution with low boiling point of 54 ℃ caused the quicker solvent evaporation, which significantly enhanced the outer sheath solution wrapping ability and resulting in a stable jet. However, fibers did not form using chloroform and methanol as a solvent mixture of intermediate PCL polymer. The high volatility of the intermediate PCL solution weakened the outer sheath wrapping ability and resulted in jet instability. Solvent mixture boiling point of intermediate PCL solution was increased by adding

acetic acid to lower the solvent evaporation rate. This significantly strengthened the sheath jet stability allowing full control of CA polymer to encapsulate the intermediate PCL and raising the wrapping ability of CA spinning solution. CA hollow fibers with the intermediate PCL showed significant improvement in load carrying capacity and stiffness in hydrated conditions. Endothelial cells attached and spread on these fibers suggesting non-toxic. Upon formation of the fiber, the outer sheath can be extracted, exposing the desired inner sheath the feature server polymers that cannot be electrospun on their own. Better electrospinning performance was obtained when the inner core MW was smaller or equal to that of the outer sheath. The jet appeared to be broken along the length of the spinning distance indicating an inability of low MW CA sheath to wrap the high MW PCL core.

# CHAPTER 5

# CONTROLLING THE RELEASE OF THERAPEUTIC AGENTS USING MULTIAXIAL ELECTROSPUN BIOCOMPATIBLE HYBRID FIBERS

## 5.1. Introduction

Electrospun fibers have emerged as ideal candidates for drug delivery systems, and for the regeneration of specific target tissues. Compared to competing methods such as nanoparticles, solvent casting, and spray drying for drug delivery [224], electrospinning could offer a better degree of control over the release kinetics. Also, electrospinning could address other weaknesses, including drug loading efficiency, materials selection, and difficulty in controlling particles size. Size and internal structure of fibers can be controlled by varying processes and/or system parameters [204]. Inherent to electrospun fibers is high surface area per volume ratio, ordered porous structure, high rate of adsorption and high strength to weight characteristics [225]. Various drugs have been incorporated into electrospun fibers, including growth factors, hormones, DNA, proteins, inhibitors and antibodies [130, 138, 226, 227]. Doxycycline (Dox), a commonly prescribed antibiotic to treat gum disease [228] and other bacterial infections [223] has also been explored. Dox is an inhibitor of extracellular matrix (ECM) degrading enzymes. Local administration of Dox loaded nanofibers is explored for treating aortic dissection by inhibiting the activity of ECM degrading enzymes [209].

Electrospinning is used to fabricate fibers from natural and biocompatible synthetic polymers and/or their blends [229]. Blending natural and synthetic polymers provide a heterogeneous structure with desirable properties [127]; synthetic polymer function provides better mechanical

properties with controlled degradation rate while natural polymer improves surface functionality for better cell adhesion and growth [55]. Due to their favorable properties, Polycaprolactone (PCL) and gelatin (GT) are frequently investigated in various applications [229] including controlled drug delivery [133, 134]. PCL is a non-toxic, biodegradable polyester, studied in forming many medical devices. To alter the hydrophobic characteristics and incorporate cell binding domain at the PCL surface, it is blended with many natural polymers such as collagen [221]. GT is an inexpensive, nonirritating, biocompatible, and biodegradable protein derived from the hydrolysis of collagen. It has a long history of safe use in pharmaceuticals and cosmetics, as well as in food products, and adhesives in clinics [214]. Due to its poor mechanical properties [215, 219], it is either used after cross-linking or in combination with a synthetic polymer. Since crosslinking agents show toxicity, blending synthetic polymers has been an attractive option. Some common solvents to dissolve PCL and GT have been developed for generating electrospun fibers [109, 135]. The single hybrid PCL/GT fiber has been explored to tune the native tissue biomechanics needed for skin regeneration [230]. Single PCL/GT fibers with different PCL to GT ratios [96] and solvent configurations [108], are also reported [101, 214]. Some reported phase separation issues after mixing the solution of PCL/GT [109]. Nevertheless, some solvents such as 2, 2, 2-trifluoroethanol (TFE) have shown to provide a unique advantage to form PCL/GT single fibers.

Recent advances in electrospinning have enabled forming multilayered structures using coaxial /triaxial electrospinning [175]. Coaxial and triaxial fibers provide programming multi-release drug patterns [149, 163] such as an immediate and sustained release from the fiber core [161, 231] Loading drug molecules in shell component results in burst release [231], and loading drug in the core could help in controlled release. However, the drug release behavior from different types of hybrid core fibers has not been well understood, especially using the same solvent. Tailoring the fiber permeability with a biocompatible outer surface, and achieving a drug loading release profile from hydrophilic and hydrophobic core reservoirs in micro-size fibers are not understood. In this regard, we formed coaxial fibers from PCL and GT in five different configurations and analyzed

the matrix porosity, volume fraction, surface morphologies, internal structures and the release profile of Dox. Also, we modeled the permeability of fibers. We show that by altering the inner core, one could regulate the drug release profile utilizing the chemical nature of the drug and the polymers.

## 5.2. Materials and methods

### 5.2.1. Materials

Type A gelatin (porcine 300 Bloom), PCL (80 kDa, Mn = 80, 000), 2, 2, 2-trifluoroethanol (TFE) and Doxycycline Hyclate (Dox, pharmaceutical secondary standard) were purchased from Sigma-Aldrich (St. Louis, USA) and were used as received. A phosphate buffer solution (PBS, pH = 7.2) was prepared in-house.

### 5.2.2. Electrospinning PCL/GT matrix

PCL and GT were dissolved separately in 10 mL TFE at 10% and 17 % (wt/v) (**Table 5.1**) and then blended at appropriate ratios (50:50 v/v). Prior to electrospinning, 153mg of Dox was added (**Figure 5.1**) to a 10 mL polymer solution (9 wt% of Dox based on the total mass of dissolved polymers). All solutions were stirred for 24h and temporarily stored at room temperature.

The custom-built electrospinning setup used is similar to our previous publication [127, 216], with minor modification to allow for dual-flow. In brief, setup consisted of two syringe pumps (74900 series, Cole-Parmer Instrument Company, Vernon Hills, IL), coaxial/triaxial needles, syringes, high voltage power supply (ES30P-5W/DAM, Gamma High Voltage Research, Ormond Beach, FL), earth grounding, and a collection mandrel. Syringes were connected to the spinneret via 30-cm long PTFE tubing purchased from Sigma-Aldrich (St. Louis, MO). PCL/GT spinning solution was loaded into a 10 mL syringe and fed to an electrospinning spinneret connected to a high voltage power supply held at 17kV. The distance between collector and spinneret was set at 18 cm. Core solution was pumped independently at a controlled rate (1 ml/h) while shell and intermediate

solutions were pumped at 3 mL/h. Five different configurations of hybrid PCL/GT polymers were formed: i) single; ii) coaxial with GT as the core and PCL/GT as the shell; iii) coaxial single phase with PCL/GT in both core and shell; iv) coaxial with GT as the core and PCL/GT as the shell; and v) triaxial with PCL/GT inner core and outer shell separated by intermediate GT. Dox loading was in the core in multiaxial fibers. All fibers were collected on a 3 × 3 cm aluminum foil and a relative humidity of about 45%.

**Table 5.1.** The ranges of operating parameters used for electrospinning of PCL/GT.

| **Parameter** | **Operation value** |
|---|---|
| PCL/GT Concentration | 10% - 17% (wt/v) |
| Shell/intermediate flow rate | 2 - 3 mL/h |
| Core flow rate | 1 – 1.5 mL/h |
| Spinning distance | 17- 19 cm |
| Polymer ratio | 50/50 (v/v) |
| Voltage applied | 17-18 kV |
| Core needle ID | 0.4 mm |
| Intermediate needle ID | 1.00 mm |
| Shell needle ID | 2.00 mm |

v/v volume percent or volume/volume percent ID needle internal diameter

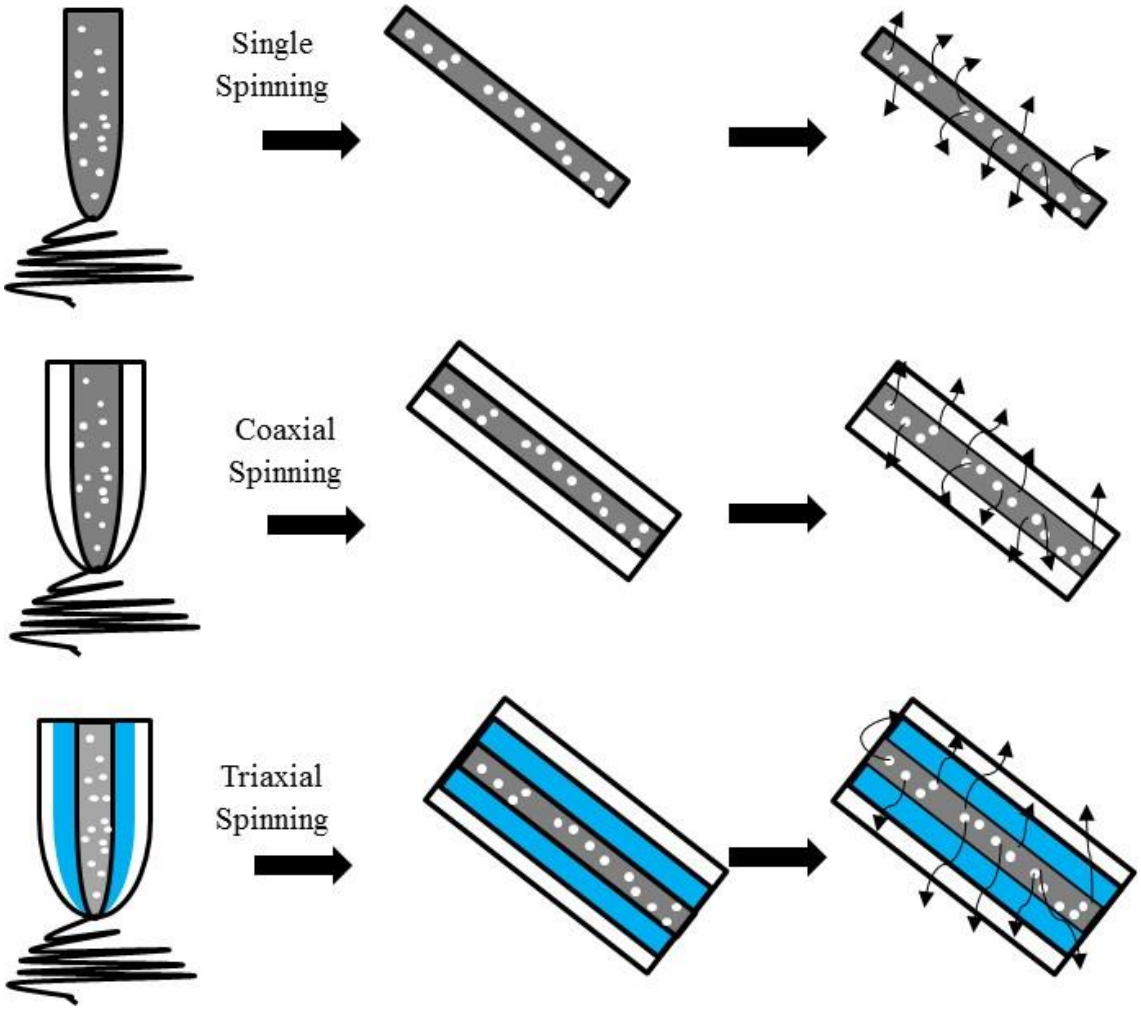


**Figure 5.1.** Schematic diagram of different configurations and drug loading in single, coaxial and triaxial PCL/GT fibers.

### 5.2.3. Microstructure characterization

To characterize the matrix surface morphology and porosity, dry electrospun fibers were analyzed using a scanning electron microscope (Jeol JOEL 6360USA Inc., Peabody, MA), similar to our previous study [127]. In brief, samples were cut into about 2-mm long strips, placed on an aluminum stub using a double sided conductive tape and sputter-coated with gold for 1 min. Samples were visualized at 15 kV accelerating voltage. The diameter or radius (r) of electrospun fibers were analyzed using ImageJ analysis software at random locations and, at least, three images

per sample were measured to determine fiber size distribution. In a known image area, open space, i.e., not occupied by the fiber per unit area were quantified. Assuming negligible open space along the thickness, porosity ($\varepsilon_p$) was calculated as the ratio of open space to the analyzed total image area. The fiber volume fraction ($\phi$) was calculated as (1- $\varepsilon_p$).

Digital micrographs of the matrix thickness were captured using an inverted microscope (Nikon TE2000, Melville, NY) equipped with a CCD camera. Fibrous matrix thickness was measured using Image J, calibrated using an image of a hemocytometer at similar magnifications.

Multiple layers within each fiber were analyzed using a transmission electron microscope (TEM) JEOL JEM-2100. Samples were mounted on the top of a copper grid, loaded in the TEM chamber, and visualized at 200 kV accelerating voltage.

### 5.2.4. Determining the presence of various components

The chemical compositions of fibers were characterized using a Thermo-Nichole-50 FTIR spectrometer equipped with a DTGS detector. Spectral scans were obtained at ambient conditions at a resolution of 4 $cm^{-1}$ with an accumulation of 64 scans, using the associated software. Obtained data were plotted in Sigma Plot 12 (SPSS) and used to analyze the characteristic peaks.

To determine the distribution of GT within the fiber, samples were soaked in PBS (pH 7.2), and 2 μM CFDA SE was added to the solution and incubated for 30 min at 37°C. Then samples were analyzed using an inverted microscope (Nikon TE2000, Melville, NY) and fluorescent micrographs were collected using the CCD camera.

### 5.2.5. In vitro Dox release determination

Samples were cut into 1.5 × 1 cm slices, immersed in 20 mL PBS (pH = 7.2) and incubated at 37 °C. At various times 0, 8, 24, 48, 72, 96 and 120h, 1 mL of the sample was retrieved after mixing. The absorbance of Dox was measured in each sample using UV spectrophotometer (Cary 50 Bio) at 375nm wavelength [232]. Dox content was determined using a calibration plot obtained from a

linear fit to the absorbance of various concentrations of Dox solutions (0.2 to 0.8 mg/L) prepared in a PBS buffer. The absorbance of each sample was measured, and Dox concentration was determined using the calibration equation.

To determine the decay rate $k_D$ values, Dox solution was prepared directly in PBS and incubated at 37 °C. Dox concentration ($C_{Dox}$) was measured in samples retrieved at various times until 48 h. Using an exponential decay rate, Dox concentration at any time "t" was related to the initial concentration $C_{doxy,0}$ when t= 0. This is written as

$$\frac{C_{Dox}}{C_{Dox,0}} = e^{-k_D t} \quad (1)$$

Obtained concentration values were plotted as a ratio of the initial concentration against corresponding time, and exponential function was fitted from which $k_D$ values were obtained.

To determine Dox content in different fiber configurations, fresh fibers were cut into 1.5 × 1 cm segments and dissolved using 1 mL of TFE. Then 9 mL PBS was added to the final volume of 10 mL. During mixing, hydrophobic PCL separated from the PBS solution containing Dox. The absorbance of 1 mL of PBS solution was measured, and Dox content per matrix was calculated.

Dox content from different time points was normalized with the Dox in the matrix to obtain the percentage release. Cumulative release was calculated by accounting decay and was plotted to obtain the release profile. At least, triplicate samples per condition were used, and experiments were performed multiple times.

### 5.2.6. Modeling permeability of different layers

To understand the changes in permeability due to multiple layering, we assumed that: i) Dox release primarily occurred from the upper and lower matrix surfaces with a negligible release along the thickness (**Figure 5.2**); ii) there were no chemical reactions other than Dox decay; iii) released Dox was uniformly distributed in the entire PBS, and iv) the temperature is uniform at 37°C. Then Fick's first law in terms of permeability was written as

$$\frac{dC_{Dox,0}}{dt} = \frac{PS}{V}\left(C_{Matrix} - C_{Dox,0}\right) \quad (2)$$

Where S is the total surface area of the matrix (300 $mm^2$), and V is the volume ($mm^3$) of the PBS incubated, $C_{Matrix}$ is the Concentration of Dox content in the matrix, and $C_{Dox,0}$ is the actual Dox concentration in the solution prior to decay. To calculate $C_{Matrix}$, first volume of solids in the matrix was calculated using the fiber fraction $\phi$ along with the sample volume (**Table 5.2**). Then, Dox loaded in each matrix was divided by the fiber volume to obtain $C_{Matrix}$. Since, measured concentrations at any given time have Dox degradation rather than the actual $C_{Dox,0}$ released from the matrix, we substituted Equation (1) into Equation (2)

$$\frac{dC_{Dox}e^{k_D t}}{dt} = \frac{PS}{V}\left(C_{Matrix} - C_{Dox}e^{k_D t}\right)$$

Using the initial boundary condition when t=0, $C_{Dox} = 0$, integrating Equation (4) gives

Substituting $\frac{C_{Dox}}{C_{Matrix}} = e^{-k_D t} - e^{-\left(k_D + \frac{PS}{V}\right)t}$

Rearranging $Ln\left(1 - \frac{C_{Dox}}{C_{Matrix}e^{-k_D t}}\right) = -P\frac{tS}{V}$ (3)

From the obtained concentrations at various times, $Ln\left(1 - \frac{C_{Dox}}{C_{Matrix}e^{-k_D t}}\right)$ was calculated. These values were plotted for the corresponding time and volume of the solution. Using a linear fit, permeability (mm/h) was calculated from the slope of the line. At least, triplicate samples per condition were used. Average values along with standard deviation were calculated.

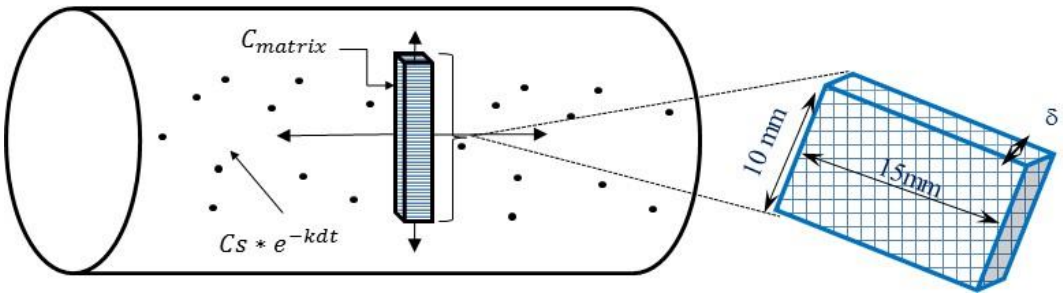


**Figure 5.2.** Schematic diagram showing the model development for determining Dox permeability of electrospun matrix.

### 5.2.7. Cell Viability

Adipocyte stem cells (hASCs) were purchased from Thermo Fisher Scientific and cultured in MesenPRO following vendor's protocol. Culture medium was changed every 3 days. Cells were detached with TRypLE™ express and stained with CFDA-SE at a concentration of 2 µM for 25 min at 37 °C. Fifty thousand stained cells were seeded onto the tissue culture plastic (TCP) surface, and various fibers [127, 216]. One day after seeding, cells viability were analyzed using an inverted microscope (Nikon TE2000, Melville, NY) and images were collected using a CCD camera. The cell-containing samples were fixed in 3.7 % formaldehyde for 30 min at room temperature, dried using ethanol and then sputter coated with gold at 40 mA prior to observing under an SEM.

## 5.3. Results

### 5.3.1. Process optimization

We utilized only one solvent and fixed the ratio of PCL to GT to 1:1 but wanted to confirm our process first with single fibers. Hence, the effect of important parameters (applied voltages, collector plate distances, and flow rate) in the formation of PCL/GT hybrid fibers were evaluated. The range of each parameter was based on previous studies using the same solvent [55, 102]. First, applied voltage was varied from 10 to 20 kV (**Figure 5.3a**). When 10 kV was used, formed fibers were not uniform, similar to other publications [17]. Instead of adding a co-solvent or a surfactant

to assist jet stability, we increased the applied voltage to 17 kV and formed uniform fibers. At 20 kV, unstable jet was observed, which resulted in the formation of smaller fiber size. Hence, applied voltage was maintained at 17 kV.

Next, the effect of spinning distance was determined by varying collector plate distance from 10 to 20 cm (**Figure 5.3b**). The spinning distance affects the jet traveling time and the strength of electric field. At a short spinning distance, wet fibers are obtained due to incomplete evaporation of the solvent. Increasing the distance beyond the optimum causes jet instability or few fiber formations. Fibers produced at 17-18 cm spinning distance appeared more uniform and free of beads. Therefore, subsequent experiments were conducted at a distance of 18 cm. The solution flow rate was varied from 0.5 to 2 mL/h (**Figure 5.3c**). Increasing the polymer solution flow rate increases the fiber diameter, because of the large mass of solution withdrawals from the spinneret. However, if the spinning solution flow rate is too high, the excess solution will drop out. The optimum flow rate was found to be 1 to 2 mL/h with respect to the fiber size.

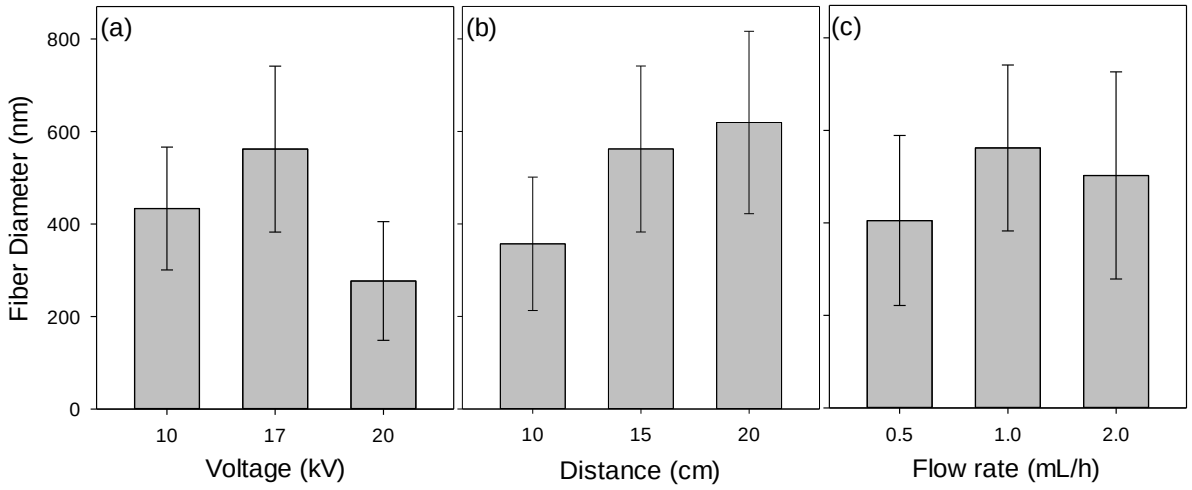


**Figure 5.3.** Effect of process parameters on fiber size of PCL/GT single fiber Dox-free electrospun from 10 wt % polymer concentration and 50/50 polymers ratio. (a) Applied voltage. (b) Collector plate distance. (c) Solution flow rate.

### 5.3.2. Fabrication of Dox loaded PCL/GT

Previously, we reported on the formation of coaxial and triaxial structured fibers using cellulose acetate and PCL. In this study, the same electrospinning system was used to form PCL/GT hybrid coaxial structures with the same solvent for all layers [127, 216]. We also used Dox as a drug model compound and evaluated the effect of changing fiber structure and size on the Dox release profile. When GT was introduced as a core while holding the polymer concentration constant, jet dripping with difficulty in maintaining a stable coaxial jet was observed. Low polymer concentration (10 wt %) in the solution could lead to an unstable jet and/or formation of beaded fibers. In particular, the low viscosity of 10 wt% PCL/GT solution could weaken the shell solution wrapping and encapsulating ability to maintain the coaxial jet spinning. The number and size of polymer chains control entanglements and ability to form continuous fibers. Therefore, the solution concentration was increased to 17 wt% of both polymers (PCL and GT). Then, the coaxial Taylor cone visually appeared to be more stable along its length, and most of the fibers maintained their integrity at the collector plate. We successfully electrospun all three configurations with no difficulty, using only one solvent for all layers.

Conditions that were suitable for coaxial fibers were also suitable for forming a triaxial fiber. We successfully formed triaxial fibers. Also, single fibers were formed with Dox added to the PCL/GT mixture, directly prior to electrospinning as a control. Single PCL/GT fibers were fabricated at the same setting as coaxial and triaxial fibers.

### 5.3.3. Characterization of Dox loaded PCL/GT

The internal structures of electrospun fibers characterized by TEM indicated the presence of multiple layers in coaxial and triaxial fibers (**Figure 5.4**). The interface between the core and shell found in the coaxial and triaxial structure was due to the density variation of core and shell materials. In coaxial electrospinning, fibers with the core PCL had a larger diameter than the fibers with core GT, despite the process parameters being the same. This could be due to PCL having a

much stronger structure than GT structure. Also, PCL has better electrospinning performance compared with GT. In coaxial single phase, however, the two layers were indistinguishable due to the absence of interface boundary between shell (PCL/GT) and core (PCL/GT). Micrographs of the triaxial fiber showed the presence of all three layers.

Using the scanning electron micrographs (**Figure 5.4**), I analyzed the surface structure of fibers and determined the average fiber diameter, overall morphology, porosity of the matrix, volume, thickness and Dox concentration. Most obtained fibers were in a microscale range (**Table 5.2**). No beaded fibers were observed, which attributes to the stability of electrospinning jet in the whipping region, and the lack of phase separation and solvent interactions between spinning solution mixtures at the tip of the spinneret. Increased polymer composition increased the fiber diameters in single phase fiber compared with the single fiber as a result of an increase in the volume of spinning solution being drawn from the tip of the spinneret. In coaxial spinning, adding the core layer increased the fiber size as expected. Triaxial fibers had the largest diameter with a wide range of fiber diameters and were nearly triple the size of the single fiber.

Matrix porosity (**Table 5.2**) was similar to coaxial single phase and triaxial fibers, while coaxial with core GT showed a reduction in porosity. Coaxial fiber with core PCL and single fibers also showed similar porosity. The differences in porosity could be due to the variation in fiber density distribution throughout the matrix. The presence of the core layer or multiple layers in the fiber did not have an impact on the porosity.

Fiber volume fraction was the same in coaxial fibers and was proximate to triaxial fibers. The matrix of single fibers showed an increase in fiber volume.

No significant differences in fiber structures were observed between loaded and unloaded Dox fibers, indicating that the Dox solubility in the solution mixture was homogeneous. When the drug loading efficiency was compared in the fibers, coaxial core GT showed highest Dox loading, followed by coaxial single phase. Coaxial core PCL showed the least in coaxial fibers, despite the fact that the same solvent was used. This could be attributed to the fact that Dox and GT are

hydrophilic, which could facilitate weak internal attractive forces while forming fibers. On the contrary, PCL is hydrophobic, and it could lead to weak internal repulsive forces. Single fibers had lower Dox than coaxial GT and same phase GT fibers. Triaxial showed lowest Dox loading. Thus, the addition of layers may have an effect on loading of the drug.

**Table 5.2.** Electrospun fiber-matrix characteristics

| | **Single** | **Co-SP** | **Co-G** | **Co-PCL** | **Triaxial** |
|---|---|---|---|---|---|
| Outer DI ± STD (μm) | 10.12 ± 3.9 | 15.08 ± 9.5 | 21.23 ± 8.3 | 17.13 ± 5.5 | 30.02 ± 17.0 |
| δ ± STD (μm) | 280 ± 56 | 229 ± 60 | 142 ± 35 | 186 ± 33 | 318 ± 29 |
| Volume ($mm^3$) | 42 ± 0.084 | 34.3 ± 0.09 | 21.3 ± 0.052 | 27.9 ± 0.05 | 47.7 ± 0.043 |
| $\varepsilon_p$ ± STD (porosity) | 0.46 ± 0.097 | 0.60 ± 0.012 | 0.35 ± 0.054 | 0.5 ± 0.056 | 0.65 ± 0.095 |
| $(1 - \varepsilon_p)$ | 0.54 | 0.40 | 0.65 | 0.5 | 0.35 |
| Fiber volume ($mm^3$) | 22.7 ± 0.045 | 13.7 ± 0.036 | 13.8 ± 0.034 | 13.9 ± 0.025 | 16.7 ± 0.015 |
| Dox mass in matrix (μg/mL) | 1.59± 0.013 | 2.08± 0.004 | 2.48± 0.009 | 0.84± 0.019 | 0.55± 0.098 |

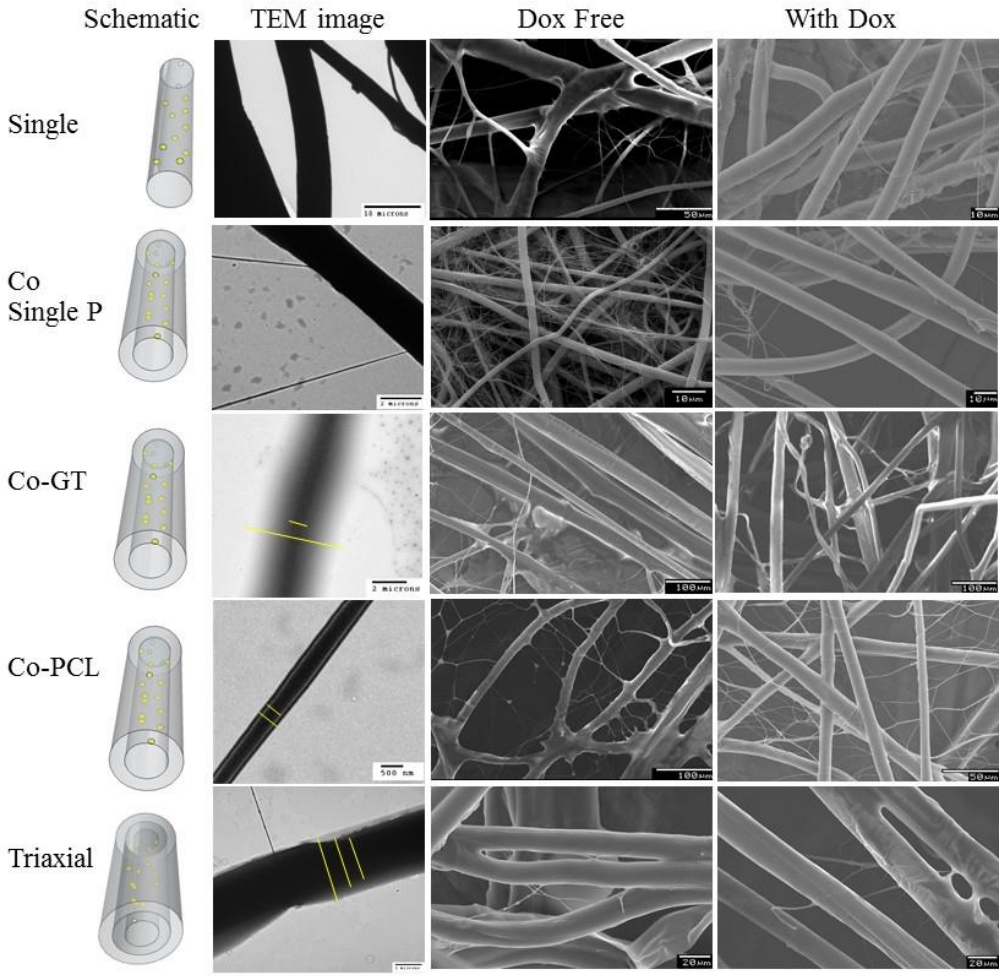


**Figure 5.4.** Microstructure of different configurations of PCL/GT matrixes. Shown are schematics, transmission electron micrographs of fibers with Dox, scanning electron micrographs without and with Dox. All images were obtained from fresh samples.

### 5.3.4. FTIR analysis

In Fourier transform infrared (FTIR) spectra of electrospun fibers **(Figure 5.5),** PCL characteristic stretching peaks consist of C=O, C-H asymmetric stretching, and C-H symmetric stretching, which appeared at 1700 $cm^{-1}$, 2920 $cm^{-1}$ and 2840 $cm^{-1}$ respectively. GT displayed several characteristic peaks consisting of an amide bond (N-H) stretching at 3555 $cm^{-1}$, C=O stretching at 1650 $cm^{-1}$ and N-H stretching (amide I) at 1520 $cm^{-1}$. Others have reported similar results [145, 233]. Same

absorption band of PCL and GT appeared in coaxial and triaxial PCL/GT, suggesting the presence of both components in the fabricated fibers. Other characteristic peaks were observed in single, coaxial and triaxial PCL/GT (C=O at 1660 $cm^{-1}$) which attributed to the functional groups of Dox loaded in the fibers. Spectra of all configurations showed that loading Dox into the fibers had no influence on the chemical components of the electrospun fibers.

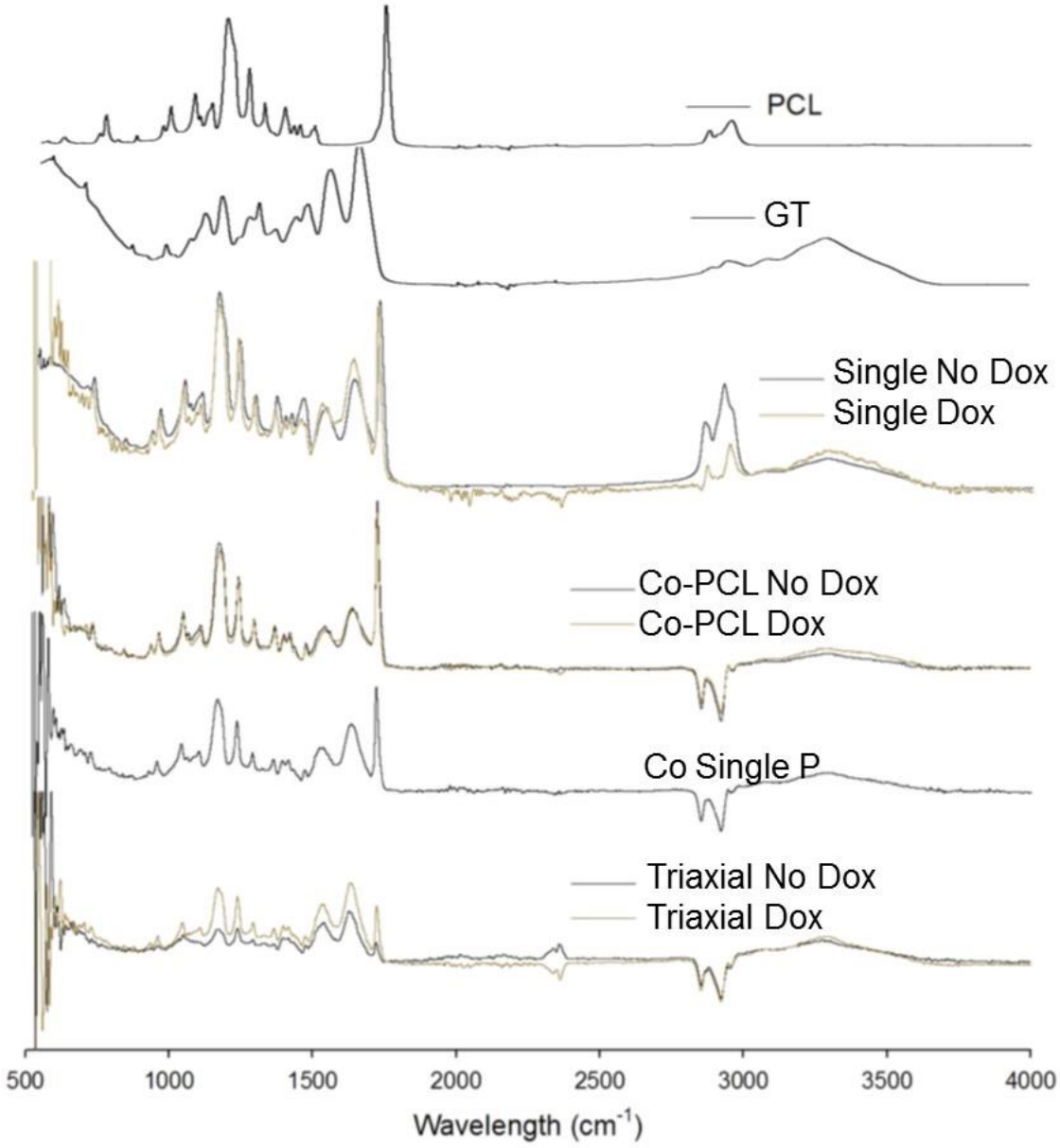


**Figure 5.5.** FTIR spectra of electrospun PCL, G and PCL/G hybrid fibers at various frequencies obtained at ambient conditions at a resolution of 4 $cm.^{-1}$

### 5.3.5. Cell Viability and Spreading

The cellular activity was evaluated on the hybrid electrospun fibers PCL/GT to understand the advantages of blending PCL and GT for cell attachment and proliferation. We tested the effect of viability after one day of culture. The pre-stained cell was evaluated for viability using CFDA-SE staining present in the cytoplasm of the cells. Fluorescent images showed that cells had attached to all GT containing fibers and also showed spreading. However, in cells on PCL only fibers had limited spreading (**Figure 5.6**). Also, the presence of CFDA inside also suggested that cells were viable. Hence, the overall process is not toxic.

Cell morphology and the interactions between cells and fibers in the matrix were also evaluated using SEM. Micrographs revealed (**Figure 5.6**) that the cells attached to the fibers and were entangled by them throughout the matrix. In some locations, cells showed numerous lamellipodia and filopodia with anchorage points to the fibers. This is indicative of a good cell attachment, implying the cytocompatibility of the implants. However, the effect of these configurations on long-term viability cell growth and tissue regeneration still needs to be investigated.

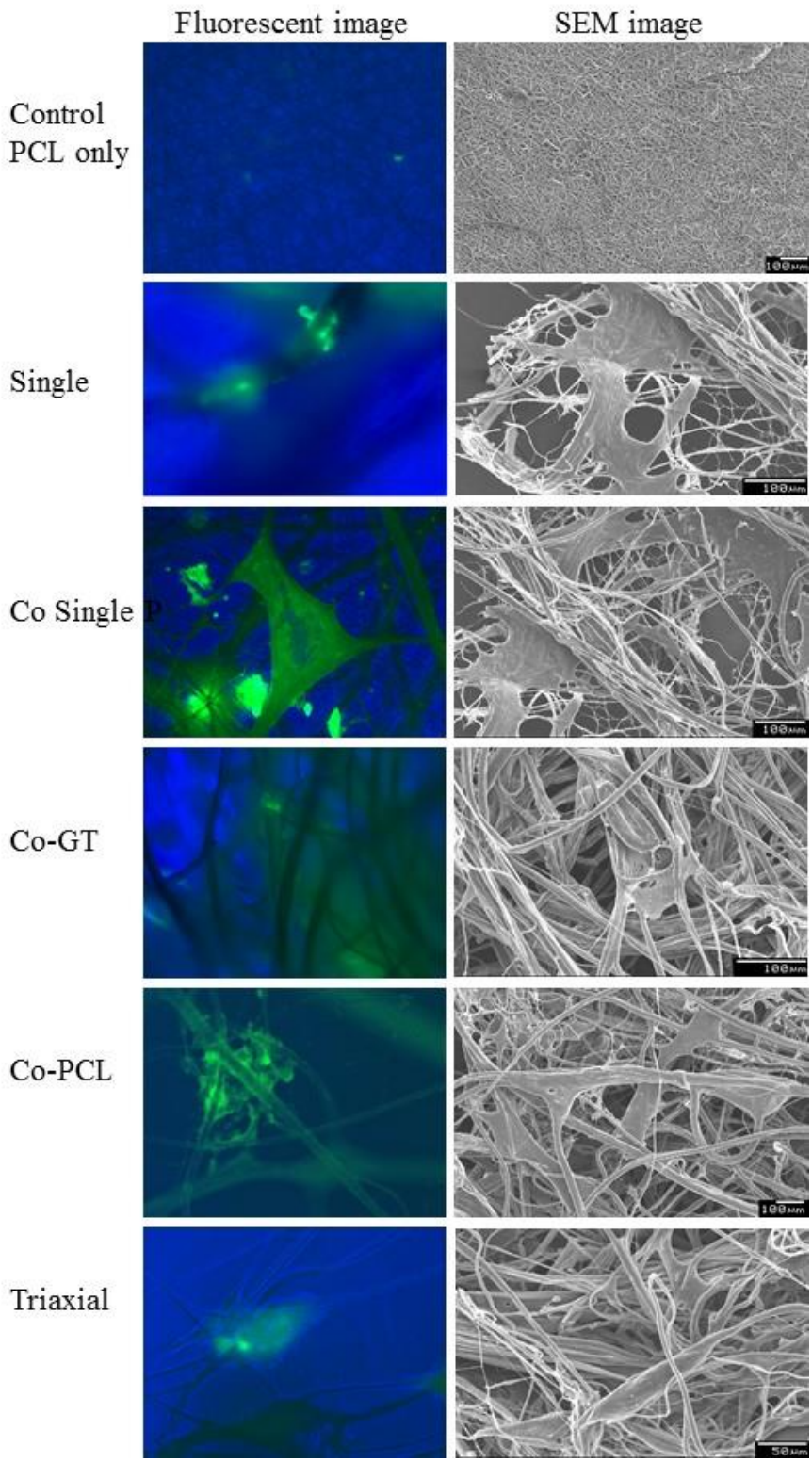


**Figure 5.6.** Adipocyte stem cells interaction on PCL/GT fibers: Fluorescent micrographs of CFDA SE stained cells on different fibers showing viability. Also, scanning electron micrographs on the same fibers showing cell attachment.

### 5.3.6. Influence of fiber configuration on Dox release profiles

The intent of forming different configurations was to understand the effect on releasing Dox. In this regard, release from different types of fibers was compared (**Figure 5.7a)**. There was nearly

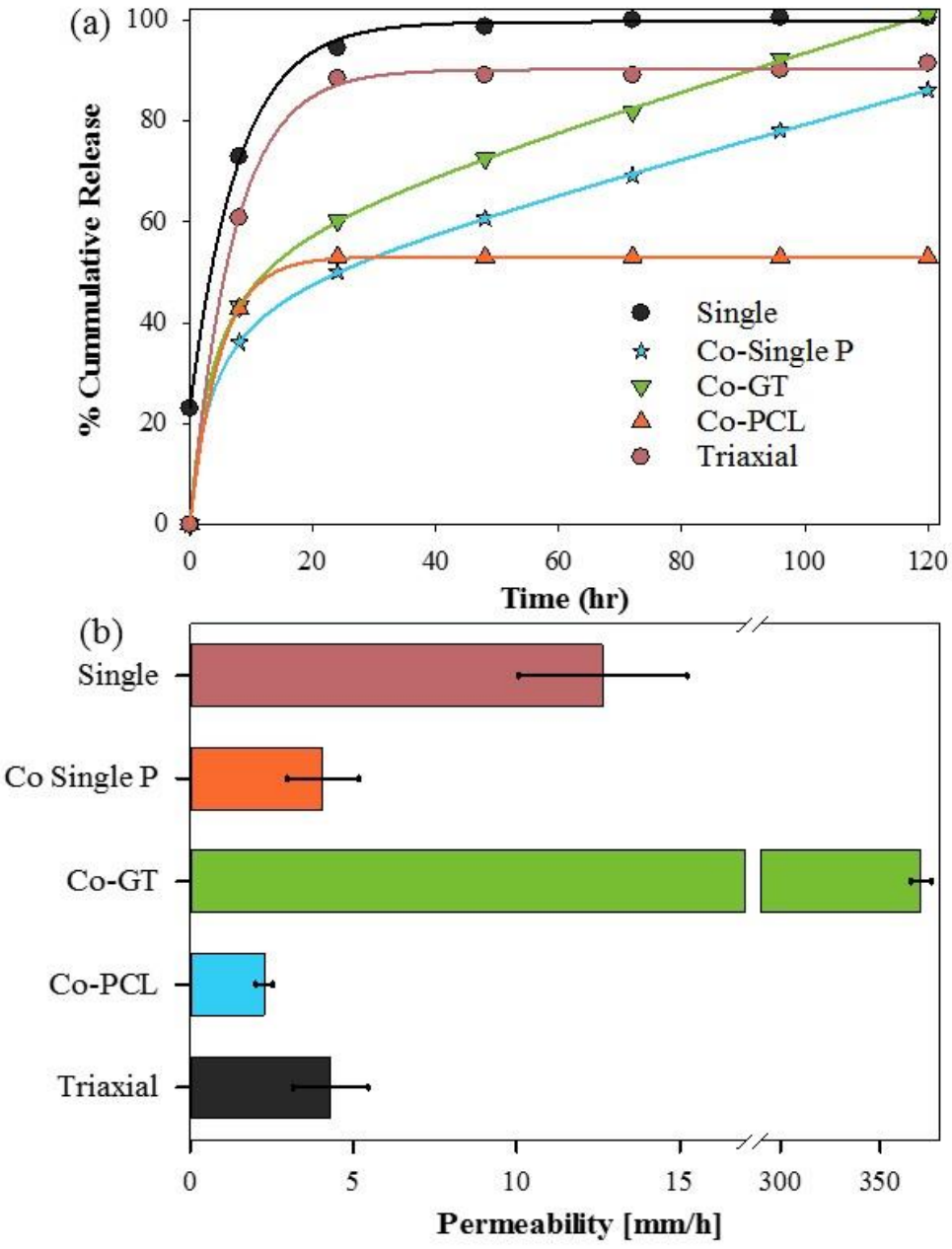


**Figure 5.7.** Comparison of drug permeability constant and release behaviors from a different type of PCL/GT matrixes. (a) The drug release behavior from various type of fibers matrix. (b) Effect of type of fiber on the permeability constant.

20-30% increase of burst release in a single fiber. When single fibers are used with a combination of PCL with other hydrophilic polymers [221], initial burst releases is expected similar to the release from membranes [234]. Also, release profiles show very short duration; nearly 95 % of Dox was released at 24h when incubated in a pH of 7.2 and at 37°C from single fibers. In coaxial fibers with core GT and core single phase, only 50% was released at 24 h. Adding a second layer controlled the release of Dox. More importantly, no burst release of Dox was observed in any of the coaxial and triaxial fibers. Coaxial fibers with PCL core released only 50%, probably due to the hydrophobic nature of PCL not attracting a liquid medium necessary for the mobility of Dox. Since PCL is a hydrophobic polymer, less than 20% release of Dox was reported for the first six days, but release rate increased at a later time point by 14 days. Triaxial fibers showed larger deviation due to inhomogeneity in the thicknesses of multiple layers, which requires more careful optimization. Successful drug loading and release was dependent on ensuring that the hydrophilic polymer is loaded up with the hydrophilic drug.

### 5.3.7. Modeling the matrix permeability

Since different core configurations were used, the permeability of each fiber configuration towards Dox was calculated (**Figure 5.7b)** using the modeling strategy described above. Coaxial fibers with core GT showed the highest permeability, probably due to the hydrophilic Dox. This could allow most of the Dox to escape from GT to the fiber surface. Single fiber matrix had the second highest permeability, with a value of 13 μm/h, which is similar to the 20μm/h value reported by others for porous films [235], using a reservoir-based drug delivery system. This also confirms our modeling approach. The shorter distance between the Dox molecules and the outer surface through which Dox diffuses near the surface leads to a small driving force. Both coaxial single phase and triaxial fibers showed similar permeability but lower than single fiber; the presence of GT layer in triaxial fibers had little contribution to resist Dox release, which is supported by the high GT

permeability value. Although reduction is expected due to the presence of additional layers and mass contribution from hydrophobic PCL, Dox is present in the same PCL/GT combination in all three configurations. Coaxial fibers with core PCL showed the least permeability to Dox, which is expected due to the hydrophobic nature of PCL; Dox is hydrophilic although more lipophilic than other members of the tetracycline family.

### 5.3.8. Stability of GT in PCL/GT fiber

Since high permeability was observed in fibers with core GT, it could be due to the instability of GT during incubation as GT is water soluble. To test this possibility, we investigated the stability of fibers structure after incubation in PBS at 37℃ for 5 days. SEM micrographs of PCL/GT of single and multilayered fibers (**Figure 5.8**) revealed rough, fibrous surface, relative to fresh fibers. Fiber sizes were similar and had no significant swelling or contractions, which could be detected via cracks within the fibers when dried for SEM evaluation. Fibers from all configurations showed similar behavior. To understand *in situ* distribution of GT in incubated and fresh samples, fibers were stained with a fluorescent marker, CFDA SE; the amino groups in GT specifically conjugate with activated CFDA. Fluorescent micrographs (**Figure 5.7)** showed the absence of GT in PCL-alone fiber, confirming specificity due to the lack of amino groups in PCL.

## 5.4. Discussion

Electrospinning allows forming natural and synthetic heterogeneous structured fibers with desirable properties useful in biomedical applications; synthetic polymers provide mechanical strength while natural polymer provides cellular attachment and growth. Many have formed single PCL/GT hybrid nanofibers while some have reported on phase separation issues due to high humidity environment and the need for various solvents such as chloroform, a mixture of acetic acid and methanol, hexafluoro-2-propanol (HFIP) and TFE [168]. We previously reported on the effect of solvent volatility and miscibility on coaxial and triaxial fiber formation [127]. While

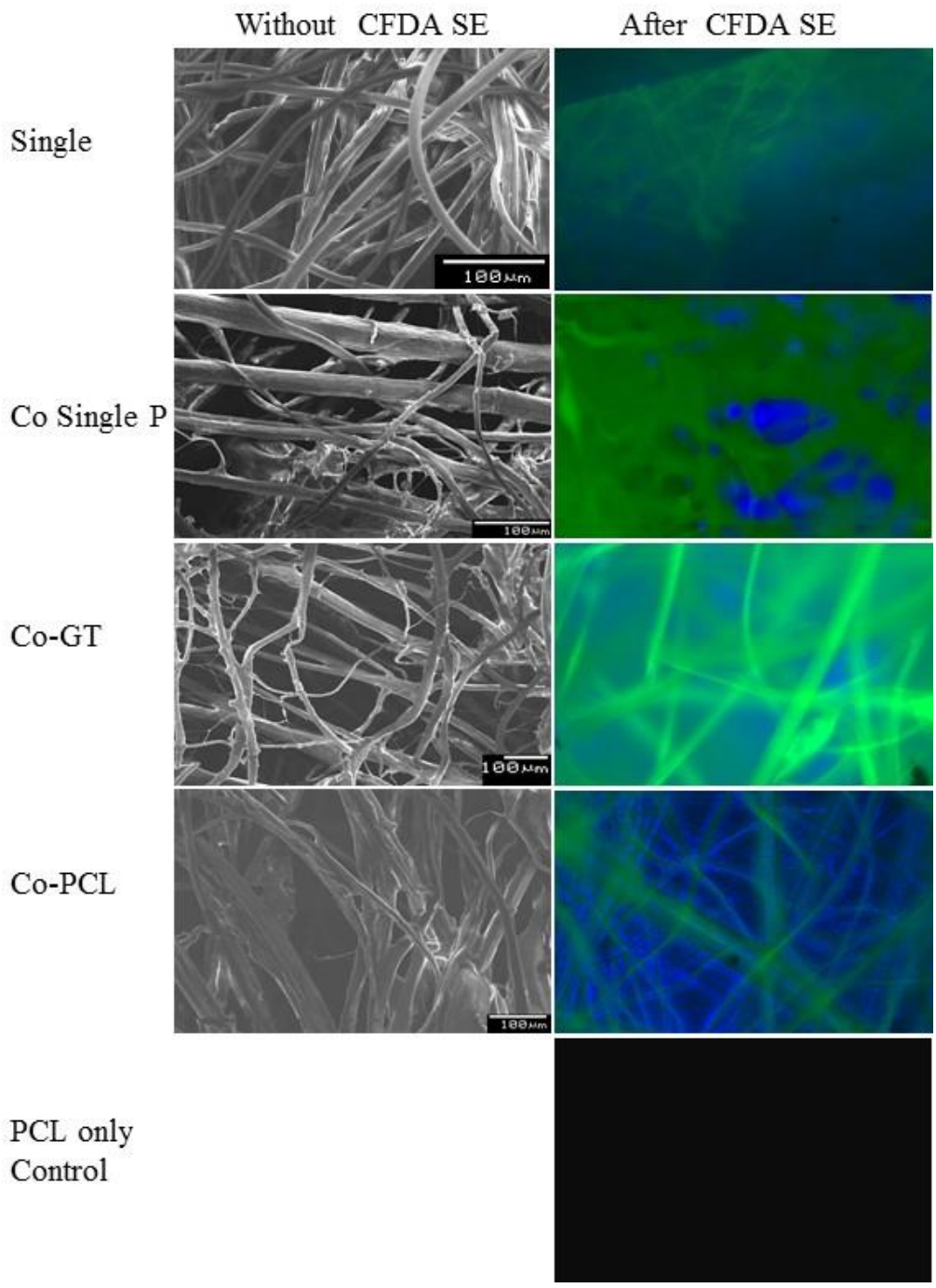


**Figure 5.8**. Stability of GT in fibers after incubation in PBS at 37℃ at day 5. Shown are micrographs acquired from SEM before CFDA SE staining and fluorescent micrographs after CFDA SE staining. As a control, PCL fibers were prepared in the same solvent at same settings.

forming PCL/GT fibers in all five configurations, we utilized the same TFE solvent to address

solvent compatibility at the interfaces. If the common solvent is not possible, one needs to look at the compatibility of solvents and solvent evaporation rate.

Formed fibers were larger in diameter compared to other reports. In particular, the advantage of coaxial and triaxial electrospun fibers is in forming thicker fibers. Our results show that fiber sizes are in micrometer range rather than nanometers. However, matrix porosity depends on fiber density variation and void content distribution in the matrix. Others have reported on the importance of material porosity in providing air mobility at high porosity and preventing the wound from a bacterial infection at low porosity [178]. Also, one could control the porosity by using void collector plates [58], if necessary.

Some have explored releasing Dox using a single electrospun PCL nanofiber matrix for periodontal diseases [236]. However, it is not clear what their loading efficiency was and how they determined the percentage release. Also, Dox release kinetics is affected by the pH, percentage of the drug loading, and the nature of the polymer matrix [178]. Others have incorporated drugs into PCL blended GT and explored its utility in a subcutaneous implantation model [58, 237]. However, these studies do not provide a good understanding of the complex transport mechanism of the drug in hybrid and multi-layered fibers, such as programming multi-release drug patterns for immediate and sustained release from the fiber core. Also, tailoring the drug release behavior from different types of hybrid core fibers has not been yet investigated, especially using the same solvent.

We altered the internal core structure of PCL blended GT by adding Dox to three different core configurations: i) PCL/GT, ii) GT, and iii) PCL. Inner core PCL/GT provides a single phase with the outer PCL/GT, but by loading Dox in the core, we increased the distance for Dox release. Alternatively, GT core with Dox allows evaluating the Dox release when loaded in a hydrophilic polymer. Replacing GT core with PCL core helps understand the effect of loading Dox in a hydrophobic polymer on the release profile. Encapsulation of the drug in the shell component of coaxial fibers will result in burst release as the drug molecules are on or near the fiber surface [236]. This is useful if a drug or a stimulating factor is required for short-term treatment only while another

drug/stimulating factor that is required for long-term treatment can be loaded into the fiber core. Thus, coaxial/triaxial fibers can be designed to provide dual release profiles consisting of an immediate and sustained release from the fiber core [238]. Also, the drug can be programmed for a multi release pattern [47, 208]. The increased distance between Dox molecules and fiber shell surface is useful in eliminating the burst release. In triaxial fibers, Dox was loaded in the inner PCL/GT core layer, which was surrounded by an intermediate layer of GT and a PCL/GT outer shell. Triaxial fibers allow the evaluation of Dox release when encapsulated with two layers of hydrophilic and blended hydrophobic/hydrophilic layer microfiber. Coaxial fibers with core GT provided the most sustained release of Dox. This could be due to the hydrophilic core GT absorbing water and providing a favorable environment for a better release. Others have shown a similar Dox release profile from coaxial nanofibers of PCL blended with Collagen with core hydrophilic polyvinyl alcohol [178]. Although these fibers are nanometers in size, released Dox provided the antibacterial environment and prevented infection, suggesting Dox is functional.

Our cell culture analysis showed that the cells attach in multiple layers, and they are viable. Further, GT is stable during the study period. An advantage of adding many layers is altering the permeability of each fiber. However, while forming a multiaxial fiber, polymer density could change, which controls the permeability to any component. Also, the partition coefficient of a molecule will affect the matrix permeability. At nanoscale or microscale, one could control the permeability with appropriate combinations of drug and the polymer. Permeability is a function of the type of diffusing molecules and its partition coefficient in different solvents. Layers at nanoscale can partition the drug effectively. Nevertheless, we need to explore what would be the release profile in a triaxial fiber with PCL layer sandwiched between two PCL/GT layers. All samples containing GT showed a uniform distribution of GT, even after a 5-day incubation. Distribution was similar to fresh samples, suggesting no dissolution of GT after 5 days. Hence, the increased permeability is not due to the instability of GT in the fibers. When one has to create a heterogeneous environment for differentiating stem cells, one could deliver various growth factors

or inhibitors at different time scales. This will allow development of composite tissues. However, we need to extend our results to understanding the status of hASCs, combine hydrophobic drugs or stimulating factors and assess what inner core controls better.

### 5.5. Summary

PCL/GT fibers with micrometer thickness were successfully electrospun into single, coaxial and triaxial configurations using a common solvent. This was possible with increasing PCL and GT concentration from 10 wt% to 17 wt%. Formed fibers were uniform, and no beaded fibers were observed in any of the configurations. Comparison of fibers with and without Dox loading showed no changes in fibers structure. Microstructure analysis confirmed the presence of different layers in each configuration. Further, FTIR analysis confirmed the presence of various components. Dox release over 5 days showed improved release profile in coaxial GT-core-fiber. Permeability modeling showed an increase in Dox permeability in hydrophilic GT core. CFDA SE staining of fibers showed that GT distribution in PCL/GT fiber was uniform and was stable over a 5-day period. The presence of GT allowed viable cells to attach to the fibers. Using electrospinning, one can control the release behavior of various components by adding another layer to the fiber and combining hydrophilic-hydrophobic polymer. Because of the unique fabrication process, release characteristics, biocompatibility, biodegradability and antibacterial properties of PCL/GT loaded Dox it could potentially be a useful matrix for tissue regeneration.

# CHAPTER 6

# CONCLUSIONS AND RECOMMENDATIONS

## 6.1 Conclusions

The primary aim of the research is to fabricate natural and synthetic heterogeneous electrospun structured fibers with desirable properties whereas synthetic polymer function as backing material providing mechanical properties while natural polymer act as promoters of cellular attachment in tissue engineering and as a sustained release agent in drug delivery. Additional proposed applications for electrospun structured fibers include wound dressings, medical implants, sensor technology, filtration, and catalysis. The study investigates the use of new types of electrospun fibers with different structure and functions such as altered surface (hydrophobic and hydrophilic), mechanical and biological properties and the ability to manipulate the polymer solution composition in control drug delivery and promote cellular growth. Forming solid fibers cannot impart all the required properties such as morphological, biological, and mechanical features. For example, embedded drug in solid fiber is subjected to fast release kinetics from the fiber surface exposed to the surrounding environment. To better control the release kinetics of embedded drugs, new modifications in fiber formation such as coaxial and triaxial electrospinning are developed. Objectives of the study are divided into three specific aims. Aim 1 investigates the effect of type core and sheath fluids on hollow and core-sheath fiber formation using cellulose acetate (CA) as polymer model for better understanding of the impact of the type of core on the size and morphology of the electrospun

fibers. Aim 2 focus on investigating the influence of solvent characteristics in triaxial electrospun fiber formation to understand the influence of solvevolatility on the mechanism of encapsulating the core polymer in coaxial and triaxial electrospinning. Aim 3 explores the beneficial of the fabricated coaxial and triaxial structured fabricated in aim one and two in controlling the release of therapeutic agents. Obtained conclusions for the three specific objectives are given below.

### 6.1.1 Cellulose acetate core–shell electrospun fiber: fabrication and characterization.

- CA was successfully electrospun into hollow and core–sheath structured fibers c by coaxial electrospinning. Varying the type of core in coaxial electrospinning of CA provided unique features for the fibers such as reinforced core, porous and hollow structure. PCL molecular weight ranges of 10, 43, and 80 kDa were evaluated for their ability to electrospun core–sheath structure. The configuration of 43 kDa PCL solution showed better jet stability. Gelatin and chitosan could be used as a core fluid, but the operation range is limited, and their electrospinning solutions perspiration requires an expensive solvent.
- Tensile strength testing in hydrated conditions CA–PCL fibers showed significant improvement in break stress and strain relative to solid or hollow CA fibers. Hydrated CA–43 kDa PCL fibers showed a nearly ten-fold increase in a break point and stiffness.
- DSC and FTIR analysis confirmed the presence of CA and PCL. Fiber morphologies from SEM analysis indicated incomplete encapsulation by the CA when 80 kDa PCL molecular weight was used.
- The rheology results suggest that the fibers could be formed when the viscosity of the core is less than that of the sheath.

- Incubation with human umbilical vein endothelial cells showed increased attachment and viability in both hollow CA and CA–PCL fibers relative to tissue culture plastic. All CA fibers configurations exhibited no toxicity against human umbilical vein endothelial cells

### 6.1.2 Influence of solvent characteristics in triaxial electrospun fiber formation.

- Successful fiber formation was dependent on ensuring that the outer shell formed first, i.e., the relative solvent volatility of encapsulating core polymer to lower than that of the shell polymer. Better electrospinning performance was obtained when the inner core MW was smaller or equal to that of the outer sheath. The jet appeared to be broken along the length of the spinning distance indicating an inability of low MW CA sheath to wrap the high MW PCL core.
- Scanning electron micrographs showed the formation of structured triaxial fiber of outer hydrophobic PCL/CA/Hollow, PCL/PVA/Hollow, and outer hydrophilic CA/PCL/Hollow fibers. Uniform and smooth fiber obtained from PCL/CA configurations.
- FTIR and DSC analysis indicated the presence of PCL and CA in all certified configurations. FTIR results suggested that further heat treatment could help in removing residual mineral oil from fabricated fibers.
- Results from tensile tests (both wet and dry) revealed that PCL/CA/Hollow fibers had increased stiffness and load carrying capacity than CA/PCL/Hollow fibers. CA hollow fibers with the intermediate PCL showed significant improvement in load carrying capacity and stiffness in hydrated conditions.
- Endothelial cells attached and spread on these fibers suggesting non-toxic. The cell features on the different surfaces demonstrated no significant differences in morphology

and spreading. This desirable feature is indicative of a good cell attachment, implying the cytocompatibility of the implants.

### 6.1.3 Controlling the release of therapeutic agents using multiaxial electrospun biocompatible hybrid fibers

- In this study, PCL/GT fibers with micrometer thickness were successfully electrospun into single, coaxial and triaxial configurations using a common solvent. This was possible with increasing PCL and GT concentration from 10 wt% to 17 wt%. Formed fibers were uniform, and no beaded fibers were observed in any of the configurations.
- Dox release over 5-days showed improved release profile in coaxial GT-core-fiber.
- Comparison of fibers with and without Dox loading showed no changes in fibers structure. Microstructure analysis confirmed the presence of different layers in each configuration. Further, FTIR analysis confirmed the presence of various components.
- The presence of GT allowed viable cells to attach to the fibers and entangled by them throughout the matrix. In some locations, cells showed numerous lamellipodia and filopodia with anchorage points to the fibers.
- CFDA SE staining of fibers showed that GT distribution in PCL/GT fiber was uniform and was stable over 5-day period.
- Permeability modeling showed an increase in permeability of Dox in hydrophilic GT core.

## 6.2 Recommendations

Specific recommendations for interesting future directions for this research are shown below:

- Electrospun fibers prepared in this work were collected on clean aluminum foils or a small rotating drum. Setting-up the electrospinning process for large lab-scale is still an issue. Scaling up fiber production rate is important especially when large sample volume is

needed. Next generation of coaxial electrospinning apparatus should include capabilities of digital controlling for the distance and position of the collector plate as well as the temperature and surrounded humidity during the electrospinning process to reach higher production rate and produce better quality and strength fiber material.

- Blending natural and synthetic polymers provided a new biomaterial with appropriate biocompatibility and improved mechanical, physical and chemical properties which are beneficial for cell adhesion and degradation rate. We evaluated the fabrication of hybrid electrospun fibers to provide controlled release of an antibiotic drug in a short and long term delivery. The fabricated scaffold loaded Dox will provide bacteria free environment for cell proliferation and tissue regeneration. However, this activity was not evaluated in this study. Assays to measure the inhibition of bacterial growth for a different type of electrospun fibers configurations with various drug content should be included in future work.
- In this research, we evaluated the fabrication of hybrid electrospun fibers to provide biocompatible surface and controlled the release of Doxycycline (Dox). Coaxial and triaxial fibers were formed with same PCL/GT shell surface but with different core materials containing Dox: Dox was loaded in GT alone (hydrophilic core), PCL alone (hydrophobic core), and PCL/GT (same phase). Also, triaxial fibers were formed with GT layer sandwiched between PCL/GT layers. Controlled release from dox encapsulated in the fiber core has been obtained due to the present of the additional layer. Develop dual drug delivery system that provided different release profiles for two different drug models separately loaded in the shell or the core of the electrospun fiber is a potential area of study. For example, fabrication coaxial or triaxial electrospun fiber that has an outer shell material loaded with x drug and core with y drug can be used to reduce pain at an early stage using drug x and inhibit infection throughout the entire healing process using drug y i.e. the drug can be programmed for multi release pattern.

- The permeability model developed in this work was used to understand the changes in permeability due to multiple layering. In the model assumptions, the fibers loaded drug were assumed to be uniformly distributed throughout the matrix which is not always possible. Developing a device to control fiber distribution would be helpful in complementing the modeling and experimental work.
- Other interesting topics to investigate include:
    - Investigate the effect of drug/polymer solubility parameter, polymer degradation rate, and drug diffusion pathway on the drug release profile.
    - Compare the drug release kinetics from coaxial and or triaxial electrospun fibers to that of nanoparticles drug delivery systems.
    - Evaluate the drug release kinetic by varying the polymer and drug properties such as hydrophobicity and hydrophilicity in coaxial and triaxial electrospun fibers.

# REFERENCES


1. Li, D. and Y.N. Xia, *Electrospinning of nanofibers: Reinventing the wheel?* Advanced Materials, 2004. **16**(14): p. 1151-1170.
2. Raghavan, P., et al., *Electrospun polymer nanofibers: The booming cutting edge technology.* Reactive & Functional Polymers, 2012. **72**(12): p. 915-930.
3. Garg, K. and G.L. Bowlin, *Electrospinning jets and nanofibrous structures.* Biomicrofluidics, 2011. **5**(1).
4. Neves, N.M., et al., *Patterning of polymer nanofiber meshes by electrospinning for biomedical applications.* International Journal of Nanomedicine, 2007. **2**(3): p. 433-448.
5. Reneker, D.H. and A.L. Yarin, *Electrospinning jets and polymer nanofibers.* Polymer, 2008. **49**(10): p. 2387-2425.
6. Nezarati, R.M., M.B. Eifert, and E. Cosgriff-Hernandez, *Effects of humidity and solution viscosity on electrospun fiber morphology.* Tissue Eng Part C Methods, 2013. **19**(10): p. 810-9.
7. Qu, H.L., S.Y. Wei, and Z.H. Guo, *Coaxial electrospun nanostructures and their applications.* Journal of Materials Chemistry A, 2013. **1**(38): p. 11513-11528.
8. Liang, D., B.S. Hsiao, and B. Chu, *Functional electrospun nanofibrous scaffolds for biomedical applications.* Adv Drug Deliv Rev, 2007. **59**(14): p. 1392-412.
9. Gupta, K.C., et al., *Nanofibrous scaffolds in biomedical applications.* Biomater Res, 2014. **18**: p. 5.
10. Homaeigohar, S. and M. Elbahri, *Nanocomposite Electrospun Nanofiber Membranes for Environmental Remediation.* Materials, 2014. **7**(2): p. 1017-1045.

11. Sarkar, K., et al., *Electrospinning to Forcespinning (TM).* Materials Today, 2010. **13**(11): p. 12-14.

12. A., F., U. patent, Editor. 1934: US.

13. A, F., U. patent, Editor. 1939: US.

14. A, F., U. patent, Editor. 1940: US.

15. Formhals, U. patent, Editor. 1943: US.

16. HL, S., U. patent, Editor. 1966: US.

17. Ayutsede, J., et al., *Carbon nanotube reinforced Bombyx mori silk nanofibers by the electrospinning process.* Biomacromolecules, 2006. **7**(1): p. 208-14.

18. Sun, Z.C., et al., *Compound core-shell polymer nanofibers by co-electrospinning.* Advanced Materials, 2003. **15**(22): p. 1929-+.

19. Srivastava, Y., et al., *Electrospinning of hollow and core/sheath nanofibers using a microfluidic manifold.* Microfluidics and Nanofluidics, 2008. **4**(3): p. 245-250.

20. Teo, W.E. and S. Ramakrishna, *A review on electrospinning design and nanofibre assemblies.* Nanotechnology, 2006. **17**(14): p. R89-R106.

21. Yang, Y., et al., *A Shield Ring Enhanced Equilateral Hexagon Distributed Multi-needle Electrospinning Spinneret.* Ieee Transactions on Dielectrics and Electrical Insulation, 2010. **17**(5): p. 1592-1601.

22. Liu, Y., et al., *Multi-jet electrospinning via auxiliary electrode.* Materials Letters, 2015. **141**: p. 153-156.

23. Eda, G., J. Liu, and S. Shivkumar, *Solvent effects on jet evolution during electrospinning of semi-dilute polystyrene solutions.* European Polymer Journal, 2007. **43**(4): p. 1154-1167.

24. Yang, R.R., et al., *Bubble-electrospinning for fabricating nanofibers.* Polymer, 2009. **50**(24): p. 5846-5850.

25. Niu, H.T. and T. Lin, *Fiber Generators in Needleless Electrospinning.* Journal of Nanomaterials, 2012.

26. El-Newehy, M.H., et al., *Nanospider Technology for the Production of Nylon-6 Nanofibers for Biomedical Applications.* Journal of Nanomaterials, 2011.

27. Fukushima, S., Y. Karube, and H. Kawakami, *Preparation of ultrafine uniform electrospun polyimide nanofiber.* Polymer Journal, 2010. **42**(6): p. 514-518.

28. Wang, H., H. Shao, and X. Hu, *Structure of silk fibroin fibers made by an electrospinning process from a silk fibroin aqueous solution.* Journal of Applied Polymer Science, 2006. **101**(2): p. 961-968.

29. Zhao, S., et al., *Electrospinning of ethyl–cyanoethyl cellulose/tetrahydrofuran solutions.* Journal of Applied Polymer Science, 2004. **91**(1): p. 242-246.

30. Camposeo, A., et al., *Local Mechanical Properties of Electrospun Fibers Correlate to Their Internal Nanostructure.* Nano Letters, 2013. **13**(11): p. 5056-5062.

31. Ramakrishna, S., et al., *An Introduction to Electrospinning and Nanofibers*. 2005.

32. BHARGAVA, A.K., *ENGINEERING MATERIALS: POLYMERS, CERAMICS AND COMPOSITES*. 2012: PHI Learning.

33. Khorshidi, S., et al., *A review of key challenges of electrospun scaffolds for tissue-engineering applications.* J Tissue Eng Regen Med, 2015.

34. Reneker, D.H., et al., *Bending instability of electrically charged liquid jets of polymer solutions in electrospinning.* Journal of Applied Physics, 2000. **87**(9): p. 4531-4547.

35. Wu, X.F., Y. Salkovskiy, and Y.A. Dzenis, *Modeling of solvent evaporation from polymer jets in electrospinning.* Applied Physics Letters, 2011. **98**(22).

36. Shahreen, L. and G.G. Chase, *Effects of Electrospinning Solution Properties on Formation of Beads in Tio2 Fibers with PdO Particles.* Journal of Engineered Fibers and Fabrics, 2015. **10**(3): p. 136-145.

37. Dayal, P. and T. Kyu, *Porous fiber formation in polymer-solvent system undergoing solvent evaporation.* Journal of Applied Physics, 2006. **100**(4): p. 043512.

38. Chi Wang, K.-W.Y., Yi-Dong Lin,and Patrick C. H. Hsieh, *biodegradable core/shell fibers by coaxial electrospinning: Processing, fiber characterization, and its application in sustained drugh release.* Macromolecules, 2010. **43**: p. 6389-6397.

39. Chakraborty, S., et al., *Electrohydrodynamics: A facile technique to fabricate drug delivery systems.* Advanced Drug Delivery Reviews, 2009. **61**(12): p. 1043-1054.

40. Jiang, H., L. Wang, and K. Zhu, *Coaxial electrospinning for encapsulation and controlled release of fragile water-soluble bioactive agents.* J Control Release, 2014.

41. Beachley, V. and X.J. Wen, *Polymer nanofibrous structures: Fabrication, biofunctionalization, and cell interactions.* Progress in Polymer Science, 2010. **35**(7): p. 868-892.

42. Su, Y., et al., *Controlled release of dual drugs from emulsion electrospun nanofibrous mats.* Colloids and Surfaces B-Biointerfaces, 2009. **73**(2): p. 376-381.

43. Xu, X.L., et al., *Preparation of core-sheath composite nanofibers by emulsion electrospinning.* Macromolecular Rapid Communications, 2006. **27**(19): p. 1637-1642.

44. Yang, Y., et al., *Structural stability and release profiles of proteins from core-shell poly (DL-lactide) ultrafine fibers prepared by emulsion electrospinning.* Journal of Biomedical Materials Research Part A, 2008. **86A**(2): p. 374-385.

45. Xu, X.L., et al., *The release behavior of doxorubicin hydrochloride from medicated fibers prepared by emulsion-electrospinning.* European Journal of Pharmaceutics and Biopharmaceutics, 2008. **70**(1): p. 165-170.

46. Sahay, R., V. Thavasi, and S. Ramakrishna, *Design Modifications in Electrospinning Setup for Advanced Applications.* Journal of Nanomaterials, 2011.

47. Han, D. and A.J. Steckl, *Triaxial electrospun nanofiber membranes for controlled dual release of functional molecules.* ACS Appl Mater Interfaces, 2013. **5**(16): p. 8241-5.

48. Md. Fazley Elahi, W.L., Guan Guoping and Farzana Khan, *Core-shell Fibers for Biomedical Applications-A Review*. Bioengineering & Biomedical Sciences, 2013. **3**(1): p. 2155-9538.

49. Lam, C.X.F., S.H. Teoh, and D.W. Hutmacher, *Comparison of the degradation of polycaprolactone and polycaprolactone-(beta-tricalcium phosphate) scaffolds in alkaline medium.* Polymer International, 2007. **56**(6): p. 718-728.

50. Ghorbani, F.M., et al., *PCL/chitosan/Zn-doped nHA electrospun nanocomposite scaffold promotes adipose derived stem cells adhesion and proliferation.* Carbohydrate Polymers, 2015. **118**: p. 133-142.

51. Hong, J.K. and S.V. Madihally, *Next Generation of Electrosprayed Fibers for Tissue Regeneration.* Tissue Engineering Part B-Reviews, 2011. **17**(2): p. 125-142.

52. Kim, Y.E. and Y.J. Kim, *Effect of biopolymers on the characteristics and cytocompatibility of biocomposite nanofibrous scaffolds.* Polymer Journal, 2013. **45**(8): p. 845-853.

53. Lee, H.J., et al., *Biomedical Applications of Magnetically Functionalized Organic/Inorganic Hybrid Nanofibers.* International Journal of Molecular Sciences, 2015. **16**(6): p. 13661-13677.

54. Fu, W., et al., *Electrospun gelatin/PCL and collagen/PLCL scaffolds for vascular tissue engineering.* International Journal of Nanomedicine, 2014. **9**: p. 2335-2344.

55. Chong, E.J., et al., *Evaluation of electrospun PCL/gelatin nanofibrous scaffold for wound healing and layered dermal reconstitution.* Acta Biomaterialia, 2007. **3**(3): p. 321-330.

56. Tokiwa, Y., et al., *Biodegradability of Plastics.* International Journal of Molecular Sciences, 2009. **10**(9): p. 3722-3742.

57. Woodruff, M.A. and D.W. Hutmacher, *The return of a forgotten polymer-Polycaprolactone in the 21st century.* Progress in Polymer Science, 2010. **35**(10): p. 1217-1256.

58. Zhu, X., et al., *Anti-Neoplastic Cytotoxicity of SN-38-Loaded PCL/Gelatin Electrospun Composite Nanofiber Scaffolds against Human Glioblastoma Cells In Vitro.* J Pharm Sci, 2015. **104**(12): p. 4345-54.

59. Gomes, S.R., et al., *In vitro and in vivo evaluation of electrospun nanofibers of PCL, chitosan and gelatin: A comparative study.* Materials Science & Engineering C-Materials for Biological Applications, 2015. **46**: p. 348-358.

60. Yeo, M. and G. Kim, *Fabrication of cell-laden electrospun hybrid scaffolds of alginate-based bioink and PCL microstructures for tissue regeneration.* Chemical Engineering Journal, 2015. **275**: p. 27-35.

61. Zhang, Y.Z., et al., *Coaxial electrospinning of (fluorescein isothiocyanate-conjugated bovine serum albumin)-encapsulated poly(epsilon-caprolactone) nanofibers for sustained release*. Biomacromolecules, 2006. **7**(4): p. 1049-1057.

62. Pok, S.W., K.N. Wallace, and S.V. Madihally, *In vitro characterization of polycaprolactone matrices generated in aqueous media.* Acta Biomaterialia, 2010. **6**(3): p. 1061-1068.

63. Dash, T.K. and V.B. Konkimalla, *Polymeric Modification and Its Implication in Drug Delivery: Poly-epsilon-caprolactone (PCL) as a Model Polymer*. Molecular Pharmaceutics, 2012. **9**(9): p. 2365-2379.

64. Xue, J.J., et al., *Drug loaded homogeneous electrospun PCL/gelatin hybrid nanofiber structures for anti-infective tissue regeneration membranes.* Biomaterials, 2014. **35**(34): p. 9395-9405.

65. Han, J., et al., *Electrospun shikonin-loaded PCL/PTMC composite fiber mats with potential biomedical applications.* Int J Pharm, 2009. **382**(1-2): p. 215-21.

66. Bognitzki, M., et al., *Nanostructured fibers via electrospinning.* Advanced Materials, 2001. **13**(1): p. 70-+.

67. Yu, H., et al., *Fabrication of core/sheath PCL/PEG-PNIPAAm fibers as thermosensitive release carriers by a new technique combining blend electrospinning and ultraviolet-induced graft polymerization.* Materials Letters, 2016. **164**: p. 505-508.

68. Ferrand, A., et al., *Osteogenetic Properties of Electrospun Nanofibrous PCL Scaffolds Equipped With Chitosan-Based Nanoreservoirs of Growth Factors.* Macromolecular Bioscience, 2014. **14**(1): p. 45-55.

69. Roozbahani, F., et al., *Effects of Chitosan Alkali Pretreatment on the Preparation of Electrospun PCL/Chitosan Blend Nanofibrous Scaffolds for Tissue Engineering Application.* Journal of Nanomaterials, 2013.

70. Roozbahani, F., et al., *Effects of Chitosan Concentration on the Protein Release Behaviour of Electrospun Poly(epsilon-caprolactone)/Chitosan Nanofibers.* Journal of Nanomaterials, 2015.

71. Duda, S., et al., *Outer electrospun polycaprolactone shell induces massive foreign body reaction and impairs axonal regeneration through 3D multichannel chitosan nerve guides.* Biomed Res Int, 2014. **2014**: p. 835269.

72. Park, J.C., et al., *Electrospun poly(vinyl alcohol) nanofibers: effects of degree of hydrolysis and enhanced water stability.* Polymer Journal, 2010. **42**(3): p. 273-276.

73. Yao, L., et al., *Electrospinning and stabilization of fully hydrolyzed poly(vinyl alcohol) fibers.* Chemistry of Materials, 2003. **15**(9): p. 1860-1864.

74. Koosha, M. and H. Mirzadeh, *Electrospinning, mechanical properties, and cell behavior study of chitosan/PVA nanofibers.* Journal of Biomedical Materials Research Part A, 2015. **103**(9): p. 3081-3093.

75. Alhosseini, S.N., et al., *Synthesis and characterization of electrospun polyvinyl alcohol nanofibrous scaffolds modified by blending with chitosan for neural tissue engineering.* International Journal of Nanomedicine, 2012. **7**: p. 25-34.

76. Linh, N.T., et al., *Fabrication of polyvinyl alcohol/gelatin nanofiber composites and evaluation of their material properties.* J Biomed Mater Res B Appl Biomater, 2010. **95**(1): p. 184-91.

77. Puls, J., S.A. Wilson, and D. Holter, *Degradation of Cellulose Acetate-Based Materials: A Review.* Journal of Polymers and the Environment, 2011. **19**(1): p. 152-165.

78. Han, S.O., et al., *Electrospinning of cellulose acetate nanofibers using a mixed solvent of acetic acid/water: Effects of solvent composition on the fiber diameter.* Materials Letters, 2008. **62**(4–5): p. 759-762.

79. Tungprapa, S., et al., *Electrospun cellulose acetate fibers: effect of solvent system on morphology and fiber diameter.* Cellulose, 2007. **14**(6): p. 563-575.

80. Huang, C.B., et al., *Electrospun cellulose acetate phthalate fibers for semen induced anti-HIV vaginal drug delivery.* Biomaterials, 2012. **33**(3): p. 962-969.

81. Wu, X.M., et al., *Ester prodrug-loaded electrospun cellulose acetate fiber mats as transdermal drug delivery systems.* Journal of Materials Science-Materials in Medicine, 2010. **21**(8): p. 2403-2411.

82. Reshmi, G., P.M. Kumar, and M. Malathi, *Preparation, characterization and dielectric studies on carbonyl iron/cellulose acetate hydrogen phthalate core/shell nanoparticles for drug delivery applications.* International Journal of Pharmaceutics, 2009. **365**(1-2): p. 131-135.

83. Gouda, M., A.A. Hebeish, and A.I. Aljafari, *Synthesis and characterization of novel drug delivery system based on cellulose acetate electrospun nanofiber mats.* Journal of Industrial Textiles, 2014. **43**(3): p. 319-329.

84. Zhu, X., et al., *Electrospun fibrous mats with high porosity as potential scaffolds for skin tissue engineering.* Biomacromolecules, 2008. **9**(7): p. 1795-801.

85. Chantarodsakun, T., et al., *[6]-Gingerol-loaded cellulose acetate electrospun fibers as a topical carrier for controlled release.* Polymer Bulletin, 2014. **71**(12): p. 3163-3176.

86. Chen, C.Z., Y.Y. Zhao, and W.M. Liu, *Electrospun polyethylene glycol/cellulose acetate phase change fibers with core-sheath structure for thermal energy storage.* Renewable Energy, 2013. **60**: p. 222-225.

87. Khatri, Z., et al., *Effect of deacetylation on wicking behavior of co-electrospun cellulose acetate/polyvinyl alcohol nanofibers blend.* Carbohydrate Polymers, 2012. **87**(3): p. 2183-2188.

88. Li J, H.A., Aheng J, Han CC. , *Gelatin and gelatin hyaluronic acid nanofibrous membranes produced by electrospinning of their aqueous solutions.* Biomacromolecules, 2006(7): p. 2243-2247.

89. Liu X, S.L., Hu J, Ma PX, *Biomimetic nanofibrous gelatin/apatite compsite scaffolds for bone tissue engineering.* Biomaterials, 2009(30): p. 2252-2258.

90. Zhang Y, O.H., Lim CT, Ramakrishna S, Huang Zm, *Electrospinning of gelatin fibers and gelatin/PCL composite fibrous scafolds.* J Biomed Mater REs B Appl Biomater, 2005(72): p. 156-165.

91. Erencia, M., et al., *Electrospinning of gelatin fibers using solutions with low acetic acid concentration: Effect of solvent composition on both diameter of electrospun fibers and cytotoxicity.* Journal of Applied Polymer Science, 2015. **132**(25).

92. Choktaweesap, N., et al., *Electrospun gelatin fibers: Effect of solvent system on morphology and fiber diameters.* Polymer Journal, 2007. **39**(6): p. 622-631.

93. Huang, Z.M., et al., *Electrospinning and mechanical characterization of gelatin nanofibers.* Polymer, 2004. **45**(15): p. 5361-5368.

94. Lee, J., et al., *The effect of gelatin incorporation into electrospun poly(L-lactide-co-epsilon-caprolactone) fibers on mechanical properties and cytocompatibility.* Biomaterials, 2008. **29**(12): p. 1872-9.

95. Kolbuk, D., et al., *Structure and morphology of electrospun polycaprolactone/gelatine nanofibres.* European Polymer Journal, 2013. **49**(8): p. 2052-2061.

96. Zheng, R., et al., *The influence of Gelatin/PCL ratio and 3-D construct shape of electrospun membranes on cartilage regeneration.* Biomaterials, 2014. **35**(1): p. 152-64.

97. Yazdanpanah, A., et al., *Fabrication and characterization of electrospun poly-L-lactide/gelatin graded tubular scaffolds: Toward a new design for performance enhancement in vascular tissue engineering.* Progress in Natural Science-Materials International, 2015. **25**(5): p. 405-413.

98. Jaiswal, A.K., et al., *Improved functionalization of electrospun PLLA/gelatin scaffold by alternate soaking method for bone tissue engineering.* Applied Surface Science, 2013. **268**: p. 477-488.

99. Gautam, S., A.K. Dinda, and N.C. Mishra, *Fabrication and characterization of PCL/gelatin composite nanofibrous scaffold for tissue engineering applications by electrospinning method.* Materials Science & Engineering C-Materials for Biological Applications, 2013. **33**(3): p. 1228-1235.

100. Gautam, S., et al., *Surface modification of nanofibrous polycaprolactone/gelatin composite scaffold by collagen type I grafting for skin tissue engineering.* Materials Science & Engineering C-Materials for Biological Applications, 2014. **34**: p. 402-409.

101. Rajzer, I., et al., *Electrospun gelatin/poly(epsilon-caprolactone) fibrous scaffold modified with calcium phosphate for bone tissue engineering.* Mater Sci Eng C Mater Biol Appl, 2014. **44**: p. 183-90.

102. Feng, B., et al., *Effect of inhomogeneity of the electrospun fibrous scaffolds of gelatin/polycaprolactone hybrid on cell proliferation.* Journal of Biomedical Materials Research Part A, 2015. **103**(2): p. 431-438.

103. Zhang, Y.Z., et al., *Preparation of core-shell structured PCL-r-gelatin Bi-component nanofibers by coaxial electrospinning.* Chemistry of Materials, 2004. **16**(18): p. 3406-3409.

104. Kiatyongchai, T., S. Wongsasulak, and T. Yoovidhya, *Coaxial Electrospinning and Release Characteristics of Cellulose Acetate-Gelatin Blend Encapsulating a Model Drug.* Journal of Applied Polymer Science, 2014. **131**(8).

105. Sakuldao, S., T. Yoovidhya, and S. Wongsasulak, *Coaxial electrospinning and sustained release properties of gelatin-cellulose acetate core-shell ultrafine fibres.* Scienceasia, 2011. **37**(4): p. 335-343.

106. Zhao, P.C., et al., *Biodegradable fibrous scaffolds composed of gelatin coated poly(epsilon-caprolactone) prepared by coaxial electrospinning.* Journal of Biomedical Materials Research Part A, 2007. **83A**(2): p. 372-382.

107. Merkle, V. and W. Xiaoyi. *Coaxial electrospinning of gelatin/polyvinyl alcohol composite nanofibers and evaluation of their material properties*. in *Bioengineering Conference (NEBEC), 2012 38th Annual Northeast*. 2012.

108. Lee, J., et al., *The effect of controlled release of PDGF-BB from heparin-conjugated electrospun PCL/gelatin scaffolds on cellular bioactivity and infiltration.* Biomaterials, 2012. **33**(28): p. 6709-20.

109. Xue, J., et al., *Drug loaded homogeneous electrospun PCL/gelatin hybrid nanofiber structures for anti-infective tissue regeneration membranes.* Biomaterials, 2014. **35**(34): p. 9395-405.

110. Sikareepaisan, P., A. Suksamrarn, and P. Supaphol, *Electrospun gelatin fiber mats containing a herbal-Centella asiatica-extract and release characteristic of asiaticoside.* Nanotechnology, 2008. **19**(1): p. 015102.

111. Hu, J., et al., *Preparation and characterization of electrospun PLGA/gelatin nanofibers as a drug delivery system by emulsion electrospinning.* Journal of Biomaterials Science-Polymer Edition, 2013. **24**(8): p. 972-985.

112. Fathollahipour, S., et al., *Electrospinning of PVA/chitosan nanocomposite nanofibers containing gelatin nanoparticles as a dual drug delivery system.* Journal of Biomedical Materials Research Part A, 2015. **103**(12): p. 3852-3862.

113. Chew, S.Y., et al., *Mechanical properties of single electrospun drug-encapsulated nanofibres.* Nanotechnology, 2006. **17**(15): p. 3880-3891.

114. Gunn, J. and M.Q. Zhang, *Polyblend nanofibers for biomedical applications: perspectives and challenges.* Trends in Biotechnology, 2010. **28**(4): p. 189-197.

115. Agarwal, S., J.H. Wendorff, and A. Greiner, *Use of electrospinning technique for biomedical applications.* Polymer, 2008. **49**(26): p. 5603-5621.

116. Duconseille, A., et al., *Gelatin structure and composition linked to hard capsule dissolution: A review.* Food Hydrocolloids, 2015. **43**: p. 360-376.

117. Liu, X., Y. Won, and P.X. Ma, *Porogen-induced surface modification of nano-fibrous poly(L-lactic acid) scaffolds for tissue engineering.* Biomaterials, 2006. **27**(21): p. 3980-7.

118. Liu, X., et al., *Biomimetic nanofibrous gelatin/apatite composite scaffolds for bone tissue engineering.* Biomaterials, 2009. **30**(12): p. 2252-2258.

119. Zhang, R. and P.X. Ma, *Synthetic nano-fibrillar extracellular matrices with predesigned macroporous architectures.* J Biomed Mater Res, 2000. **52**(2): p. 430-8.

120. Walser, J. and S.J. Ferguson, *Oriented nanofibrous membranes for tissue engineering applications: Electrospinning with secondary field control.* J Mech Behav Biomed Mater, 2015.

121. Dhandayuthapani, B., et al., *Polymeric Scaffolds in Tissue Engineering Application: A Review.* International Journal of Polymer Science, 2011.

122. Bach, A.D., et al., *Engineering of muscle tissue.* Clin Plast Surg, 2003. **30**(4): p. 589-99.

123. Lee, K., E.A. Silva, and D.J. Mooney, *Growth factor delivery-based tissue engineering: general approaches and a review of recent developments.* J R Soc Interface, 2011. **8**(55): p. 153-70.

124. Berthiaume, F., T.J. Maguire, and M.L. Yarmush, *Tissue engineering and regenerative medicine: history, progress, and challenges.* Annu Rev Chem Biomol Eng, 2011. **2**: p. 403-30.

125. Rim, N.G., C.S. Shin, and H. Shin, *Current approaches to electrospun nanofibers for tissue engineering.* Biomedical Materials, 2013. **8**(1).

126. Wenjing Lu, J.S.a.X.J., *Recent advances in electrospinning technology and biomedical applications of electrospun fibers.* Journal of Materials Chemistry B, 2014. **2**: p. 2369.

127. Khalf, A., K. Singarapu, and S.V. Madihally, *Influence of solvent characteristics in triaxial electrospun fiber formation.* Reactive & Functional Polymers, 2015. **90**: p. 36-46.

128. Li, W., et al., *Formation of controllable hydrophilic/hydrophobic drug delivery systems by electrospinning of vesicles.* Langmuir, 2015. **31**(18): p. 5141-6.

129. Diaz, J.E., et al., *Controlled encapsulation of hydrophobic liquids in hydrophilic polymer nanofibers by co-electrospinning.* Advanced Functional Materials, 2006. **16**(16): p. 2110-2116.

130. Zamani, M., M.P. Prabhakaran, and S. Ramakrishna, *Advances in drug delivery via electrospun and electrosprayed nanomaterials.* Int J Nanomedicine, 2013. **8**: p. 2997-3017.

131. Kruger, B., et al., *Drug-induced impairment of renal function.* Deutsche Medizinische Wochenschrift, 2012. **137**(38): p. 1873-1877.

132. Natu, M.V., H.C. Sousa, and M.H. Gil, *Electrospun Drug-Eluting Fibers for Biomedical Applications*, in *Active Implants and Scaffolds for Tissue Regeneration*, M. Zilberman, Editor. 2011, Springer Berlin Heidelberg: Berlin, Heidelberg. p. 57-85.

133. Luong-Van, E., et al., *Controlled release of heparin from poly(epsilon-caprolactone) electrospun fibers.* Biomaterials, 2006. **27**(9): p. 2042-2050.

134. Wang, H., et al., *Controlled heparin release from electrospun gelatin fibers.* J Control Release, 2011. **152 Suppl 1**: p. e28-9.

135. Ji, W., et al., *Incorporation of stromal cell-derived factor-1alpha in PCL/gelatin electrospun membranes for guided bone regeneration.* Biomaterials, 2013. **34**(3): p. 735-45.

136. Viness Pillay, C.D., Yahya E. Choonara, Charu Tyagi, Lomas Tomar, Pradeep Kumar, Lisa C. du Toit, and Valence M. K. Ndesendo, *A Review of the Effect of Processing*

*Variables on the Fabrication of Electrospun Nanofibers for Drug Delivery Applications.* Journal of Nanomaterials, 2012. **2013**: p. 22.

137. Sill, T.J. and H.A. von Recum, *Electrospinning: applications in drug delivery and tissue engineering.* Biomaterials, 2008. **29**(13): p. 1989-2006.

138. Son, Y.J., W.J. Kim, and H.S. Yoo, *Therapeutic applications of electrospun nanofibers for drug delivery systems.* Arch Pharm Res, 2014. **37**(1): p. 69-78.

139. Khampieng, T., G.E. Wnek, and P. Supaphol, *Electrospun DOXY-h loaded-poly(acrylic acid) nanofiber mats: in vitro drug release and antibacterial properties investigation.* Journal of Biomaterials Science-Polymer Edition, 2014. **25**(12): p. 1292-1305.

140. Jiang, H., et al., *Modulation of protein release from biodegradable core-shell structured fibers prepared by coaxial electrospinning.* J Biomed Mater Res B Appl Biomater, 2006. **79**(1): p. 50-7.

141. Bochu Wang , Y.W., Tieying Yin & Qingsong Yu, *Applications of Electrospinning Technique in Drug Delivery* Chem. Eng. Comm, 2010. **197**: p. 1315–1338.

142. Sultanova, Z., et al., *Controlled release of a hydrophilic drug from coaxially electrospun polycaprolactone nanofibers.* Int J Pharm, 2016. **505**(1-2): p. 133-138.

143. Repanas, A. and B. Glasmacher, *Dipyridamole embedded in Polycaprolactone fibers prepared by coaxial electrospinning as a novel drug delivery system.* Journal of Drug Delivery Science and Technology, 2015. **29**: p. 132-142.

144. He, M., et al., *Fibrous guided tissue regeneration membrane loaded with anti-inflammatory agent prepared by coaxial electrospinning for the purpose of controlled release.* Applied Surface Science, 2015. **335**: p. 121-129.

145. Yu, H., et al., *PCL/PEG core/sheath fibers with controlled drug release rate fabricated on the basis of a novel combined technique.* International Journal of Pharmaceutics, 2014. **469**(1): p. 17-22.

146. Thuy, T.T.N., et al., *Porous core/sheath composite nanofibers fabricated by coaxial electrospinning as a potential mat for drug release system.* International Journal of Pharmaceutics, 2012. **439**(1-2): p. 296-306.

147. Llorens, E., et al., *Biocompatibility and drug release behavior of scaffolds prepared by coaxial electrospinning of poly(butylene succinate) and polyethylene glycol.* Materials Science & Engineering C-Materials for Biological Applications, 2015. **49**: p. 472-484.

148. Liao, I.C., S.Y. Chew, and K.W. Leong, *Aligned core-shell nanofibers delivering bioactive proteins.* Nanomedicine, 2006. **1**(4): p. 465-471.

149. Wang, C., et al., *Biodegradable Core/Shell Fibers by Coaxial Electrospinning: Processing, Fiber Characterization, and Its Application in Sustained Drug Release.* Macromolecules, 2010. **43**(15): p. 6389-6397.

150. Tang, Y.F., et al., *Fabrication of PLGA/HA (core)-collagen/amoxicillin (shell) nanofiber membranes through coaxial electrospinning for guided tissue regeneration.* Composites Science and Technology, 2016. **125**: p. 100-107.

151. Yang, J.M., et al., *Coaxial electrospinning with acetic acid for preparing ferulic acid/zein composite fibers with improved drug release profiles.* Colloids Surf B Biointerfaces, 2013. **102**: p. 737-43.

152. Yu, D.G., et al., *Linear drug release membrane prepared by a modified coaxial electrospinning process.* Journal of Membrane Science, 2013. **428**: p. 150-156.

153. Yu, D.G., et al., *Modified coaxial electrospinning for the preparation of high-quality ketoprofen-loaded cellulose acetate nanofibers.* Carbohydr Polym, 2012. **90**(2): p. 1016-23.

154. Castillo-Ortega, M.M., et al., *Preparation, characterization and release of amoxicillin from cellulose acetate and poly(vinyl pyrrolidone) coaxial electrospun fibrous membranes.* Materials Science & Engineering C-Materials for Biological Applications, 2011. **31**(8): p. 1772-1778.

155. Ball, C., et al., *Coaxially electrospun fiber-based microbicides facilitate broadly tunable release of maraviroc.* Materials Science and Engineering: C, 2016. **63**: p. 117-124.

156. Oliveira, M.F., et al., *Electrospun nanofibers of polyCD/PMAA polymers and their potential application as drug delivery system.* Materials Science & Engineering C-Materials for Biological Applications, 2015. **54**: p. 252-261.

157. Zupancic, S., et al., *Controlled Release of Ciprofloxacin from Core-Shell Nanofibers with Monolithic or Blended Core.* Mol Pharm, 2016. **13**(4): p. 1393-404.

158. Sohrabi, A., et al., *Sustained drug release and antibacterial activity of ampicillin incorporated poly(methyl methacrylate)–nylon6 core/shell nanofibers.* Polymer, 2013. **54**(11): p. 2699-2705.

159. Yu, D.G., et al., *Nanofibers Fabricated Using Triaxial Electrospinning as Zero Order Drug Delivery Systems.* Acs Applied Materials & Interfaces, 2015. **7**(33): p. 18891-18897.

160. Yu, H., et al., *PCL/PEG core/sheath fibers with controlled drug release rate fabricated on the basis of a novel combined technique.* Int J Pharm, 2014. **469**(1): p. 17-22.

161. Qian, W., et al., *Dual drug release electrospun core-shell nanofibers with tunable dose in the second phase.* Int J Mol Sci, 2014. **15**(1): p. 774-86.

162. Huang, Z.M., et al., *Encapsulating drugs in biodegradable ultrafine fibers through co-axial electrospinning.* J Biomed Mater Res A, 2006. **77**(1): p. 169-79.

163. Steckl, D.H.a.A.J., *triaxial electrospun nanofber membranes for controlled dual release of functional molecules.* Appl. Mater. Interfaces, 2013(5): p. 8241−8245.

164. Kim, W. and S.S. Kim, *Synthesis of biodegradable triple-layered capsules using a triaxial electrospray method.* Polymer, 2011. **52**(15): p. 3325-3336.

165. Wang, C., et al., *Biodegradable Core/Shell Fibers by Coaxial Electrospinning: Processing, Fiber Characterization, and Its Application in Sustained Drug Release.* Macromolecules, 2010. **43**(15): p. 6389-6397.

166. Tiwari, S.K., et al., *Optimizing partition-controlled drug release from electrospun core-shell fibers.* International Journal of Pharmaceutics, 2010. **392**(1-2): p. 209-217.

167. Korsmeyer, R.W., et al., *Mechanisms of solute release from porous hydrophilic polymers.* International Journal of Pharmaceutics, 1983. **15**(1): p. 25-35.

168. Hartman, O., et al., *Biofunctionalization of electrospun PCL-based scaffolds with perlecan domain IV peptide to create a 3-D pharmacokinetic cancer model.* Biomaterials, 2010. **31**(21): p. 5700-5718.

169. Hong, Y.L., et al., *Fabrication and Drug Delivery of Ultrathin Mesoporous Bioactive Glass Hollow Fibers.* Advanced Functional Materials, 2010. **20**(9): p. 1503-1510.

170. Natu, M.V., H.C. de Sousa, and M.H. Gil, *Effects of drug solubility, state and loading on controlled release in bicomponent electrospun fibers.* International Journal of Pharmaceutics, 2010. **397**(1–2): p. 50-58.

171. Xie, Z.W. and G. Buschle-Diller, *Electrospun Poly(D,L-lactide) Fibers for Drug Delivery: The Influence of Cosolvent and the Mechanism of Drug Release.* Journal of Applied Polymer Science, 2010. **115**(1): p. 1-8.

172. Tipduangta, P., et al., *Electrospun Polymer Blend Nanofibers for Tunable Drug Delivery: The Role of Transformative Phase Separation on Controlling the Release Rate.* Molecular Pharmaceutics, 2016. **13**(1): p. 25-39.

173. Du, J. and Y.L. Hsieh, *Cellulose/chitosan hybrid nanofibers from electrospinning of their ester derivatives.* Cellulose, 2009. **16**(2): p. 247-260.

174. Saraf, A., et al., *Regulated non-viral gene delivery from coaxial electrospun fiber mesh scaffolds.* J Control Release, 2010. **143**(1): p. 95-103.

175. Hong, J.K. and S.V. Madihally, *Next generation of electrosprayed fibers for tissue regeneration.* Tissue Eng Part B Rev, 2011. **17**(2): p. 125-42.

176. Yu, D.G., et al., *Zero-order drug release cellulose acetate nanofibers prepared using coaxial electrospinning.* Cellulose, 2013. **20**(1): p. 379-389.

177. Lee, Y.S. and T.L. Arinzeh, *Electrospun Nanofibrous Materials for Neural Tissue Engineering.* Polymers, 2011. **3**(1): p. 413-426.

178. Zussman, E.H., IL) , et al., *Medical Scaffold, Methods of Fabrication and Using Thereof*, U.S.P. Application, Editor. 03/19/2009

179. Woodruff, M.A. and D.W. Hutmacher, *The return of a forgotten polymer—Polycaprolactone in the 21st century.* Progress in Polymer Science, 2010. **35**(10): p. 1217-1256.

180. Oh, S.H., et al., *In vitro and in vivo characteristics of PCL scaffolds with pore size gradient fabricated by a centrifugation method.* Biomaterials, 2007. **28**(9): p. 1664-1671.

181. Sarasam, A. and S.V. Madihally, *Characterization of chitosan-polycaprolactone blends for tissue engineering applications.* Biomaterials, 2005. **26**(27): p. 5500-8.

182. Tiwari, S.K., et al., *Optimizing partition-controlled drug release from electrospun core-shell fibers.* Int J Pharm, 2010. **392**(1-2): p. 209-17.

183. Mirani, R.D., et al., *The stress relaxation characteristics of composite matrices etched to produce nanoscale surface features.* Biomaterials, 2009. **30**(5): p. 703-10.

184. Gouda, M., A.A. Hebeish, and M.A. Al-Omair, *Development of silver-containing nanocellulosics for effective water disinfection.* Cellulose, 2014. **21**(3): p. 1965-1974.

185. Zhang, Z.P., J. Hu, and P.X. Ma, *Nanofiber-based delivery of bioactive agents and stem cells to bone sites.* Advanced Drug Delivery Reviews, 2012. **64**(12): p. 1129-1141.

186. Sousa, M., et al., *Dynamical Characterization of a Cellulose Acetate Polysaccharide.* Journal of Physical Chemistry B, 2010. **114**(34): p. 10939-10953.

187. Liu, H.Q. and Y.L. Hsieh, *Ultrafine fibrous cellulose membranes from electrospinning of cellulose acetate.* Journal of Polymer Science Part B-Polymer Physics, 2002. **40**(18): p. 2119-2129.

188. Son, W.K., et al., *Electrospinning of ultrafine cellulose acetate fibers: Studies of a new solvent system and deacetylation of ultrafine cellulose acetate fibers.* Journal of Polymer Science Part B-Polymer Physics, 2004. **42**(1): p. 5-11.

189. Rodriguez, K., P. Gatenholm, and S. Renneckar, *Electrospinning cellulosic nanofibers for biomedical applications: structure and in vitro biocompatibility.* Cellulose, 2012. **19**(5): p. 1583-1598.

190. Sethuraman, V., et al., *Influence of scaffold forming techniques on stress relaxation behavior of polycaprolactone scaffolds.* Journal of Applied Polymer Science, 2013. **130**(6): p. 4237-4244.

191. Iyer, P., K.J. Walker, and S.V. Madihally, *Increased matrix synthesis by fibroblasts with decreased proliferation on synthetic chitosan-gelatin porous structures.* Biotechnol Bioeng, 2012. **109**(5): p. 1314-1325.

192. Hong, J.K., et al., *Analysis of void shape and size in the collector plate and polycaprolactone molecular weight on electrospun scaffold pore size.* Journal of Applied Polymer Science, 2013. **128**(3): p. 1583-1591.

193. Salihu, G., P. Goswami, and S. Russell, *Hybrid electrospun nonwovens from chitosan/cellulose acetate.* Cellulose, 2012. **19**(3): p. 739-749.

194. Kamide, K. and M. Saito, *Thermal-Analysis of Cellulose-Acetate Solids with Total Degrees of Substitution of 0.49, 1.75, 2.46, and 2.92.* Polymer Journal, 1985. **17**(8): p. 919-928.

195. Vince Beachley, X.W., *Effect of electrospinning parameters on the nanofiber diameter and length.* Materials Science and Engineering, 2009. **29**: p. 663–668.

196. Huanga, Z., et al., *A review on polymer nanofibers by electrospinning and their applications in nanocomposites.* Composites Science and Technology, 2003. **15**(63): p. 2223-2231.

197. Maleki, H., et al., *Influence of the solvent type on the morphology and mechanical properties of electrospun PLLA yarns.* Biofabrication, 2013. **5**(3): p. 035014.

198. Han, S.O., et al., *Ultrafine porous fibers electrospun from cellulose triacetate.* Materials Letters, 2005. **59**(24-25): p. 2998-3001.

199. Gopal, R., et al., *Electrospun nanofibrous filtration membrane.* Journal of Membrane Science, 2006. **281**(1-2): p. 581-586.

200. Tang, C., P. Chen, and H. Liu, *Cocontinuous cellulose acetate/polyurethane composite nanofiber fabricated through electrospinning.* Polymer Engineering & Science, 2008. **48**(7): p. 1296-1303.

201. Vatankhah, E., M.P. Prabhakaran, and S. Ramakrishna, *Biomimetic Nanostructures by Electrospinning and Electrospraying*, in *Stem-Cell Nanoengineering*. 2015, John Wiley & Sons, Inc. p. 123-141.

202. Du, J.M., S. Shintay, and X.W. Zhang, *Diameter control of electrospun polyacrylonitrile/iron acetylacetonate ultrafine nanofibers.* Journal of Polymer Science Part B-Polymer Physics, 2008. **46**(15): p. 1611-1618.

203. Li, D., et al., *Nanofibers of conjugated polymers prepared by electrospinning with a two-capillary spinneret.* Advanced Materials, 2004. **16**(22): p. 2062-+.

204. Pillay, V., et al., *A Review of the Effect of Processing Variables on the Fabrication of Electrospun Nanofibers for Drug Delivery Applications.* Journal of Nanomaterials, 2013.

205. Na, H.N., et al., *Fabrication of PVDF/PVA microtubules by coaxial electrospinning.* Polymer, 2012. **53**(13): p. 2736-2743.

206. Gautam, S., A.K. Dinda, and N.C. Mishra, *Fabrication and characterization of PCL/gelatin composite nanofibrous scaffold for tissue engineering applications by electrospinning method.* Mater Sci Eng C Mater Biol Appl, 2013. **33**(3): p. 1228-35.

207. Jiang, S.H., et al., *Highly Flexible and Tough Concentric Triaxial Polystyrene Fibers.* Acs Applied Materials & Interfaces, 2014. **6**(8): p. 5918-5923.

208. Liu, W.W., et al., *Preparation of Multilayer Biodegradable Nanofibers by Triaxial Electrospinning.* Acs Macro Letters, 2013. **2**(6): p. 466-468.

209. Yamawaki-Ogata, A., et al., *A doxycycline loaded, controlled-release, biodegradable fiber for the treatment of aortic aneurysms.* Biomaterials, 2010. **31**(36): p. 9554-9564.

210. Mondal, S., *Influence of solvents properties on morphology of electrospun polyurethane nanofiber mats.* Polymers for Advanced Technologies, 2014. **25**(2): p. 179-183.

211. Cascone, M.G., et al., *Bioartificial polymeric materials based on polysaccharides.* Journal of Biomaterials Science-Polymer Edition, 2001. **12**(3): p. 267-281.

212. Dias, J. and P. Bártolo, *Morphological Characteristics of Electrospun PCL Meshes – The Influence of Solvent Type and Concentration.* Procedia CIRP, 2013. **5**(0): p. 216-221.

213. Castillo-Ortega, M.M., et al., *Fibrous membranes of cellulose acetate and poly(vinyl pyrrolidone) by electrospinning method: Preparation and characterization.* Journal of Applied Polymer Science, 2010. **116**(4): p. 1873-1878.

214. Guo, Z., et al., *In vitro evaluation of random and aligned polycaprolactone/gelatin fibers via electrospinning for bone tissue engineering.* J Biomater Sci Polym Ed, 2015. **26**(15): p. 989-1001.

215. Zhang, Y., et al., *Electrospinning of gelatin fibers and gelatin/PCL composite fibrous scaffolds.* J Biomed Mater Res B Appl Biomater, 2005. **72**(1): p. 156-65.

216. Khalf, A., K. Singarapu, and S. Madihally, *Cellulose acetate core–shell structured electrospun fiber: fabrication and characterization.* Cellulose, 2015: p. 1-12.

217. Hong, J.K. and S.V. Madihally, *Three-dimensional scaffold of electrosprayed fibers with large pore size for tissue regeneration.* Acta Biomater, 2010. **6**(12): p. 4734-42.

218. Castillo-Ortega, M.M., et al., *Preparation, characterization and release of amoxicillin from cellulose acetate and poly(vinyl pyrrolidone) coaxial electrospun fibrous membranes.* Materials Science and Engineering: C, 2011. **31**(8): p. 1772-1778.

219. Zhang, S., et al., *Gelatin nanofibrous membrane fabricated by electrospinning of aqueous gelatin solution for guided tissue regeneration.* J Biomed Mater Res A, 2009. **90**(3): p. 671-9.

220. Yu, D.G., et al., *Coaxial electrospinning with sodium dodecylbenzene sulfonate solution for high quality polyacrylonitrile nanofibers.* Colloids and Surfaces a-Physicochemical and Engineering Aspects, 2012. **396**: p. 161-168.

221. Song, W., et al., *Coaxial PCL/PVA electrospun nanofibers: osseointegration enhancer and controlled drug release device.* Biofabrication, 2013. **5**(3): p. 035006.

222. Darby, R., *Chemical engineering fluid mechanics*. 2001. p. 64.

223. Anumolu, S.S., et al., *Doxycycline loaded poly(ethylene glycol) hydrogels for healing vesicant-induced ocular wounds.* Biomaterials, 2010. **31**(5): p. 964-974.

224. Kumari, A., S.K. Yadav, and S.C. Yadav, *Biodegradable polymeric nanoparticles based drug delivery systems.* Colloids Surf B Biointerfaces, 2010. **75**(1): p. 1-18.

225. Lu, W.J., J.S. Sun, and X.Y. Jiang, *Recent advances in electrospinning technology and biomedical applications of electrospun fibers.* Journal of Materials Chemistry B, 2014. **2**(17): p. 2369-2380.

226. Liao, I.C., S.Y. Chew, and K.W. Leong, *Aligned core-shell nanofibers delivering bioactive proteins.* Nanomedicine (Lond), 2006. **1**(4): p. 465-71.

227. Hu, X., et al., *Electrospinning of polymeric nanofibers for drug delivery applications.* J Control Release, 2014. **185**: p. 12-21.

228. Javali, M.A. and K.L. Vandana, *A comparative evaluation of atrigel delivery system (10% doxycycline hyclate) Atridox with scaling and root planing and combination therapy in treatment of periodontitis: A clinical study*. J Indian Soc Periodontol, 2012. **16**(1): p. 43-8.

229. Kai, D., S.S. Liow, and X.J. Loh, *Biodegradable polymers for electrospinning: Towards biomedical applications.* Materials Science & Engineering C-Materials for Biological Applications, 2014. **45**: p. 659-670.

230. Gautam, S., et al., *Surface modification of nanofibrous polycaprolactone/gelatin composite scaffold by collagen type I grafting for skin tissue engineering.* Mater Sci Eng C Mater Biol Appl, 2014. **34**: p. 402-9.

231. Huang, Z.M., et al., *Encapsulating drugs in biodegradable ultrafine fibers through co-axial electrospinning.* Journal of Biomedical Materials Research Part A, 2006. **77A**(1): p. 169-179.

232. Tormos, C.J., C. Abraham, and S.V. Madihally, *Improving the stability of chitosan-gelatin-based hydrogels for cell delivery using transglutaminase and controlled release of doxycycline.* Drug Delivery and Translational Research, 2015. **5**(6): p. 575-584.

233. Gautam, S., et al., *Fabrication and characterization of PCL/gelatin/chitosan ternary nanofibrous composite scaffold for tissue engineering applications.* Journal of Materials Science, 2014. **49**(3): p. 1076-1089.

234. Sahoo, S., et al., *Synthesis and Characterization of Chitosan-Polycaprolactone Blended with Organoclay for Control Release of Doxycycline.* Journal of Applied Polymer Science, 2010. **118**(6): p. 3167-3175.

235. Fan, Q., et al., *In vitro delivery of doxycycline hydrochloride based on a porous membrane-based aqueous–organic partitioning system.* Journal of Controlled Release, 2004. **98**(3): p. 355-365.

236. Zussman, E., et al., *Electrospun polyacrylonitrile/poly (methyl methacrylate)-derived turbostratic carbon micro-/nanotubes.* Advanced Materials, 2006. **18**(3): p. 348-353.

237. Lee, J., et al., *The effect of controlled release of PDGF-BB from heparin-conjugated electrospun PCL/gelatin scaffolds on cellular bioactivity and infiltration.* Biomaterials, 2012. **33**(28): p. 6709-6720.

238. Taepaiboon, P., U. Rungsardthong, and P. Supaphol, *Vitamin-loaded electrospun cellulose acetate nanofiber mats as transdermal and dermal therapeutic agents of vitamin A acid and vitamin E.* Eur J Pharm Biopharm, 2007. **67**(2): p. 387-97.

239. Costa, P. and J.M. Sousa Lobo, *Modeling and comparison of dissolution profiles.* Eur J Pharm Sci, 2001. **13**(2): p. 123-33.

# APPENDIX A

Polymers evaluated with ranges of operation parameters

| Polymer (wt %) | Core | Intermediate | Shell | Core FR(mL/h) | Shell FR(mL/h) | Observation | Jet behavior |
|---|---|---|---|---|---|---|---|
| -/20% | Oil | CA | - | 0.5 | 2 | Fibers membrane | Whipping |
| 20%/14% | PCL | CA | - | 1 | 2 | Thick fibers | Whipping |
| 14%/20% | CA | PCL | - | 1 | 3 | Few fibers (dripping) | Whipping |
| 2%/14% | Chitosan | CA | - | 0.5 | 2 | Poor spinning stability | Dripping |
| 14%/2% | CA | Chitosan | - | 1 | 2 | Poor spinning stability | Dripping |
| 10%/14% | Gelatin | CA | - | 0.5 | 3 | Poor spinning stability | Dripping |
| 14%/10% | CA | Gelatin | - | 1 | 3 | Poor spinning stability | Dripping |
| 14%/20% | Oil | CA | PCL | 0.1 | 3 | Uniform fibers | Whipping |
| 20%/14% | Oil | PCL | CA | 0.1 | 3 | Uniform fibers | Whipping |
| 2%/20%/14% | Chitosan | PCL | CA | 0.5 | 2 | Poor spinning stability | Dripping |
| 10%/20%/14% | Gelatin | PCL | CA | 0.5 | 2 | Poor spinning stability | Dripping |
| 20%/10% | Oil | PCL | PVA | 0.1 | 3 | Poor spinning stability | Whipping |
| 10%/20% | Oil | PVA | PCL | 0.1 | 3 | Uniform fibers | Whipping |

# APPENDIX B

## Solvent mixtures boiling points determined using a simulator

| | Liquid | | | Vapor | | |
|---|---|---|---|---|---|---|
| | 21 | | | 21 | | |
| Water Mo | Temp C | | Water Mo | Temp C | | |
| 0 | 151.772 | | 0 | 151.772 | | Water / DiMthFormamide at 101325.39 Pa By NRTL |
| 0.05 | 143.834 | | 0.236516 | 143.834 | | |
| 0.1 | 137.643 | | 0.394011 | 137.643 | | |
| 0.15 | 132.616 | | 0.506327 | 132.616 | | |
| 0.2 | 128.417 | | 0.590383 | 128.417 | 102 ℃ | |
| 0.25 | 124.839 | | 0.655592 | 124.839 | | |
| 0.3 | 121.742 | | 0.70762 | 121.742 | | |
| 0.35 | 119.031 | | 0.750087 | 119.031 | T C | |
| 0.4 | 116.634 | | 0.785418 | 116.634 | | |
| 0.45 | 114.499 | | 0.815305 | 114.499 | | |
| 0.5 | 112.583 | | 0.840973 | 112.583 | | |
| 0.55 | 110.853 | | 0.863331 | 110.853 | | |
| 0.6 | 109.281 | | 0.883081 | 109.281 | | |
| 0.65 | 107.845 | | 0.900778 | 107.845 | | |
| 0.7 | 106.522 | | 0.916878 | 106.522 | | |
| 0.75 | 105.294 | | 0.931768 | 105.294 | | |
| 0.8 | 104.144 | | 0.945797 | 104.144 | | |
| 0.85 | 103.056 | | 0.959291 | 103.056 | | 90% water 0.9 |
| 0.9 | 102.012 | | 0.972579 | 102.012 | | |
| 0.95 | 100.999 | | 0.986014 | 100.999 | | |
| 1 | 99.9985 | | 1 | 99.9985 | | |

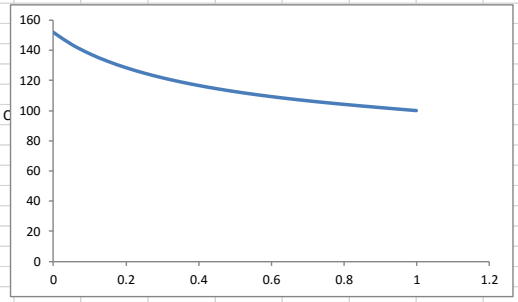


| | Liquid | | | Vapor | | |
|---|---|---|---|---|---|---|
| | 21 | | | 21 | | |
| Water Mo | Temp C | | Water Mo | Temp C | | |
| 0 | 64.4818 | | 0 | 64.4818 | | Water / Methanol at 101325.39 Pa By NRTL |
| 0.05 | 65.1876 | | 0.022141 | 65.1876 | | |
| 0.1 | 65.9076 | | 0.043683 | 65.9076 | | |
| 0.15 | 66.643 | | 0.064716 | 66.643 | 87.7℃ | |
| 0.2 | 67.3955 | | 0.085347 | 67.3955 | | |
| 0.25 | 68.1679 | | 0.105695 | 68.1679 | | |
| 0.3 | 68.9639 | | 0.125908 | 68.9639 | T C | |
| 0.35 | 69.7887 | | 0.146161 | 69.7887 | | |
| 0.4 | 70.6497 | | 0.166677 | 70.6497 | | |
| 0.45 | 71.5568 | | 0.187739 | 71.5568 | | |
| 0.5 | 72.5236 | | 0.209718 | 72.5236 | | |
| 0.55 | 73.5691 | | 0.233115 | 73.5691 | | |
| 0.6 | 74.7194 | | 0.258623 | 74.7194 | | |
| 0.65 | 76.0116 | | 0.287238 | 76.0116 | | |
| 0.7 | 77.4986 | | 0.320437 | 77.4986 | | |
| 0.75 | 79.2578 | | 0.360514 | 79.2578 | | |
| 0.8 | 81.4056 | | 0.411222 | 81.4056 | | 90% Water 0.9 |
| 0.85 | 84.1242 | | 0.479098 | 84.1242 | | |
| 0.9 | 87.7106 | | 0.576493 | 87.7106 | | |
| 0.95 | 92.6807 | | 0.729304 | 92.6807 | | |
| 1 | 99.9985 | | 1 | 99.9985 | | |

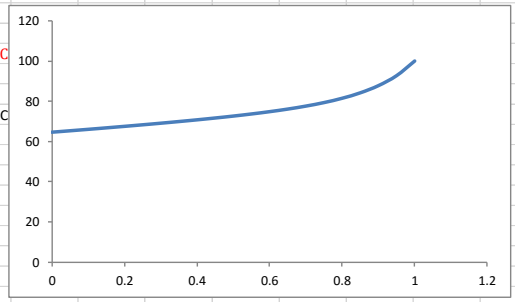

| | Liquid | | Vapor | | | |
|---|---|---|---|---|---|---|
| | 21 | | | 21 | | Chloroform / Acetic acid at 101325.39 Pa By NRTL |
| Chlorofori | Temp C | | Chlorofori | Temp C | | |
| 0 | 118.009 | | 0 | 118.009 | | |
| 0.05 | 104 | | 0.390953 | 104 | | |
| 0.1 | 95.5187 | | 0.564008 | 95.5187 | | |
| 0.15 | 89.7731 | | 0.659698 | 89.7731 | | |
| 0.2 | 85.5145 | | 0.721218 | 85.5145 | 69℃ | |
| 0.25 | 82.1414 | | 0.765034 | 82.1414 | | |
| 0.3 | 79.3399 | | 0.798514 | 79.3399 | | |
| 0.35 | 76.9351 | | 0.825378 | 76.9351 | T C | |
| 0.4 | 74.8245 | | 0.847685 | 74.8245 | | |
| 0.45 | 72.944 | | 0.866669 | 72.944 | | |
| 0.5 | 71.2539 | | 0.883117 | 71.2539 | | |
| 0.55 | 69.728 | | 0.897561 | 69.728 | | |
| 0.6 | 68.3488 | | 0.910387 | 68.3488 | | |
| 0.65 | 67.104 | | 0.921892 | 67.104 | | |
| 0.7 | 65.9843 | | 0.932327 | 65.9843 | | |
| 0.75 | 64.9811 | | 0.941934 | 64.9811 | | |
| 0.8 | 64.0845 | | 0.950991 | 64.0845 | | |
| 0.85 | 63.2792 | | 0.959901 | 63.2792 | | 55% Chloroform 0.54 |
| 0.9 | 62.5401 | | 0.969398 | 62.5401 | | |
| 0.95 | 61.8274 | | 0.981155 | 61.8274 | | |
| 1 | 61.0999 | | 1 | 61.0999 | | |

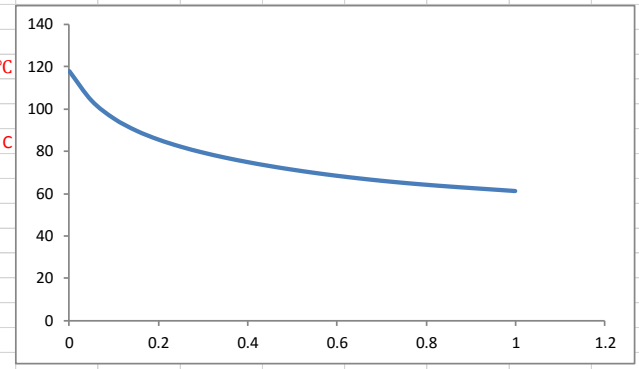


| | Liquid | | | Vapor | | |
|---|---|---|---|---|---|---|
| | 21 | | | 21 | | |
| Acetone M | Temp C | | Acetone M | Temp C | | |
| 0 | 101.444 | | 0 | 101.444 | | |
| 0.05 | 97.0285 | | 0.170383 | 97.0285 | | Acetone / 4-Dioxane at 101325.39 Pa By NRTL |
| 0.1 | 93.0506 | | 0.306539 | 93.0506 | | |
| 0.15 | 89.4475 | | 0.416834 | 89.4475 | | |
| 0.2 | 86.1666 | | 0.507302 | 86.1666 | | |
| 0.25 | 83.1645 | | 0.582358 | 83.1645 | | |
| 0.3 | 80.4046 | | 0.645276 | 80.4046 | 65.8 ℃ | |
| 0.35 | 77.8566 | | 0.698521 | 77.8566 | | |
| 0.4 | 75.4948 | | 0.743967 | 75.4948 | T C | |
| 0.45 | 73.2974 | | 0.783064 | 73.2974 | | |
| 0.5 | 71.2465 | | 0.816939 | 71.2465 | | |
| 0.55 | 69.3255 | | 0.846483 | 69.3255 | | |
| 0.6 | 67.5213 | | 0.872404 | 67.5213 | | |
| 0.65 | 65.8222 | | 0.895274 | 65.8222 | | |
| 0.7 | 64.2181 | | 0.915552 | 64.2181 | | |
| 0.75 | 62.7 | | 0.933618 | 62.7 | | |
| 0.8 | 61.2604 | | 0.949783 | 61.2604 | | |
| 0.85 | 59.8923 | | 0.964304 | 59.8923 | | |
| 0.9 | 58.5897 | | 0.977398 | 58.5897 | | |
| 0.95 | 57.3474 | | 0.989246 | 57.3474 | | 66% Acetone 0.6 |
| 1 | 56.1606 | | 1 | 56.1606 | | |

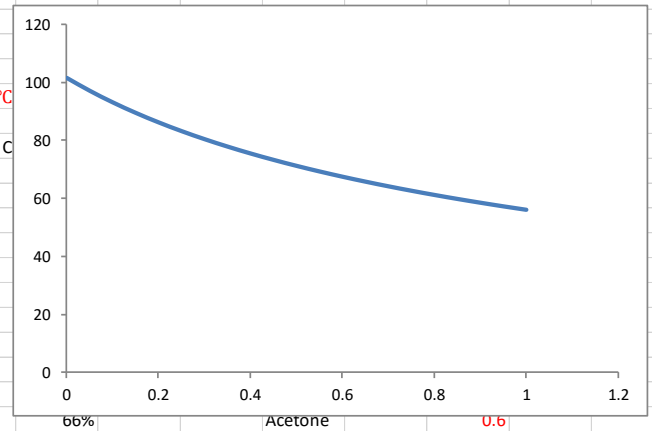

# APPENDIX C

## In vitro drug release data

| | control | Single | | single phase | | G+D | | PCL+D | | Tri+D | |
|---|---|---|---|---|---|---|---|---|---|---|---|
| Time (hr) | | | net | | net | | net | | net | | net |
| 0 | 0.2006 | 0.2944 | 0.094 | 0.1947 | -0.0059 | 0.21 | 0.0061 | 0.189 | -0.0116 | 0.1893 | -0.0113 |
| 8 | 0.1831 | 0.4055 | 0.222 | 0.3304 | 0.1473 | 0.32 | 0.1352 | 0.2281 | 0.045 | 0.2365 | 0.0534 |
| 24 | 0.1801 | 0.3922 | 0.212 | 0.3156 | 0.1355 | 0.3 | 0.1222 | 0.2204 | 0.0403 | 0.2355 | 0.0554 |
| 48 | 0.2177 | 0.3797 | 0.162 | 0.3055 | 0.0878 | 0.3 | 0.0795 | 0.2224 | 0.0047 | 0.2378 | 0.0201 |
| 72 | 0.236 | 0.3661 | 0.13 | 0.3 | 0.064 | 0.29 | 0.058 | 0.2198 | -0.0162 | 0.2361 | 0.0001 |
| 96 | 0.2338 | 0.3622 | 0.128 | 0.2979 | 0.0641 | 0.29 | 0.0584 | 0.2222 | -0.0116 | 0.2366 | 0.0028 |
| 120 | 0.2375 | 0.3636 | 0.126 | 0.2981 | 0.0606 | 0.3 | 0.0581 | 0.2174 | -0.0201 | 0.2423 | 0.0048 |
| | | | | | | | | | | | |
| Run # 2 | | | | | | | | | | | |
| Time (hr) | | | | | | | | | | | |
| | | | | | | | | | | | |
| 0 | 0.2006 | 0.2658 | 0.065 | 0.2108 | 0.0102 | 0.21 | 0.0089 | 0.1942 | -0.0064 | 0.188 | -0.0126 |
| 8 | 0.1831 | 0.4294 | 0.246 | 0.4037 | 0.2206 | 0.36 | 0.177 | 0.242 | 0.0589 | 0.2263 | 0.0432 |
| 24 | 0.1801 | 0.4049 | 0.225 | 0.3823 | 0.2022 | 0.34 | 0.1593 | 0.2344 | 0.0543 | 0.2172 | 0.0371 |
| 48 | 0.2177 | 0.3865 | 0.169 | 0.3677 | 0.15 | 0.33 | 0.1149 | 0.2473 | 0.0296 | 0.2235 | 0.0058 |
| 72 | 0.236 | 0.3806 | 0.145 | 0.3582 | 0.1222 | 0.33 | 0.0933 | 0.2349 | -0.0011 | 0.2235 | -0.0125 |
| 96 | 0.2338 | 0.3723 | 0.139 | 0.3533 | 0.1195 | 0.32 | 0.0911 | 0.2334 | -0.0004 | 0.2235 | -0.0103 |
| 120 | 0.2375 | 0.3731 | 0.136 | 0.3515 | 0.114 | 0.32 | 0.0864 | 0.2352 | -0.0023 | 0.2276 | -0.0099 |
| | | | | | | | | | | | |
| Run # 3 | | | | | | | | | | | |
| Time (hr) | | | | | | | | | | | |
| | | | | | | | | | | | |
| 0 | 0.2006 | 0.3123 | 0.112 | 0.1997 | -0.0009 | 0.21 | 0.0076 | 0.1882 | -0.0124 | 0.193 | -0.0076 |
| 8 | 0.1831 | 0.5022 | 0.319 | 0.4121 | 0.229 | 0.33 | 0.145 | 0.2185 | 0.0354 | 0.2162 | 0.0331 |
| 24 | 0.1801 | 0.4736 | 0.294 | 0.3862 | 0.2061 | 0.31 | 0.132 | 0.2158 | 0.0357 | 0.2133 | 0.0332 |
| 48 | 0.2177 | 0.4501 | 0.232 | 0.3659 | 0.1482 | 0.31 | 0.0938 | 0.2203 | 0.0026 | 0.224 | 0.0063 |
| 72 | 0.236 | 0.4372 | 0.201 | 0.3559 | 0.1199 | 0.31 | 0.072 | 0.2151 | -0.0209 | 0.2271 | -0.0089 |
| 96 | 0.2338 | 0.4341 | 0.2 | 0.3505 | 0.1167 | 0.31 | 0.0736 | 0.2133 | -0.0205 | 0.2224 | -0.0114 |
| 120 | 0.2375 | 0.4375 | 0.2 | 0.3544 | 0.1169 | 0.3 | 0.0648 | 0.2204 | -0.0171 | 0.2314 | -0.0061 |

| | Concentration | | | | | |
|---|---|---|---|---|---|---|
| | single | single phase | G | PCL | triaxial | |
| | | | | | | |
| 0 | 0.038068182 | -0.002394481 | 0.002475649 | -0.004707792 | -0.004586039 | |
| 8 | 0.09025974 | 0.059780844 | 0.05487013 | 0.018262987 | 0.021672078 | |
| 24 | 0.086079545 | 0.054991883 | 0.049594156 | 0.016355519 | 0.022483766 | |
| 48 | 0.065746753 | 0.035633117 | 0.03226461 | 0.001907468 | 0.008157468 | |
| 72 | 0.052800325 | 0.025974026 | 0.023538961 | -0.006574675 | 4.05844E-05 | |
| 96 | 0.05211039 | 0.02601461 | 0.023701299 | -0.004707792 | 0.001136364 | |
| 120 | 0.051176948 | 0.024594156 | 0.023579545 | -0.008157468 | 0.001948052 | |
| | | | | | | |
| | | | | | | |
| | single | Sinlge-ph | G | PCL | triaxial | |
| | | | | | | |
| 0 | 0.026461039 | 0.00413961 | 0.003612013 | -0.002597403 | -0.005113636 | |
| 8 | 0.099959416 | 0.089529221 | 0.071834416 | 0.023904221 | 0.017532468 | |
| 24 | 0.091233766 | 0.082061688 | 0.064650974 | 0.022037338 | 0.015056818 | |
| 48 | 0.068506494 | 0.060876623 | 0.046631494 | 0.012012987 | 0.002353896 | |
| 72 | 0.058685065 | 0.049594156 | 0.03786526 | -0.000446429 | -0.005073052 | |
| 96 | 0.056209416 | 0.048498377 | 0.036972403 | -0.000162338 | -0.004180195 | |
| 120 | 0.055032468 | 0.046266234 | 0.035064935 | -0.000933442 | -0.004017857 | |
| | | | | | | |
| | | | | | | |
| | | | | | | |
| | single | Sinlge-ph | G | PCL | triaxial | |
| 0 | 0.045332792 | -0.00036526 | 0.003084416 | -0.005032468 | -0.003084416 | |
| 8 | 0.12950487 | 0.092938312 | 0.058847403 | 0.014366883 | 0.013433442 | |
| 24 | 0.11911526 | 0.083644481 | 0.053571429 | 0.014488636 | 0.013474026 | |
| 48 | 0.094318182 | 0.060146104 | 0.038068182 | 0.001055195 | 0.002556818 | |
| 72 | 0.081655844 | 0.048660714 | 0.029220779 | -0.008482143 | -0.003612013 | |
| 96 | 0.081290584 | 0.047362013 | 0.02987013 | -0.008319805 | -0.004626623 | |
| 120 | 0.081168831 | 0.047443182 | 0.026298701 | -0.006939935 | -0.002475649 | |

| | | | | | concentratioin of doxy in the solution | | | | |
|---|---|---|---|---|---|---|---|---|---|
| | micro/mL | | | | Mass | | | | |
| | | | | **single** | | | | | K= |
| 0 | 0.0381 | 0.02646 | 0.04533 | **0.03662** | 0.028950216 | -0.203192641 | 0.174242424 | **7.4015E-17** | |
| 8 | 0.0903 | 0.09996 | 0.1295 | **0.10657** | 1.019142316 | 1.203436147 | 1.764799784 | **1.32912608** | |
| 24 | 0.0861 | 0.09123 | 0.11912 | **0.09881** | 0.89025974 | 0.983035714 | 1.484902597 | **1.11939935** | |
| 48 | 0.0657 | 0.06851 | 0.09432 | **0.07619** | 0.495143398 | 0.542058983 | 0.980857684 | **0.67268669** | |
| 72 | 0.0528 | 0.05869 | 0.08166 | **0.06438** | 0.258874459 | 0.353030303 | 0.720562771 | **0.44415584** | |
| 96 | 0.0521 | 0.05621 | 0.08129 | **0.0632** | 0.232345779 | 0.293831169 | 0.670048701 | **0.39874188** | |
| 120 | 0.0512 | 0.05503 | 0.08117 | **0.06246** | 0.203787879 | 0.257765152 | 0.623674242 | **0.36174242** | |
| | | | | | | | | | |
| | | | | | | | | | |
| | | | | Sinlge-ph | | | | | |
| 0 | -0.002 | 0.00414 | -0.0004 | **0.00046** | -0.057088745 | 0.073593074 | -0.016504329 | **0** | |
| 8 | 0.0598 | 0.08953 | 0.09294 | **0.08075** | 1.127096861 | 1.692316017 | 1.757088745 | **1.52550054** | |
| 24 | 0.055 | 0.08206 | 0.08364 | **0.07357** | 0.981574675 | 1.468831169 | 1.497321429 | **1.31590909** | |
| 48 | 0.0356 | 0.06088 | 0.06015 | **0.05222** | 0.597943723 | 1.027083333 | 1.014664502 | **0.87989719** | |
| 72 | 0.026 | 0.04959 | 0.04866 | **0.04141** | 0.408225108 | 0.786147186 | 0.771212121 | **0.65519481** | |
| 96 | 0.026 | 0.0485 | 0.04736 | **0.04063** | 0.383319805 | 0.720576299 | 0.703530844 | **0.60247565** | |
| 120 | 0.0246 | 0.04627 | 0.04744 | **0.03943** | 0.337878788 | 0.641287879 | 0.657765152 | **0.54564394** | |
| | | | | | | | | | |
| | | | | G | | | | | |
| 0 | 0.0025 | 0.00361 | 0.00308 | **0.00306** | -0.011634199 | 0.011093074 | 0.000541126 | -2.891E-18 | |
| 8 | 0.0549 | 0.07183 | 0.05885 | **0.06185** | 0.984442641 | 1.306764069 | 1.060010823 | 1.11707251 | |
| 24 | 0.0496 | 0.06465 | 0.05357 | **0.05594** | 0.837662338 | 1.108685065 | 0.909253247 | 0.95186688 | |
| 48 | 0.0323 | 0.04663 | 0.03807 | **0.03899** | 0.496523268 | 0.740760281 | 0.595183983 | 0.61082251 | |
| 72 | 0.0235 | 0.03787 | 0.02922 | **0.03021** | 0.327705628 | 0.556926407 | 0.418614719 | 0.43441558 | |
| 96 | 0.0237 | 0.03697 | 0.02987 | **0.03018** | 0.309659091 | 0.508725649 | 0.402191558 | 0.40685877 | |
| 120 | 0.0236 | 0.03506 | 0.0263 | **0.02831** | 0.287310606 | 0.448106061 | 0.325378788 | 0.35359848 | |
| | | | | **PCL** | | | | | |
| 0 | -0.005 | -0.0026 | -0.005 | **-0.0041** | -0.011904762 | 0.03030303 | -0.018398268 | 1.1565E-17 | |
| 8 | 0.0183 | 0.0239 | 0.01437 | **0.01884** | 0.425135281 | 0.532318723 | 0.351109307 | 0.43618777 | |
| 24 | 0.0164 | 0.02204 | 0.01449 | **0.01763** | 0.368425325 | 0.470698052 | 0.334821429 | 0.39131494 | |
| 48 | 0.0019 | 0.01201 | 0.00106 | **0.00499** | 0.102340368 | 0.274134199 | 0.087851732 | 0.15477543 | |
| 72 | -0.007 | -0.00045 | -0.0085 | **-0.0052** | -0.039393939 | 0.058658009 | -0.06991342 | -0.0168831 | |
| 96 | -0.005 | -0.00016 | -0.0083 | **-0.0044** | -0.008928571 | 0.059253247 | -0.063108766 | -0.0042614 | |
| 120 | -0.008 | -0.00093 | -0.0069 | **-0.0053** | -0.056628788 | 0.044507576 | -0.039583333 | -0.0172348 | |
| | | | | | | | | | |
| | | | | triaxial | | | | | |
| 0 | 0 | 0 | 0 | **0** | 0 | 0 | 0 | 0 | |
| 8 | 0.0217 | 0.01753 | 0.01343 | **0.01755** | 0.411769481 | 0.333116883 | 0.25523539 | 0.33337392 | |
| 24 | 0.0225 | 0.01506 | 0.01347 | **0.017** | 0.404707792 | 0.271022727 | 0.242532468 | 0.30608766 | |
| 48 | 0.0082 | 0.00235 | 0.00256 | **0.00436** | 0.138676948 | 0.040016234 | 0.043465909 | 0.07405303 | |
| 72 | 4E-05 | -0.00507 | -0.0036 | **-0.0029** | 0.000649351 | -0.081168831 | -0.057792208 | -0.0461039 | |
| 96 | 0.0011 | -0.00418 | -0.0046 | **-0.0026** | 0.017045455 | -0.062702922 | -0.069399351 | -0.0383523 | |
| 120 | 0.0019 | -0.00402 | -0.0025 | **-0.0015** | 0.027272727 | -0.05625 | -0.034659091 | -0.0212121 | |

| | | | | | | | | | |
|---|---|---|---|---|---|---|---|---|---|
| | | | | | Cummulative | | | | |
| K=kd.Cdox/(1-exp(-kd*t)) | | | | | | | | | |
| 0 | 0 | 0 | 0 | 0.0366 | 0 | 0 | 0 | **0** | **0** |
| 8 | 14.472 | 17.089 | 25.06 | | 14.47182089 | 17.088793 | 25.06015693 | **18.87359** | **5.51519** |
| 24 | 12.642 | 13.959 | 21.086 | | 27.1135092 | 31.0479 | 46.14577381 | **34.76906** | **10.047** |
| 48 | 7.031 | 7.6972 | 13.928 | | 34.14454545 | 38.745138 | 60.07395292 | **44.32121** | **13.8348** |
| 72 | 3.676 | 5.013 | 10.232 | 0 | 37.82056277 | 43.758168 | 70.30594426 | **50.62823** | **17.2981** |
| 96 | 3.2993 | 4.1724 | 9.5147 | | 41.11987284 | 47.930571 | 79.82063582 | **56.29036** | **20.6604** |
| 120 | 2.8938 | 3.6603 | 8.8562 | | 44.01366071 | 51.590836 | 88.67681006 | **70.13382** | **23.9011** |
| | | | | | | | | **#REF!** | |
| | | | | | | | | | |
| | | | | | | | | | |
| 0 | 0 | 0 | 0 | | 0 | 0 | 0 | **0** | **0** |
| 8 | 16.005 | 24.031 | 24.951 | | 16.00477543 | 24.030887 | 24.95066017 | **21.66211** | **4.92093** |
| 24 | 13.938 | 20.857 | 21.262 | | 29.94313582 | 44.88829 | 46.21262446 | **40.34802** | **9.03519** |
| 48 | 8.4908 | 14.585 | 14.408 | | 38.43393669 | 59.472873 | 60.62086039 | **52.84256** | **12.4914** |
| 72 | 5.7968 | 11.163 | 10.951 | | 44.23073323 | 70.636163 | 71.57207251 | **62.14632** | **15.5224** |
| 96 | 5.4431 | 10.232 | 9.9901 | | 49.67387446 | 80.868347 | 81.5622105 | **70.70148** | **18.2137** |
| 120 | 4.7979 | 9.1063 | 9.3403 | | 54.47175325 | 89.974635 | 90.90247565 | **78.44962** | **20.7706** |
| | | | | | | | | **#REF!** | |
| | | | | | | | | | |
| 0 | 0 | 0 | 0 | | 0 | 0 | 0 | **0** | **0** |
| 8 | 13.979 | 18.556 | 15.052 | | 13.9790855 | 18.55605 | 15.05215368 | **15.86243** | **2.39365** |
| 24 | 11.895 | 15.743 | 12.911 | | 25.87389069 | 34.299378 | 27.96354978 | **29.37894** | **4.38745** |
| 48 | 7.0506 | 10.519 | 8.4516 | | 32.9245211 | 44.818174 | 36.41516234 | **38.05262** | **6.11357** |
| 72 | 4.6534 | 7.9084 | 5.9443 | | 37.57794102 | 52.726529 | 42.35949134 | **44.22132** | **7.74401** |
| 96 | 4.3972 | 7.2239 | 5.7111 | | 41.97510011 | 59.950433 | 48.07061147 | **49.99871** | **9.14146** |
| 120 | 4.0798 | 6.3631 | 4.6204 | | 46.05491071 | 66.313539 | 52.69099026 | **55.01981** | **10.3281** |
| | | | | | | | | **#REF!** | |
| 0 | 0 | 0 | 0 | | 0 | 0 | 0 | **0** | **0** |
| 8 | 6.0369 | 7.5589 | 4.9858 | | 6.036920996 | 7.5589259 | 4.985752165 | **6.193866** | **1.29375** |
| 24 | 5.2316 | 6.6839 | 4.7545 | | 11.26856061 | 14.242838 | 9.74021645 | **11.75054** | **2.28968** |
| 48 | 1.4532 | 3.8927 | 1.2475 | | 12.72179383 | 18.135544 | 10.98771104 | **13.94835** | **3.72843** |
| 72 | -0.5594 | 0.8329 | -0.9928 | | 12.16239989 | 18.968488 | 9.994940476 | **13.70861** | **4.68233** |
| 96 | -0.1268 | 0.8414 | -0.8961 | | 12.03561418 | 19.809884 | 9.098795996 | **13.6481** | **5.53461** |
| 120 | -0.8041 | 0.632 | -0.5621 | | 11.23148539 | 20.441891 | 8.536712662 | **13.40336** | **6.24268** |
| | | | | | | | | | |
| | | | | | | | | | |
| 0 | 0 | 0 | 0 | | | | | | |
| 8 | 5.8471 | 4.7303 | 3.6243 | | | | | | |
| 24 | 5.7469 | 3.8485 | 3.444 | | | | | | |
| 48 | 1.9692 | 0.5682 | 0.6172 | | | | | | |
| 72 | 0.0092 | -1.1526 | -0.8206 | | | | | | |
| 96 | 0.242 | -0.8904 | -0.9855 | | | | | | |
| 120 | 0.3873 | -0.7987 | -0.4922 | | | | | | |
| | | | | | | | | | |
| | | | | | | | | | |
| | | | | | | | | | |

| | | | | | | | |
|---|---|---|---|---|---|---|---|
| 0 | 0 | 0 | 0 | **0** | **0** | 0.036620671 | 0. |
| 8 | 0.328802936 | 0.331236991 | 0.28260102 | **0.3142136** | **0.027404378** | | |
| 24 | 0.61602486 | 0.601810376 | 0.52038153 | **0.5794056** | **0.051608068** | | |
| 48 | 0.775771542 | 0.751008143 | 0.67744829 | **0.7347427** | **0.051139909** | | |
| 72 | 0.85929146 | 0.84817715 | 0.79283348 | **0.833434** | **0.035597546** | | |
| 96 | 0.934252506 | 0.929052029 | 0.90012976 | **0.9211448** | **0.018384343** | | |
| 120 | 1 | 1 | 1 | **1** | **0** | | |
| | | | | | | | |
| | | | | | | | |
| | | | | | | | |
| 0 | 0 | 0 | 0 | **0** | **0** | | |
| 8 | 0.322197042 | 0.297160612 | 0.30590956 | **0.3084224** | **0.012705963** | | |
| 24 | 0.60279445 | 0.555078616 | 0.56659358 | **0.5748222** | **0.024899459** | **average** | |
| 48 | 0.773725366 | 0.735428331 | 0.7432469 | **0.7508002** | **0.020234993** | **STD** | **0.** |
| 72 | 0.890422455 | 0.873471094 | 0.87751511 | **0.8804696** | **0.008853456** | | Ne |
| 96 | 1 | 1 | 1 | **1** | **0** | | |
| | | | | | | | |
| | | | | | | **average** | |
| | | | | | | **STD** | |
| 0 | 0 | 0 | 0 | **0** | **0** | | |
| 8 | 0.333032809 | 0.309523199 | 0.3131259 | **0.3185606** | **0.012662057** | | |
| 24 | 0.616410458 | 0.572128941 | 0.5817182 | **0.5900859** | **0.023296492** | | |
| 48 | 0.784382194 | 0.747587157 | 0.75753483 | **0.7631681** | **0.019033356** | **average** | |
| 72 | 0.895243631 | 0.879502051 | 0.8811931 | **0.8853129** | **0.008641704** | **STD** | |
| 96 | 1 | 1 | 1 | **1** | **0** | | |
| | | | | | | | |
| | | | | | | | |
| 0 | 0 | 0 | 0 | **0** | **0** | | |
| 8 | 0.537499786 | 0.369776249 | 0.54795735 | **0.4850778** | **0.099990876** | | |
| 24 | 0.936268016 | 0.696747578 | 1.07049509 | **0.9011702** | **0.189329586** | | |
| 48 | 1.057012434 | 0.887175439 | 1.20760055 | **1.0505961** | **0.160308887** | | |
| 72 | 1.010534212 | 0.92792234 | 1.09849045 | **1.0123157** | **0.085298006** | | |
| 96 | 1 | 0.969082725 | 1 | **0.9896942** | **0.017850097** | | |
| | | 1 | | | | | |
| | | | | | | | |

| The total amount of Doxy loaded | | | | | | | |
|---|---|---|---|---|---|---|---|
| | Control | Single | Co single | Co G | Co PCL | Triaxial | Final |
| | | | | | | | |
| 0.036620671 | 0.2092 | 2.7042 | 2.1752 | 1.861 | 1.3 | 1.4535 | 1.2 |
| | 0.3032 | 2.8142 | 2.3276 | 2.2996 | 1.095 | 1.5539 | 1.22 |
| | 0.2411 | 2.8329 | 2.6928 | 2.3365 | 1.063 | 2.2465 | 1.21 |
| | 0.2899 | | | | | | |
| | 0.2785 | | | | | | |
| | | | | | | | |
| | | | | | | | |
| | | | | | | | |
| | | | | | | | |
| | | | | | | | |
| | | | | | | | |
| | | | | | | | |
| **0.26438** | **2.783766667** | **2.39853333** | **2.1657** | **1.1526667** | **1.7513** | | |
| **0.038550058** | **0.069538215** | **0.26599078** | **0.264522154** | **0.1285937** | **0.43178388** | | |
| Net | 2.43982 | 1.91082 | 1.59662 | 1.03562 | 1.18912 | 0.93562 | |
| | 2.54982 | 2.06322 | 2.03522 | 0.83062 | 1.28952 | 0.95562 | |
| | 2.56852 | 2.42842 | 2.07212 | 0.79862 | 1.98212 | 0.94562 | |
| | **2.519386667** | **2.13415333** | **1.90132** | **0.8882867** | **1.48692** | **0.94562** | |
| | **0.069538215** | **0.26599078** | **0.264522154** | **0.1285937** | **0.43178388** | **0.01** | |
| | 34.65653409 | 27.1423295 | 22.67926136 | 14.710511 | 16.8909091 | 132.90057 | |
| | 36.21903409 | 29.3071023 | 28.909375 | 11.79858 | 18.3170455 | 135.74148 | |
| | #VALUE! | 34.4946023 | 29.43352273 | 11.344034 | 28.1551136 | 134.32102 | |
| | **#VALUE!** | **30.314678** | **27.00738636** | **12.617708** | **21.1210227** | **134.32102** | **average** |
| | **#VALUE!** | **3.77827808** | **3.757416961** | **1.8266147** | **6.13329377** | **1.4204545** | **STD** |

| Control | | Single | | Co single | | Co G | | Co PCL | | Triaxial | | |
|---|---|---|---|---|---|---|---|---|---|---|---|---|
| 0.21 | 0.28 | 2.7 | 0.83 | 2.18 | 1.2 | 1.86 | 1.22 | 1.3 | 0.68 | 1.45 | 0.596 | |
| 0.3 | 0.28 | 2.81 | 0.83 | 2.33 | 1.22 | 2.3 | 1.23 | 1.095 | 0.68 | 1.55 | 0.597 | |
| 0.24 | 0.28 | 2.83 | 0.83 | 2.69 | 1.21 | 2.34 | 1.23 | 1.063 | 0.67 | 2.25 | 0.598 | |
| | | | | | | | | | | | | |
| | | | | | 0.72 | | 0.66 | | 0.44 | | 0.381 | |
| | | | | | | | 0.65 | | 0.44 | | 0.383 | |
| | | | | | | | 0.65 | | 0.44 | | 0.382 | |
| **0.25** | **0.28** | | **0.83** | | **1.21** | | | | | | | |
| pure s | Control | | Single | | Co single | | Co G | | Co PCL | | Triaxial | |
| 0.18 | 0.24 | | 0.64 | | 0.761 | | 0.86 | | 0.45 | | 0.406 | A |
| 0.18 | 0.25 | | 0.64 | | 0.76 | | 0.86 | | 0.46 | | 0.382 | A |
| 0.18 | 0.25 | | 0.64 | | 0.759 | | 0.86 | | 0.46 | | 0.357 | A |
| ave(c | 0.25 | | | | | | | | | | | |
| | | | | | Net = actual -ave control | | | | | | | |
| | -0 | | 0.4 | | 0.515 | | 0.61 | | 0.2 | | 0.159 | |
| | 0 | | 0.39 | | 0.513 | | 0.61 | | 0.21 | | 0.135 | |
| | -0 | | 0.39 | | 0.512 | | 0.61 | | 0.21 | | 0.111 | |
| | | | | | | | | | | | | micrg/ml |
| | 0.01 | | 0.16 | 1.61 | 0.209 | 2.09 | 0.25 | 2.471 | 0.08 | 0.81 | 0.065 | 0.6465 |
| | 0.01 | | 0.16 | 1.58 | 0.208 | 2.08 | 0.25 | 2.482 | 0.08 | 0.85 | 0.055 | 0.5495 |
| | 0.01 | | 0.16 | 1.59 | 0.208 | 2.08 | 0.25 | 2.489 | 0.08 | 0.85 | 0.045 | 0.4501 |
| | | | ave | 1.59 | | 2.08 | | 2.481 | | 0.84 | | 0.5487 |
| The weight averate | | | st | 0.01 | | 0 | | 0.009 | | 0.02 | | 0.0982 |
| **avera** | **0.01** | | **0.16** | | **0.208** | | **0.25** | | **0.08** | | **0.055** | |
| **std** | **0** | | **0** | | **4E-04** | | **0** | | **0** | | **0.01** | |
| | | | y | Abs | | | | | | | | |
| | | | | | x | Conc | | | | | | |
| | volume | 10 ml | | | | | | | | | | |
| | y=x*0.0704 | | x=y/0.0704 | | | | | | | | | |
| | | c=g/v | g=c*v | | | | | | | | | |
| | | | | | | | | | ave | st | | |
| | | | | | | Single | | | 1.59 | 0.01 | | |
| | | | | | | Co-axial Single pha | | | 2.08 | 0 | | |
| | | | | | | Co-axial CG/G | | | 2.48 | 0.01 | | |
| | | | | | | Co-axial CG/PCL | | | 0.84 | 0.02 | | |
| | | | | | | Tri-axial PCLG/G/P | | | 0.55 | 0.1 | | |

| Control | | Single | | Co single | | Co G | | Co PCL | | Triaxial | |
|---|---|---|---|---|---|---|---|---|---|---|---|
| 0.28 | 0.28 | 2.91 | 0.83 | 2.92 | 0.682 | 2.64 | 0.45 | 0.916 | 0.35 | 2.54 | 0.306 |
| 0.3 | 0.28 | 2.98 | 0.83 | 3.17 | 0.557 | 2.88 | 0.33 | 0.797 | 0.3 | 2.94 | 0.26 |
| 0.31 | 0.28 | 3.04 | 0.83 | 3.43 | 0.432 | 3.12 | 0.21 | 0.679 | 0.25 | 3.34 | 0.214 |

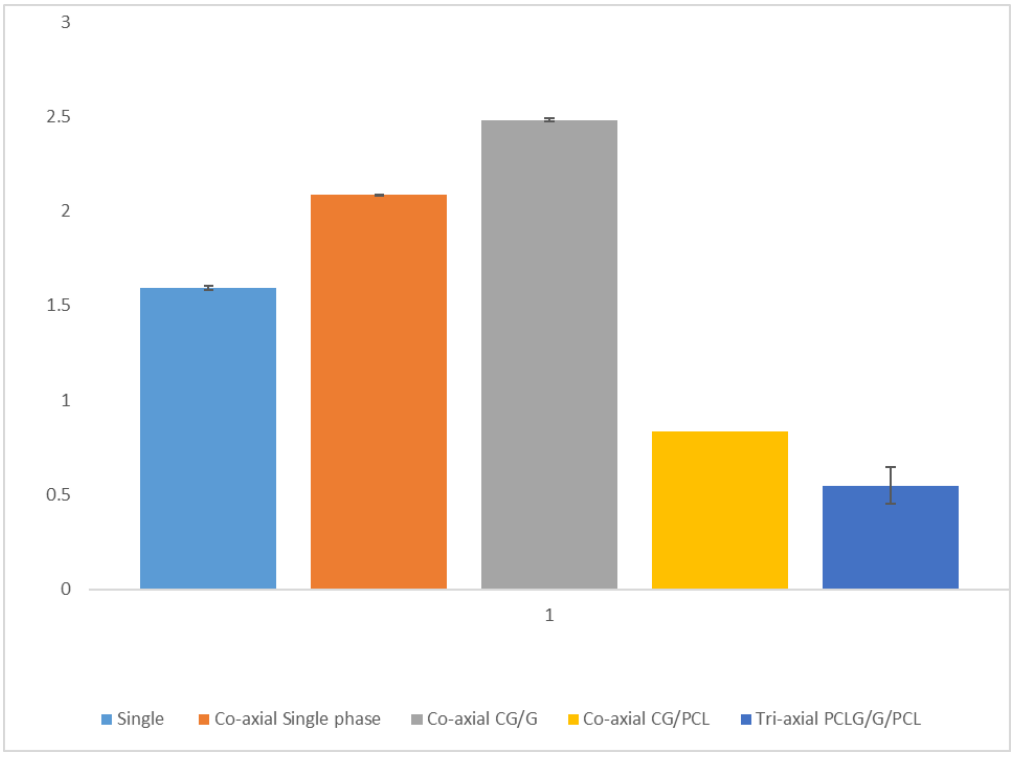
3
2.5
2
1.5
1
0.5
0
1
Single
Co-axial Single phase
Co-axial CG/G
Co-axial CG/PCL
Tri-axial PCLG/G/PCL

# APPENDIX D

## Permeability model

In order to determine $k_d$ values, Dox concentration was measured by incubating Dox directly in PBS various times until 48 hr. Then a first order decay rate [239] given by

$$\frac{dC_{Dox}}{dt} = -k_D C_{Dox} \tag{1}$$

was used to determine the decay constant $k_d$ ($h^{-1}$) where $C_{Dox}$ (µg/mL) is the Dox concentration at any time t. This equation was integrated using the limits of integration of when t= 0, $C_{DOX}$= $C_{Dox,0}$ (µg/mL) and when t= t, $C_{Dox}$= $C_{Dox}$ to obtain

$$\frac{C_{Dox}}{C_{Dox,0}} = e^{-k_d t} \quad \text{or} \quad C_{Dox,0} = C_{Dox} e^{k_D t} \tag{2}$$

Obtained concentration values were then plotted as a ratio against corresponding time according to the equation. By fitting an exponential decay function, slope value corresponded to the decay constant. In order to determine the Dox release rate K (µg/mL.h), a single compartment was assumed. Writing the Fick's first law in terms of permeability gave

$$\frac{dC_{Dox,0}}{dt} = \frac{PS}{V}\left(C_{Matrix} - C_{Dox,0}\right) \tag{3}$$

where S is the surface area of the matrix (300 $mm^2$) and V is the volume ($mm^3$) of the PBS incubated. Substituting Equation (2) into Equation (3)

$$\frac{dC_{Dox}e^{k_D t}}{dt} = \frac{PS}{V}\left(C_{Matrix} - C_{Dox}e^{k_D t}\right) \rightarrow$$

$$e^{k_D t}\frac{dC_{Dox}}{dt} + k_D C_{Dox}e^{k_D t} = \frac{PS}{V}C_{Matrix} - \frac{PS}{V}C_{Dox}e^{k_D t}$$

$$\frac{dC_{Dox}}{dt} + \left(k_D + \frac{PS}{V}\right)C_{Dox} = \frac{PS}{V}C_{Matrix}e^{-k_D t}$$ ➔ This is of the form $\frac{dy}{dt} + by = ae^{-k_D t}$

Integration gives $$C_{Dox} = C_{Matrix}e^{-k_D t} + c_1\left(k_D + \frac{PS}{V}\right)e^{-(k_D + P)t}$$

Using the initial boundary condition when t = 0, $C_{Dox} = 0$, integral constant c1 is evaluated as

$$c_1 = -\frac{C_{Matrix}}{\left(k_D + \frac{PS}{V}\right)}$$

Substituting $$\frac{C_{Dox}}{C_{Matrix}} = e^{-k_D t} - e^{-\left(k_D + \frac{PS}{V}\right)t} \rightarrow \frac{C_{Dox}}{C_{Matrix}e^{-k_D t}} = 1 - e^{-\frac{PS}{V}t}$$

$$\rightarrow C_{Dox} = C_{Matrix}e^{-k_D t} - C_{Matrix}e^{-\left(k_D + \frac{PS}{V}\right)t} \rightarrow e^{-\frac{PS}{V}t} = 1 - \frac{C_{Dox}}{C_{Matrix}e^{-k_D t}} \rightarrow$$

$$Ln\left(1 - \frac{C_{Dox}}{C_{Matrix}e^{-k_D t}}\right) = -P\frac{tS}{V} \qquad (4)$$

This equation was plotted to and the slope provided the permeability values P (mm/h)

# Permeability data for single fiber (PCL/GT)

| $C_s$ | V mm3 | St/V | 70.2883 | CS |
|---|---|---|---|---|
| 0.037 | 20000 | 0.000158333 | -0.00052 | 0.036602 |
| 0.107 | 19000 | 0.126315789 | -0.00223 | 0.160285 |
| 0.099 | 18000 | 0.4 | -0.00446 | 0.444295 |
| 0.076 | 17000 | 0.847058824 | -0.01091 | 1.48217 |
| 0.064 | 16000 | 1.35 | -0.02946 | 4.75473 |
| 0.063 | 15000 | 1.92 | -0.0945 | 15.10962 |
| 0.062 | 14000 | 2.571428571 | -0.33129 | 47.8771 |

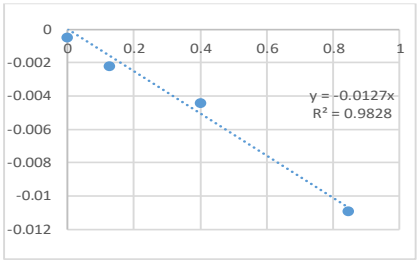


| $C_s$ | V mm3 | St/V | 70.2883 | |
|---|---|---|---|---|
| 0.038068 | 20000 | 0.000158333 | -0.00054 | 0.038049 |
| 0.09026 | 19000 | 0.126315789 | -0.00189 | 0.146093 |
| 0.08608 | 18000 | 0.4 | -0.00388 | 0.400975 |
| 0.065747 | 17000 | 0.847058824 | -0.00941 | 1.334639 |
| 0.0528 | 16000 | 1.35 | -0.02409 | 4.276288 |
| 0.05211 | 15000 | 1.92 | -0.07726 | 13.58449 |
| 0.051177 | 14000 | 2.571428571 | -0.26274 | 43.03951 |

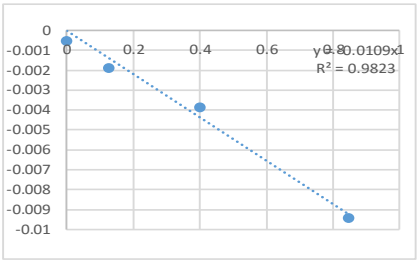


| $C_s$ | V mm3 | St/V | 70.2883 | |
|---|---|---|---|---|
| 0.045333 | 20000 | 0.000158333 | -0.00065 | 0.04531 |
| 0.099959 | 19000 | 0.126315789 | -0.00209 | 0.166447 |
| 0.091234 | 18000 | 0.4 | -0.00412 | 0.450002 |
| 0.068506 | 17000 | 0.847058824 | -0.00981 | 1.492546 |
| 0.058685 | 16000 | 1.35 | -0.02681 | 4.781871 |
| 0.056209 | 15000 | 1.92 | -0.0836 | 15.18851 |
| 0.055032 | 14000 | 2.571428571 | -0.28564 | 48.11932 |

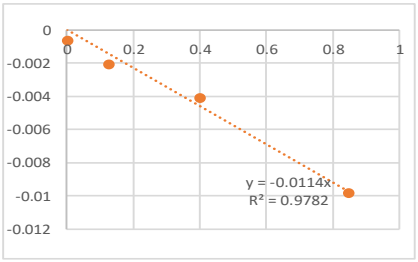


| $C_s$ | V mm3 | St/V | 70.2883 | CS |
|---|---|---|---|---|
| 0.026461 | 20000 | 0.000158333 | -0.00038 | 0.026448 |
| 0.129505 | 19000 | 0.126315789 | -0.00271 | 0.168314 |
| 0.119115 | 18000 | 0.4 | -0.00538 | 0.481908 |
| 0.094318 | 17000 | 0.847058824 | -0.01353 | 1.619324 |
| 0.081656 | 16000 | 1.35 | -0.03751 | 5.206033 |
| 0.081291 | 15000 | 1.92 | -0.12328 | 16.55586 |
| 0.081169 | 14000 | 2.571428571 | -0.45645 | 52.47246 |

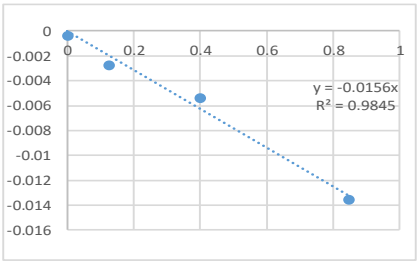


| Pm [mm/h | mm/s | 1/Pm |
|---|---|---|
| 0.0109 | 3.03E-06 | 91.74312 |
| 0.0114 | 3.17E-06 | 87.7193 |
| 0.0156 | 4.33E-06 | 64.10256 |
| **0.012633** | | |
| **0.002581** | | |

Permeability data for single-phase fiber (PCL/GT-PCL/GT)

| time | $C_s$ | V mm3 | St/V | 151.6739447 |
|---|---|---|---|---|
| 0.010556 | 0.00046 | 20000 | 0.000158 | -3.03408E-06 |
| 8 | 0.080749 | 19000 | 0.126316 | -0.000781929 |
| 24 | 0.073566 | 18000 | 0.4 | -0.001536056 |
| 48 | 0.052219 | 17000 | 0.847059 | -0.003453652 |
| 72 | 0.04141 | 16000 | 1.35 | -0.008689558 |
| 96 | 0.040625 | 15000 | 1.92 | -0.027227663 |
| 120 | 0.039435 | 14000 | 2.571429 | -0.086112614 |

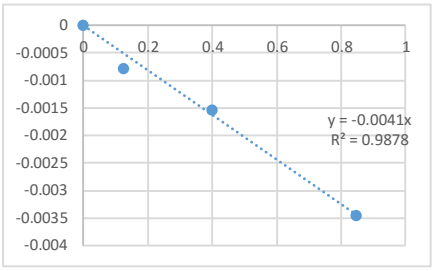


run 1

| time | Cs | V mm3 | St/V | 151.6739447 |
|---|---|---|---|---|
| 0.010556 | -0.00239 | 20000 | 0.000158 | 1.57949E-05 |
| 8 | 0.059781 | 19000 | 0.126316 | -0.000578823 |
| 24 | 0.054992 | 18000 | 0.4 | -0.001148006 |
| 48 | 0.035633 | 17000 | 0.847059 | -0.002355422 |
| 72 | 0.025974 | 16000 | 1.35 | -0.005441656 |
| 96 | 0.026015 | 15000 | 1.92 | -0.017349915 |
| 120 | 0.024594 | 14000 | 2.571429 | -0.052829741 |

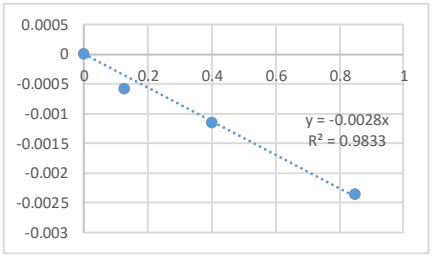


run 2

| time | Cs | V mm3 | St/V | 151.6739447 |
|---|---|---|---|---|
| 0 | 0.00414 | 20000 | 0 | -2.72932E-05 |
| 8 | 0.089529 | 19000 | 0.126316 | -0.000866984 |
| 24 | 0.082062 | 18000 | 0.4 | -0.001713597 |
| 48 | 0.060877 | 17000 | 0.847059 | -0.004027433 |
| 72 | 0.049594 | 16000 | 1.35 | -0.010416003 |
| 96 | 0.048498 | 15000 | 1.92 | -0.032591407 |
| 120 | 0.046266 | 14000 | 2.571429 | -0.101814727 |

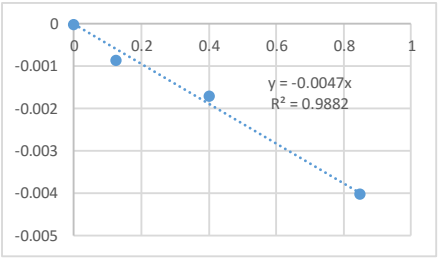


run 3

| time | Cs | V mm3 | St/V | 151.6739447 |
|---|---|---|---|---|
| 0 | -0.00037 | 20000 | 0 | 2.40819E-06 |
| 8 | 0.092938 | 19000 | 0.126316 | -0.000900012 |
| 24 | 0.083644 | 18000 | 0.4 | -0.001746678 |
| 48 | 0.060146 | 17000 | 0.847059 | -0.003979007 |
| 72 | 0.048661 | 16000 | 1.35 | -0.010218952 |
| 96 | 0.047362 | 15000 | 1.92 | -0.031815479 |
| 120 | 0.047443 | 14000 | 2.571429 | -0.104544917 |

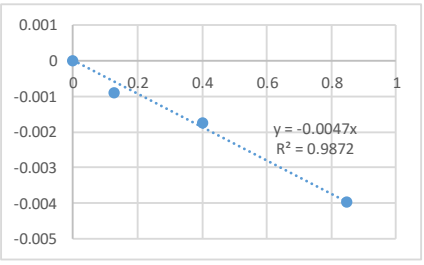


| | p mm/hr |
|---|---|
| | 0.0028 |
| | 0.0047 |
| | 0.0047 |
| **ave** | **0.004066667** |
| **std** | **0.001096966** |

Permeability data for Co-GT fiber

| time | CS | V mm3 | St/V | 179.1831017 |
|---|---|---|---|---|
| 0.010556 | 0.003057 | 20000 | 0.000158 | -5.89197E-05 |
| 8 | 0.061851 | 19000 | 0.126316 | -0.045813404 |
| 24 | 0.055939 | 18000 | 0.4 | -0.144218382 |
| 48 | 0.038988 | 17000 | 0.847059 | -0.312499761 |
| 72 | 0.030208 | 16000 | 1.35 | -0.514844811 |
| 96 | 0.030181 | 15000 | 1.92 | -0.769038506 |
| 120 | 0.028314 | 14000 | 2.571429 | -1.110533524 |

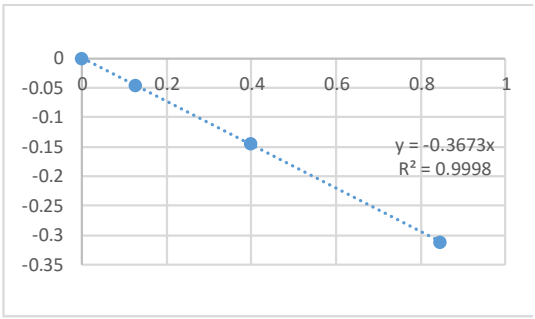


**run 1**

| time | CS | V mm3 | St/V | 179.1831017 |
|---|---|---|---|---|
| 0.010556 | 0.002476 | 20000 | 0.000158 | -5.89181E-05 |
| 8 | 0.05487 | 19000 | 0.126316 | -0.045797699 |
| 24 | 0.049594 | 18000 | 0.4 | -0.144171145 |
| 48 | 0.032265 | 17000 | 0.847059 | -0.312381398 |
| 72 | 0.023539 | 16000 | 1.35 | -0.5146293 |
| 96 | 0.023701 | 15000 | 1.92 | -0.76867854 |
| 120 | 0.02358 | 14000 | 2.571429 | -1.110070961 |

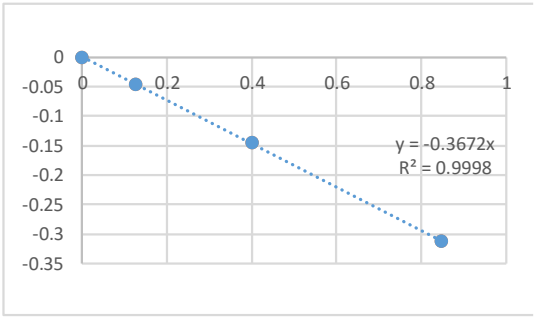


run 2

| time | Gelatin | V mm3 | St/V | 179.1831017 |
|---|---|---|---|---|
| 0.010556 | 0.003612 | 20000 | 0.000158 | -5.89213E-05 |
| 8 | 0.071834 | 19000 | 0.126316 | -0.045835875 |
| 24 | 0.064651 | 18000 | 0.4 | -0.144283273 |
| 48 | 0.046631 | 17000 | 0.847059 | -0.312634381 |
| 72 | 0.037865 | 16000 | 1.35 | -0.515092375 |
| 96 | 0.036972 | 15000 | 1.92 | -0.769416016 |
| 120 | 0.035065 | 14000 | 2.571429 | -1.111193558 |

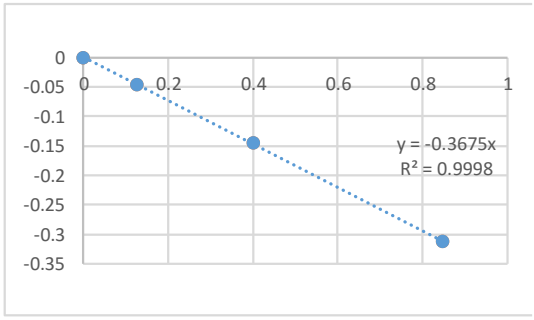


run 3

| time | Gelatin | V mm3 | St/V | 179.1831017 |
|---|---|---|---|---|
| 0.010556 | 0.003084 | 20000 | 0.000158 | -5.89198E-05 |
| 8 | 0.058847 | 19000 | 0.126316 | -0.045806646 |
| 24 | 0.053571 | 18000 | 0.4 | -0.144200754 |
| 48 | 0.038068 | 17000 | 0.847059 | -0.312483563 |
| 72 | 0.029221 | 16000 | 1.35 | -0.514812892 |
| 96 | 0.02987 | 15000 | 1.92 | -0.769021216 |
| 120 | 0.026299 | 14000 | 2.571429 | -1.110336565 |

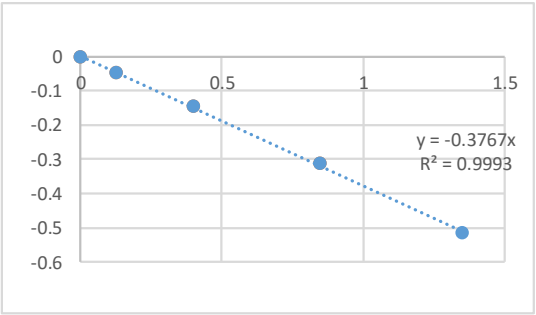


| | P(mm/hr) |
|---|---|
| | 0.3672 |
| | 0.3675 |
| | 0.3767 |
| **average** | **0.370467** |
| **stdv** | **0.0054** |

# Permeability data for Co-PCL fiber

| time | PCL | V mm3 | St/V | 60.06357594 |
|---|---|---|---|---|
| 0.15 | -0.00411 | 20000 | 0.00225 | 6.89624E-05 |
| 8 | 0.018845 | 19000 | 0.126316 | -0.00046073 |
| 24 | 0.017627 | 18000 | 0.4 | -0.00092914 |
| 48 | 0.004992 | 17000 | 0.847059 | -0.00083262 |
| 72 | -0.00517 | 16000 | 1.35 | 0.00272283 |
| 96 | -0.0044 | 15000 | 1.92 | 0.007313917 |
| 120 | -0.00534 | 14000 | 2.571429 | 0.027841994 |

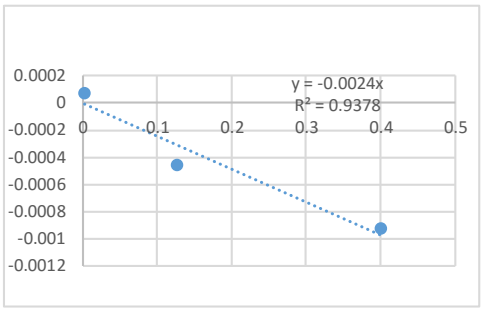


run 1

| time | CS | V mm3 | St/V | 60.06357594 |
|---|---|---|---|---|
| 0.15 | -0.00471 | 20000 | 0.00225 | 7.89434E-05 |
| 8 | 0.018263 | 19000 | 0.126316 | -0.00044651 |
| 24 | 0.016356 | 18000 | 0.4 | -0.00086208 |
| 48 | 0.001907 | 17000 | 0.847059 | -0.00031807 |
| 72 | -0.00657 | 16000 | 1.35 | 0.003462842 |
| 96 | -0.00471 | 15000 | 1.92 | 0.007829496 |
| 120 | -0.00816 | 14000 | 2.571429 | 0.042197345 |

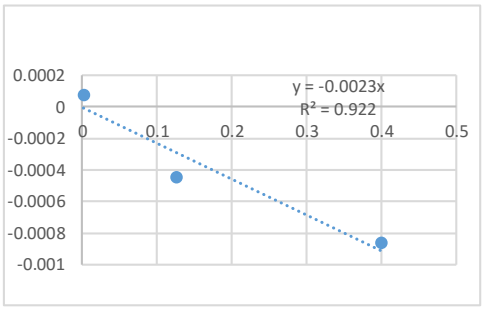


run 2

| time | PCL | V mm3 | St/V | 60.06357594 |
|---|---|---|---|---|
| 0.15 | -0.0026 | 20000 | 0.00225 | 4.35558E-05 |
| 8 | 0.023904 | 19000 | 0.126316 | -0.00058447 |
| 24 | 0.022037 | 18000 | 0.4 | -0.00116174 |
| 48 | 0.012013 | 17000 | 0.847059 | -0.00200489 |
| 72 | -0.00045 | 16000 | 1.35 | 0.000235511 |
| 96 | -0.00016 | 15000 | 1.92 | 0.000271006 |
| 120 | -0.00093 | 14000 | 2.571429 | 0.004919754 |

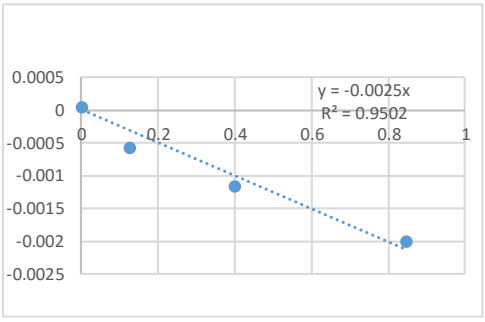


run 3

| time | PCL | V mm3 | St/V | 60.06357594 |
|---|---|---|---|---|
| 0.15 | -0.00503 | 20000 | 0.00225 | 8.43876E-05 |
| 8 | 0.014367 | 19000 | 0.126316 | -0.00035123 |
| 24 | 0.014489 | 18000 | 0.4 | -0.00076364 |
| 48 | 0.001055 | 17000 | 0.847059 | -0.00017594 |
| 72 | -0.00848 | 16000 | 1.35 | 0.004465254 |
| 96 | -0.00832 | 15000 | 1.92 | 0.013795323 |
| 120 | -0.00694 | 14000 | 2.571429 | 0.036011171 |

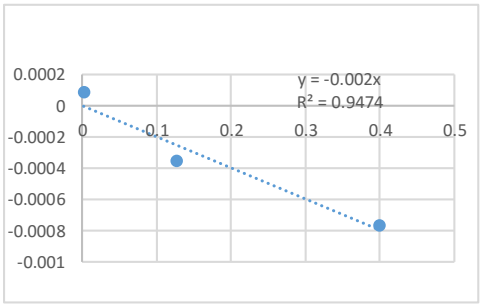


| | Pm (mm/hr) |
|---|---|
| | 0.0023 |
| | 0.0025 |
| | 0.002 |
| **average** | **0.002267** |
| **stdv** | **0.000252** |

Permeability data for triaxial fiber

| time | triaxial | V mm3 | St/V | 32.83523 |
|---|---|---|---|---|
| 0.15 | -0.00426 | 20000 | 0.00225 | 0.000131 |
| 8 | 0.017546 | 19000 | 0.126316 | -0.00078 |
| 24 | 0.017005 | 18000 | 0.4 | -0.00164 |
| 48 | 0.004356 | 17000 | 0.847059 | -0.00133 |
| 72 | -0.00288 | 16000 | 1.35 | 0.002777 |
| 96 | -0.00256 | 15000 | 1.92 | 0.007779 |
| 120 | -0.00152 | 14000 | 2.571429 | 0.014538 |

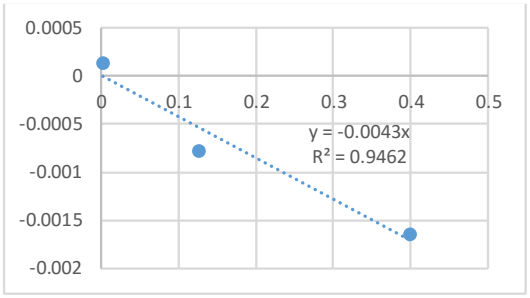


run 1

| time | triaxial | V mm3 | St/V | 32.83523 |
|---|---|---|---|---|
| 0 | -0.00459 | 20000 | 0 | 0.00014 |
| 8 | 0.021672 | 19000 | 0.126316 | -0.00097 |
| 24 | 0.022484 | 18000 | 0.4 | -0.00217 |
| 48 | 0.008157 | 17000 | 0.847059 | -0.00249 |
| 72 | 4.06E-05 | 16000 | 1.35 | -3.9E-05 |
| 96 | 0.001136 | 15000 | 1.92 | -0.00348 |
| 120 | 0.001948 | 14000 | 2.571429 | -0.01901 |

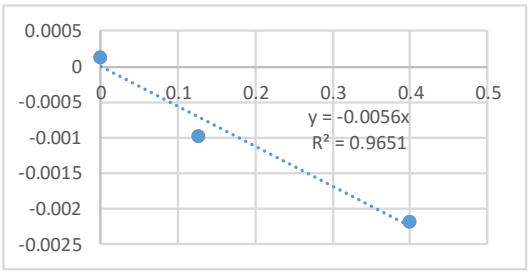


run 2

| time | triaxial | V mm3 | St/V | 32.83523 |
|---|---|---|---|---|
| 0 | -0.00511 | 20000 | 0 | 0.000156 |
| 8 | 0.017532 | 19000 | 0.126316 | -0.00078 |
| 24 | 0.015057 | 18000 | 0.4 | -0.00145 |
| 48 | 0.002354 | 17000 | 0.847059 | -0.00072 |
| 72 | -0.00507 | 16000 | 1.35 | 0.004884 |
| 96 | -0.00418 | 15000 | 1.92 | 0.012686 |
| 120 | -0.00402 | 14000 | 2.571429 | 0.038097 |

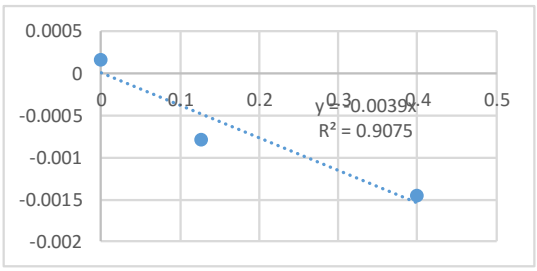


run 3

| time | triaxial | V mm3 | St/V | 32.83523 |
|---|---|---|---|---|
| 0 | -0.00308 | 20000 | 0 | 9.39E-05 |
| 8 | 0.013433 | 19000 | 0.126316 | -0.0006 |
| 24 | 0.013474 | 18000 | 0.4 | -0.0013 |
| 48 | 0.002557 | 17000 | 0.847059 | -0.00078 |
| 72 | -0.00361 | 16000 | 1.35 | 0.00348 |
| 96 | -0.00463 | 15000 | 1.92 | 0.014031 |
| 120 | -0.00248 | 14000 | 2.571429 | 0.023645 |

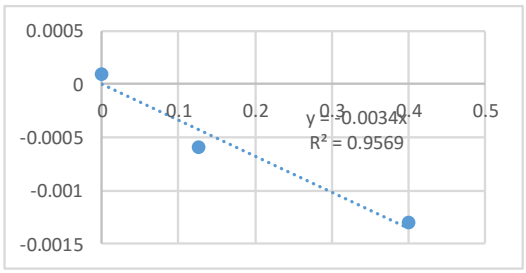


| | P(mm/hr) |
|---|---|
| | 0.0056 |
| | 0.0039 |
| | 0.0034 |
| **average** | **0.0043** |
| **stdv** | **0.001153** |

# APPENDIX E

## Concentration conversion of Dox

| gram | x (micro) | (Abs) | Y | conc micrg/ml X |
|---|---|---|---|---|
| 0 | 0 | 0.2167 | 0 | 0.00 |
| 0.000008 | 8 | 0.8446 | 0.6279 | 0.23 |
| 0.00001 | 10 | 1.126 | 0.9093 | 0.29 |
| 0.00003 | 30 | 2.243 | 2.0263 | 0.86 |

2.464

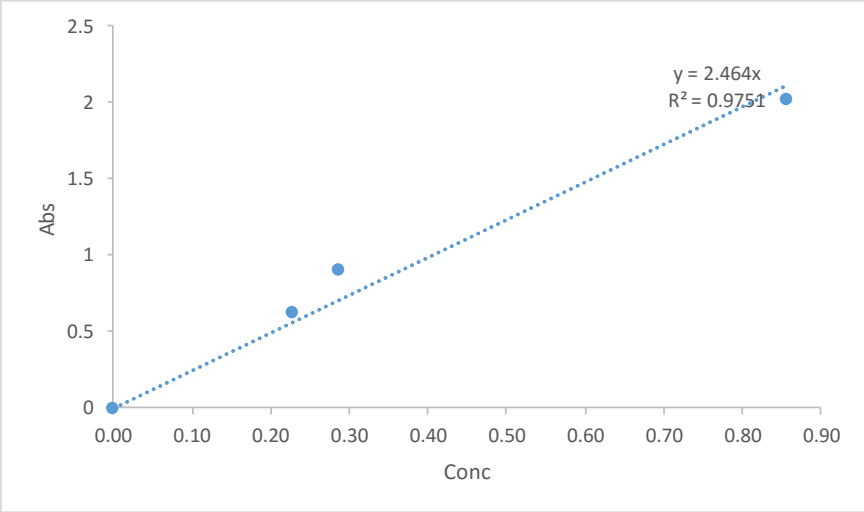

APPENDIX F

Limitations and advantageous of the electrospinning technique

| **Limitations** | **Advantageous** |
|---|---|
| Low output (limited by feed rate) | High surface area to volume ratio |
| Clogging at the spinneret | Varity of structures can be constructed |
| Stability of electric field | Varity of materials can be used |
| Fiber size consistency | Mass production capability |
| Solutions interactions | Low startup cost |

# APPENDIX G.

## Boiling point and volatility of solvents mixture

In this study, we used CHEMCAD to evaluate the solution solvents mixture volatility for the three electrospinning configuration (CA-PCL-hollow, CA-PCL-hollow, and PVA-PCL-hollow) to better understand the influence of the solvent mixture volatility on the jet behavior and the producibility, structure and morphology of core-shell fibers. Before running the simulation, the engineering units were set to Pascal for pressure and °C degrees for temperature. To run the simulation, first, we define the compounds of interest by selecting a thermophysical menu on the main CHEMCAD toolbar and then select a component from components list. On the thermodynamics simulation, it's required to enter the operation max temperature and pressure ranges of the process; both were set at 25°C and 1 atm temperature and pressure respectively. There is no need to enter or edit anything else on this screen; the program has default values for other parameters. The next step is selecting the thermodynamic model. CHEMCAD will display the components selection list. NRTL model (Non-Random Two-liquid) was selected as it is the model that recommended for polar liquid mixtures at low pressures. For data analysis, TPXY plot was selected (the process is at constant pressure) and used to plot the generated experimental data in XY diagram. For a mixture of two components, the screen will ask to enter the two component of interest along with estimate pressure and temperature (25°C, 1 atm). When you run the simulation, CHEMCAD will automatically generate TPXY plot with the selected components. The plot shows the temperature vs liquid and vapor fraction of selected component. From the plot, the approximated mixture temperature (boiling point) can be estimated at the given mass fraction. The obtained plots were analyzed and used to determine the approximate boiling point and volatility of the three selected mixtures system.

# APPENDIX G

Electrospinning system

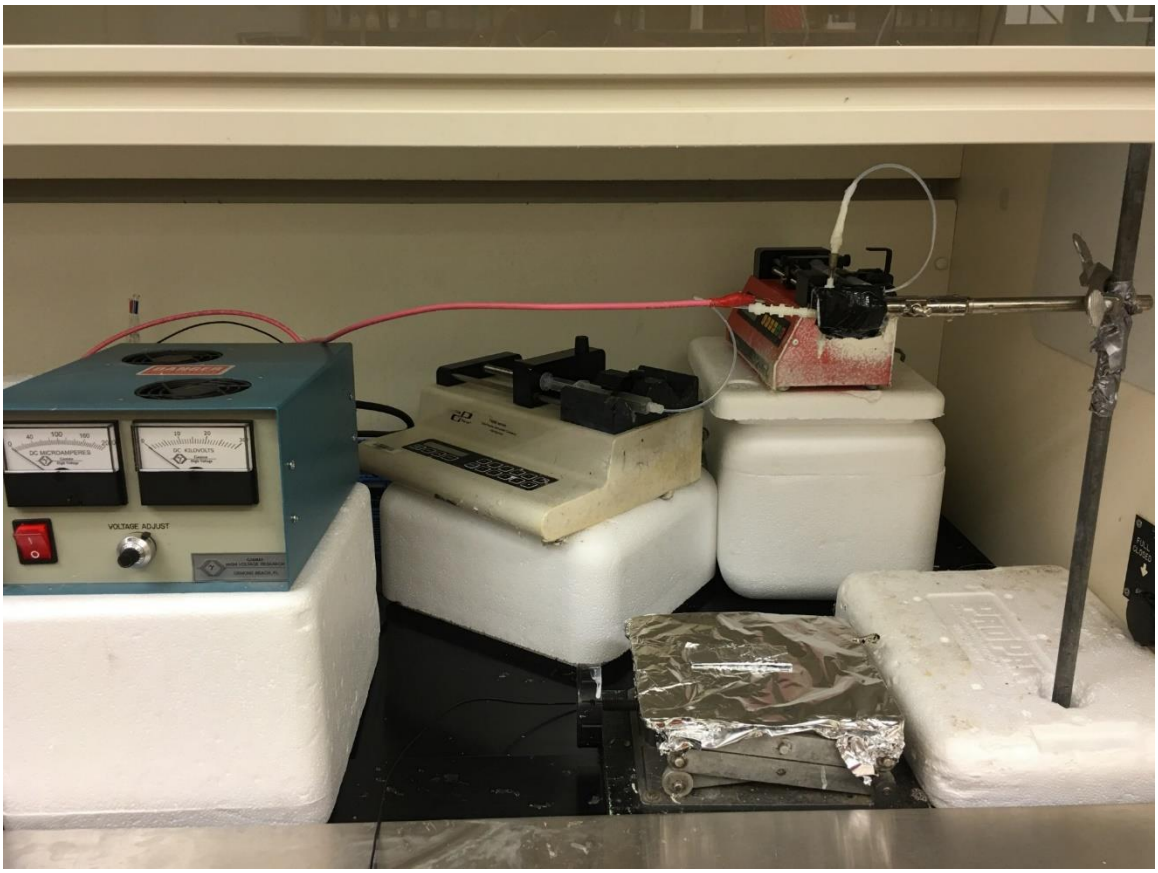

# APPENDIX H

Schematic of triaxial spinneret

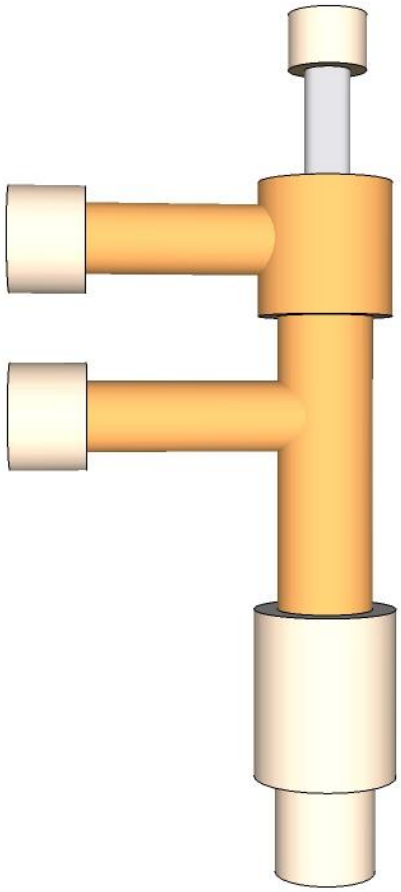

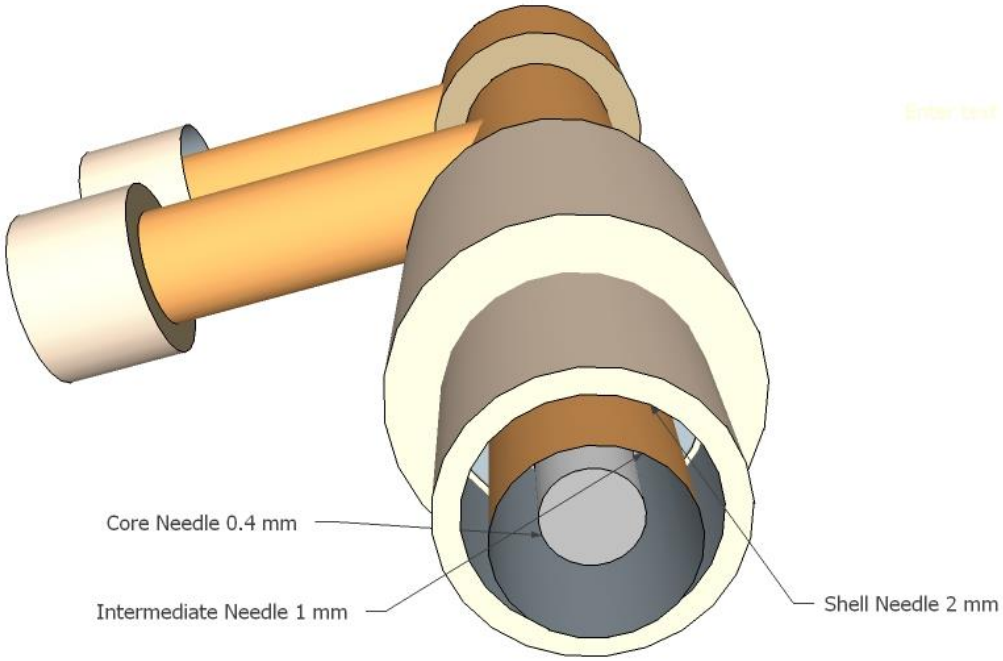
Core Needle 0.4 mm
Intermediate Needle 1 mm
Shell Needle 2 mm

VITA

Abdurizzagh Alfitori Khalf

Candidate for the Degree of

Doctor of Philosophy

Thesis: COAXIAL AND TRIAXIAL STRUCTURED FIBERS BY ELECTROSPINNING FOR TISSUE ENGINEERING AND SUSTAINED DRUG RELEASE

Major Field: Chemical Engineering

Biographical:

Education:

Completed the requirements for the Doctor of Philosophy in Chemical Engineering at Oklahoma State University, Stillwater, Oklahoma in May 2016.

Completed the requirements for the Master of Science in Chemical Engineering at University of Stellenbosch, Stellenbosch, South Africa in 2009.

Completed the requirements for the Bachelor of Science in Chemical Engineering at Sirte University, Sirte, Libya in 2002.

Experience:

Research Associate, School of Chemical Engineering, Oklahoma State University, Stillwater, Oklahoma. 2012-2015

Teaching Associate, School of Chemical Engineering, Oklahoma State University, Stillwater, Oklahoma. 2012-2013

Research Associate, Division of Polymer Science
University of Stellenbosch, Stellenbosch, South Africa. 2006-2009

Professional Memberships:
American Chemical Society (ACS)
International Society for Biomedical Polymers and Polymeric Biomaterials (ISBPPB)
Chemical Engineering Graduate Student Association (ChEGSA)
American Institute of Chemical Engineers (AIChE)